CHALMERS
UNIVERSITY OF TECHNOLOGY

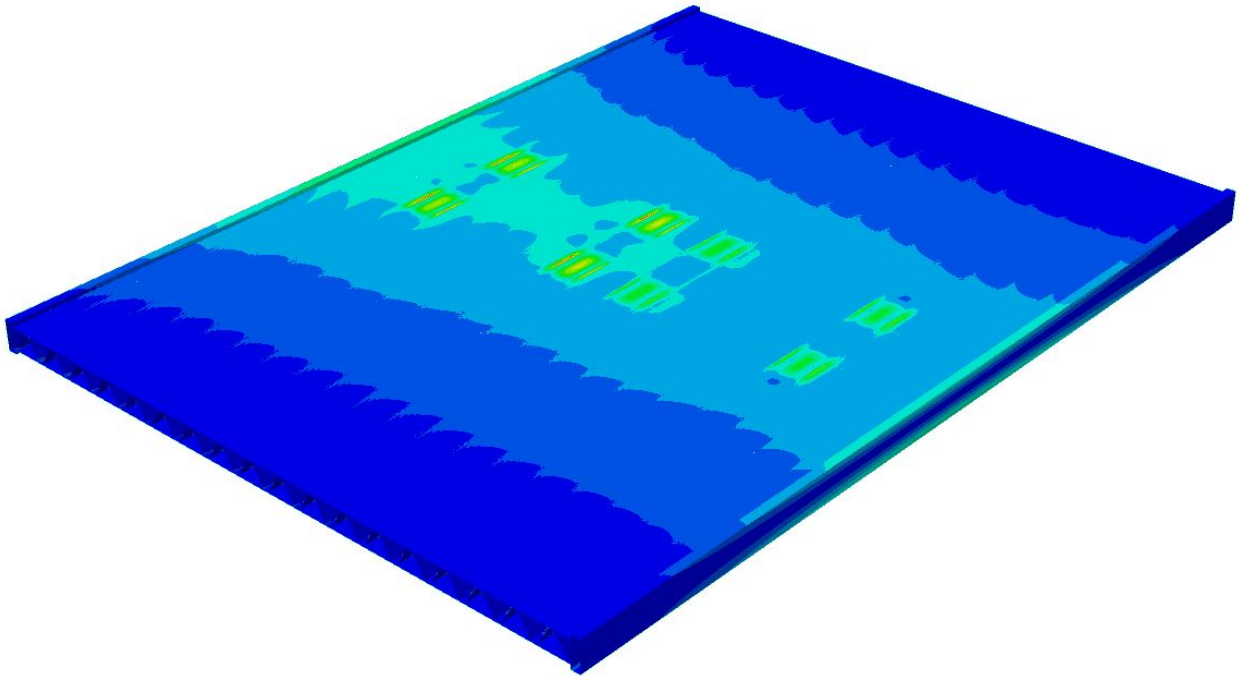

Laser welded Corrugated Core Steel Sandwich Panels for short-span bridge application

Master's thesis in Structural Engineering and Building Technology

ANNA LIBELL
HANNA LASSING

DEPARTMENT OF ARCHITECTURE AND CIVIL ENGINEERING
CHALMERS UNIVERSITY OF TECHNOLOGY

Gothenburg, Sweden 2020
www.chalmers.se

Master's thesis ACEX30

Laser welded Corrugated Core Steel Sandwich Panels for short-span bridge application

Master's Thesis in the Master's Programme Structural Engineering and Building Technology

ANNA LIBELL
HANNA LASSING

CHALMERS
UNIVERSITY OF TECHNOLOGY

Department of Architecture and Civil Engineering
Division of Structural Engineering
Steel and Timber Structures
Chalmers University of Technology
Gothenburg, Sweden 2020

Laser welded Corrugated Core Steel Sandwich Panels for short-span bridge application

Master's Thesis in the Master's Programme Structural Engineering and Building Technology

ANNA LIBELL
HANNA LASSING

Examensarbete ACEX30
Institutionen för arkitektur och samhällsbyggnadsteknik
Chalmers tekniska högskola, 2020

Department of Architecture and Civil Engineering
Division of Structural Engineering
Steel and Timber Structures
Chalmers University of Technology
SE-412 96 Gothenburg
Telephone +46 (0)31 772 1000

Cover: Model of the Laser welded Corrugated Core Steel Sandwich Panel bridge deck investigated in the thesis

Typeset in LaTeX
Printed by Chalmers Reproservice
Gothenburg, Sweden, 2020

Laser welded Corrugated Core Steel Sandwich Panels for short-span bridge application
Master's Thesis in the Master's Programme Structural Engineering and Building Technology
ANNA LIBELL
HANNA LASSING
Department of Architecture and Civil Engineering
Chalmers University of Technology

Abstract

With the environmental changes, there is a large focus on finding bridge deck solutions that are material efficient. Laser welded Corrugated Core Steel Sandwich Panels (CCSSPs) is a promising solution due to its high stiffness to mass ratio. It is of interest to investigate if CCSSPs can be used as a bridge deck for simply supported short-span bridges. This thesis aims to investigate how different cross section parameters influence the behaviour of a CCSSP used as a simply supported bridge deck for short-span bridges and the feasibility of these panels with this purpose.

A laser welded CCSSP is a Steel Sandwich Panel consisting of two face plates on each side of a corrugated core. At all positions where the core meets the face plates there are two weld lines. In welded steel structures, fatigue is a common failure mode. A method for checking the fatigue life of the CCSSP bridge deck verified. Another crucial aspect of CCSSPs is the risk of buckling of the top plate in the field between each weld pair due to biaxial compression from patch loads. Eurocode's Reduced Stress Method (RSM) is verified as a way to check the capacity of the CCSSP with respect to buckling.

Using the FE-analysis software BRIGADE/Plus with Python scripting a design program for a simply supported short-span CCSSP bridge deck is created. Using the design program, a parametric study is performed for the CCSSP bridge deck. Resolution IV Fractional Factorial Design is used to perform the study. The results of the parametric study show that the Utilization Ratio (UR) of the investigated CCSSP with respect to deflection in SLS is decreased with an increased cross section height and a decreased cell width. They also show that the UR of the CCSSP with respect to the Von Mises stress in the welds in ULS is decreased with a decreased cell width and an increased weld size. The thesis also concludes that local effects from patch loading is highly dominant for the CCSSP.

Keywords: BRIGADE/Plus, Corrugated Core Steel Sandwich Panels, Eurocode, Fractional Factorial Design, Laser welding, Reduced Stress Method

Lasersvetsade stålsandwichplattor med korrugerat liv som brodäck för kortspanniga broar
Examensarbete inom masterprogrammet Structural Engineering and Building Technology
ANNA LIBELL
HANNA LASSING
Institutionen för arkitektur och samhällsbyggnad
Chalmers Tekniska Högskola

Sammanfattning

Med dagens klimatutmaningar ligger stort fokus på att designa brodäck som är materialeffektiva. Lasersvetsade stålsandwichplattor med korrugerat liv (CCSSP) är en lovande lösning tack vare dess höga förhållande mellan styvhet och vikt. Det är av intresse att undersöka om CCSSP kan användas som brodäck för fritt upplagda, kortspanniga broar. Arbetet syftar till att undersöka hur olika tvärsnittsparametrar påverkar beteendet hos en CCSSP då den används som brodäck för en fritt upplagd, kortspannig bro samt rimligheten i att de används för detta syfte.

En lasersvetsad CCSSP är en stålsandwichplatta bestående av två ytplåtar på varsin sida av ett korrugerat liv. På alla positioner där kärnan möter ytplåtarna finns två svetslinjer. I svetsade stålkonstruktioner är utmattning en vanlig brottmod. En metod för att kontrollera utmattningskapaciteten för en CCSSP som ett brodäck verifieras. En annan kritisk aspekt för en CCSSP är risken för buckling av plåtfältet i topplattan mellan varje svetspar på grund av det biaxiella spänningstillstånd som uppstår av punktlaster. Eurocodes Reducerade spänningsmetod (RSM) verifieras som ett sätt att kolla kapaciteten för en CCSSP med avseende på buckling.

Med hjälp av finita elementanalysprogrammet BRIGADE/Plus och scriptning i Python, skapas ett designprogram för en CCSSP som ett brodäck för fritt upplagda, korstspanniga broar. Designprogrammet används för att utföra en parameterstudie av CCSSP-brodäcket. För att utföra studien används Fractional Factorial Design (FFD) med upplösning IV. Resultaten från parameterstudien visar att utnyttjandegraden för plattan med avseende på nedböjning i bruksgränstillstånd minskar med en ökad höjd på tvärsnittet och en minskad cellbredd. De visar också att utnyttjandegraden för plattan med avseende på Von Mises-spänningarna i svetsarna i brottsgränstillstånd minskar med en minskad cellbredd och en ökad svetsstorlek. Slutsatsen dras även att lokala effekter från punktlaster är dominanta för en CCSSP.

Nyckelord: BRIGADE/Plus, Eurocode, Fractional Factorial Design, Lasersvetsning, Reducerad spänningsmetod, Stålsandwichplattor med korrugerat liv

Contents

Preface

This master's thesis investigates how a Corrugated Core Steel Sandwich Panel can be designed and utilized as a simply supported bridge deck for short-span bridges. The thesis is written during the spring 2020 at the Department of Architecture and Civil Engineering at Chalmers University of Technology within the master's program Structural Engineering and Building Technology.

We would greatly like to thank our supervisor Dr. Peter Nilsson Strand for his big encouragement and with all the help he has provided us with during this project. Your help and support has been irreplaceable. We would also like to thank Associate Professor Mohammad Al-Emrani for his guidance and feedback during the project.

Finally, thanks to everyone at WSP Bridge and Hydraulics department in Gothenburg where the project was carried out.

Anna Libell and Hanna Lassing, Gothenburg, June 2020

List of Figures

List of Tables

Acronyms

CCSSP Corrugated Core Steel Sandwich Panel. 1

DOFs Degrees of Freedom. 14

ESL Equivalent Single Layer. 1

FE Finite Element. 13
FFD Fractional Factorial Design. 29
FLM4 Fatigue Load Model 4. 3
FLS Fatigue Limit State. 3

HLAW Hybrid Laser-Arc Welding. 9

LM1 Load Model 1. 3
LPF Load Proportionality Factor. 44

RSM Reduced Stress Method. 22

SLS Serviceability Limit State. 3
SSP Steel Sandwich Panel. 6

ULS Ultimate Limit State. 3
UR Utilization Ratio. 3

Glossary

biaxial stress Stress in two directions. 2

composite Composition of two or more materials to create a new one. 6

elastic-plastic Material with elastic behaviour up to the yield stress, thereafter plastic behaviour. 44

high energy density process Process with an energy density above 10^{11} $\frac{J}{m^3}$. 9

homogenized When one single property is given to something with different properties. 14

initial imperfections Imperfections of a structure before any load has been applied. 44

integration point Positions in an FE-model where the equation system is solved for. 34

longitudinal Along the length of the bridge. 1

membrane forces Forces in the plane of a very thin plate. 14

multiaxial Two or more directions. 22

notch stress Stress at the edge of a weld where the weld connects to the main material. 9

orthotropic Material with different properties in different directions. 5

plate action When the load is taken in two directions in plane. 6

quadrilateral 2D geometry with four corners. 14

seeding Dividing an edge into many parts. 34

tandem loads Traffic loads consisting of two wheel pressure points connected by an axis. 2

tied connections Connection where all degrees of freedom are locked. 40

transverse Across the width of the bridge. 1

Von Mises yield criteria Capcity criteria based on the Von Mises stress. 23

Nomenclature

α	Buckling curve coefficient
$\alpha_{1..6}$	Coefficients used to calculate the rotational spring stiffness
α_{cr}	Relation between critical buckling stress and applied stress
α_{Qi}	Reduction factor in Load Model 1
α_{qi}	Reduction factor in Load Model 1
$\alpha_{ult,k}$	Relation between ultimate capacity and applied stress
$\bar{\lambda_p}$	Slenderness of a plate
$\bar{h_g}$	Normalized gap height between welded plates
β_w	Factor in weld evaluation
χ_w	Reduction factor in shear
χ_c	Column buckling reduction factor
$\Delta\phi_{fat}$	Damage amplification factor
$\Delta\sigma_C$	Detail category used in Fatigue assessment
$\Delta\sigma_i$	Applied stress range per cycle
$\Delta\sigma_L$	Stress in Fatigue assessment
δ	Displacement in z-direction
ϵ_0	Yield strain
ϵ_1	Ultimate strain
η	Utilization ratio
γ_d	Reduction factor in Load combination
γ_{Ff}	Partial factor from Eurocode
$\gamma_{G,j,inf}$	Reduction factor in Load combination
$\gamma_{G,j,sup}$	Reduction factor in Load combination
γ_{M0}	Partial factor from Eurocode
γ_{M1}	Partial factor from Eurocode
γ_{M2}	Partial factor from Eurocode
γ_{Mf}	Partial factor from Eurocode
$\gamma_{Q,i}$	Reduction factor in Load combination
λ_{eig}	Eigenvalue
ν	Poisson's ratio
ν_x	Poisson's ratio in x-direction
ν_y	Poisson's ratio in y-direction
ω	Lever arm in column-like buckling
$\psi_{0,i}$	Reduction factor in Load combination
$\psi_{1,i}$	Reduction factor in Load combination
$\psi_{2,i}$	Reduction factor in Load combination
ρ	Plate buckling reduction factor
ρ	Reduction for RSM
ρ_z	Reduction factor in z-direction
ρ_c	Reduction factor when interation occurs
ρ_{steel}	Density of steel
ρ_x	Reduction factor in x-direction
ρ_y	Reduction factor in y-direction

σ	Stress
σ_x	Stress in x-direction
σ_y	Stress in y-direction
σ_0	Parallel stress on a weld
σ_{90}	Perpendicular stress on a weld
$\sigma_{c,Rd}$	Bending stress capacity
$\sigma_{cr,c}$	Critical buckling stress for a column
$\sigma_{cr,p}$	Critical buckling stress for a plate
σ_{cr}	Critical buckling stress
σ_{Ed}	Applied stress
σ_{VM}	Von Mises stress
$\sigma_{x,Ed}$	Applied stress in x-direction
$\sigma_{z,Ed}$	Applied stress in z-direction
τ	Shear stress
τ_0	Parallel shear stress on a weld
τ_{90}	Perpendicular shear stress on a weld
$\tau_{c,Rd}$	Shear stress capacity
τ_{Ed}	Applied shear stress
τ_{xy}	Shear stress
Θ	Corrugation angle
ξ	Interaction factor plate and column buckling
ξ_j	Reduction factor in Load combination
A	Area
a	Height of an unstiffened plate
a	Weld width
A_{eff}	Effective area
B	Total width of the deck
b	Width of an unstiffened plate
c_i	Factor used to evaluate biaxial compression
D	Damage in Fatigue Limit State
D	Distance used in the calculation of the damage amplification factor
D_x	Bending stiffness in longitudinal direction
D_y	Bending stiffness in transverse direction
D_{Qx}	Transverse shear stiffness in plane parallel to corrugation axis
D_{Qy}	Transverse shear stiffness in longitudinal direction
d_{wi}	Distance between welds
D_{xy}	Bending stiffness in xy-plane
dL	Distance from edges to support partitions
dw_1	Distance between welds in bottom plate
dw_2	Distance between welds in top plate
E	Young's modulus
e_0	Initial imperfection lever arm
$e_{y,N}$	Lever arm in y-direction
$e_{z,N}$	Lever arm in z-direction
f_1	Distance between welds in the bottom plate
f_2	Distance between welds in the top plate
f_u	Ultimate tensile strength
f_y	Yield strength
G	Shear modulus
$G_{k,i}$	Permanent load in Load combination
h	Center to center distance between top and bottom plate
k	Buckling coefficient
k_φ	Rotational spring stiffness
k_{spring}	Spring stiffness

L	Total length of the deck
M	Moment
m	Slope in an S-N curve
M_x	Moment around x-axis
m_y	Local bending moment over the welds
$M_{norm,k}$	Normalized moment
$M_{y,Ed}$	Applied bending moment in y-direction
$M_{z,Ed}$	Applied bending moment in z-direction
N_i	Number of cycles that a bridge can carry
n_i	Distance from weld to corrugation inclination
n_i	Number of cycles on a bridge
n_x	Normal stress in x-direction
n_y	Normal stress in y-direction
N_{Ed}	Applied axial force
N_{OBS}	Number of cycles in Fatigue Limit State
$nCells$	Number of cells in a cross section configuration
P	Force
P	Prestressing force in Load combination
p	Length of half a cell
P_x	Force in x-direction
P_y	Force in y-direction
P_z	Force in z-direction
P_{cr}	Critical buckling load
$P_{norm,k}$	Normalized force
q	Patch load
$q_{coating}$	Load from surface coating
Q_{ik}	Tandem load
q_{ik}	Distributed load
$Q_{k,i}$	Variable load in Load combination
R_1	Radius bottom side of the corrugation
R_2	Radius top side of the corrugation
s	Plate width
t	Plate thickness
t	Thickness of an unstiffened plate
t_1	Thickness of the bottom plate
t_2	Thickness of the top plate
t_c	Thickness of the core material
t_e	Thickness of the edge beams
t_w	Weld width
W	Sectional modulus
W_{eff}	Effective sectional modulus

1
Introduction

1.1 Background

Bridges play a large role in society and the design of bridges is an important topic. Due to the environmental changes, a large focus lies on finding solutions that use low amounts of resources and are material efficient (Trafikverket, 2019). It has been shown that a bridge deck solution using a Corrugated Core Steel Sandwich Panel (CCSSP) is promising with regard to its high stiffness to mass ratio, since this leads to high material efficiency (Nilsson, 2017, p.2). A steel sandwich bridge deck generally involves high expenses and a lot of assessment and has previously only been used in bridges when light weight is crucial (Bright & Smith, 2007, Abstract). However, research has shown that they can be prefabricated and also result in a less complex structure (Nilsson, 2017, p.2-3). According to Beneus and Koc (2014, p.52), the steel sandwich deck is well suited as a bridge deck in situations where a low structural weight is of high importance, such as in movable bridges.

A CCSSP consists of two steel plates, with a corrugated core in between (Nilsson, 2015, p.4). The purpose of the core material is to carry shear force and the face plates are intended to carry the bending moment (Frank, 2014, p.11). The CCSSPs have a few important properties that are favourable. Thanks to laser welding performed by robotics, the risk of geometrical imperfections decreases and thereby the risk of fatigue damage is decreased (Roland & Metschkow, 1997, p.183). Geometrical imperfections in the welds is a problem when using other conventional welding methods. There are also a few important structural advantages with CCSSPs. The bending stiffness in the longitudinal (along the corrugation) and the transverse (orthogonal to the corrugation) direction is increased compared to conventional orthotropic steel decks. Another advantage of a CCSSP is the possibility to utilize the deck as a flange, which increases the efficiency of the deck. This is due to a decreased shear-lag effect (Nilsson, 2017, p.3).

In order to enable structural design and optimization of bridges using a CCSSP solution, it must be possible to correctly model the panels complete behaviour in a reasonable time frame. This can be done with a 3D solid or 3D shell model. However, these types of models require vast amount of computational power. Something that has previously made it difficult to make practical use of analysis of CCSSPs. New research by Nilsson, Atashipour, and Al-Emrani (2019) has shown that a deformation driven sub-modelling technique, an Equivalent Single Layer (ESL) together

with 3D shell element models, can be used to accurately model the behaviour of CCSSPs used as bridge decks. This type of analysis requires far less computational effort than the alternative of a full 3D analysis.

Finding new effective solutions for bridge decks are of high interest. Today, most bridge decks are made of concrete which emits a lot of CO_2 and due to this a large environmental impact (Nilsson, 2017, p.1-2). Concrete is also a high density material which increases the weight on the substructure. A CCSSP could be a competitive solution, but to enable this there is need for further research in terms of parametric design and in the end an optimization of a CCSSP (Nilsson, Atashipour, & Al-Emrani, 2019, p.22). Meanwhile, there is an interest expressed from the industry to investigate if CCSSPs could be competitive to use as bridge decks, compared to other alternatives on the market. A design program could be used to investigate possible dimensions which in turn could be used to compare CCSSPs to other alternatives on the market. Such a model would require accurate controls of the panel in Ultimate Limit State (ULS), Serviceability Limit State (SLS) and Fatigue Limit State (FLS). The tandem loads on a CCSSP bridge deck cause a biaxial stress state. There are uncertainties regarding how to correctly perform capacity checks of this phenomena and this is yet to be investigated.

1.2 Aim and objectives

The aim of this thesis is to investigate how different cross section parameters influence the behaviour of a Corrugated Core Steel Sandwich Panel (CCSSP) used as a simply supported bridge deck for short-span bridges and the feasibility of these panels with this purpose.

In order to fulfil the aim of the thesis, the following objectives have been specified:

- Verify the use of the Reduced Stress Method to evaluate biaxial compression in the CCSSP bridge deck
- Find a suitable way to verify the fatigue life of a CCSSP bridge deck
- Create a design program for a CCSSP bridge deck using the software BRIGADE/-Plus with Python scripting
- Perform a parametric study to investigate how certain cross section parameters influence the response of a CCSSP bridge deck

1.3 Limitations

The thesis is limited to simply supported Laser welded Corrugated Core Steel Sandwich Panels. The number of lanes are limited to two and the bridge length is limited to 10 meters with a span of 9.6 meters between supports. The design program is based on linear elastic analysis. The loads applied on the bridge are limited to the following:

- Self-weight
- Pavement

- Traffic loads according to Eurocode's Load Model 1 (LM1)
- Traffic load for fatigue life evaluation according to Eurocode's Fatigue Load Model 4 (FLM4)

The capacity checks are performed according to Eurocode by calculating the Utilization Ratio (UR) of the CCSSP in the following areas:

- Ultimate Limit State (ULS)
- Serviceability Limit State (SLS)
- Fatigue Limit State (FLS)

The parametric study is limited to the influence of some cross section parameters on the UR of the CCSSP bridge deck in SLS and ULS as well as the fatigue damage of the welds in FLS.

1.4 Methodology

A literature study is performed to gain knowledge about the production, behaviour and the modelling techniques of CCSSPs. This is followed by producing a design program using Python scripting and the software BRIGADE/Plus with the purpose of performing a parametric study on certain cross section parameters.

The areas of study covered in the literature study are; what the properties of a CCSSP are, how CCSSPs are produced, how CCSSPs respond to different loads, what the critical issues are with regard to the design of CCSSPs, how CCSSPs can be modelled using numerical analysis, how to perform controls according to Eurocode and how to design a parametric study.

To create a design program two different important areas are investigated; how to evaluate biaxial compression- and how to evaluate the fatigue damage of a CCSSP bridge deck. This is done using one cross section configuration and performing investigations. Results, discussion and conclusions are drawn continuously within each chapter. These conclusions are used when building the design program. The design program is tested on one specific cross section configuration. Conclusions are drawn from this case and are the basis of a parametric study.

The parametric study uses the experimental design methodology Fractional Factorial Design with resolution IV. The purpose of the parametric study is to gain knowledge about the influence of different cross section parameters on the URs of a CCSSP.

1.5 Overview

The report is divided into 9 chapters.

In Chapter 1, the topic is introduced and a background is given presenting the purpose of the thesis and how the project is carried out.

In Chapter 2, the theory for the project is presented. This involves information regarding the production, behaviour and the modelling techniques of CCSSPs as well as Eurocode regulations on loads and controls relevant for CCSSPs.

In Chapter 3, the modelling conditions used in the thesis are described. These are the properties of the model used throughout the thesis.

In Chapter 4, a study of the Reduced Stress Method (RSM) is presented. This done using the model described in Chapter 3 with a specific cross section of the CCSSP. The aim of this investigation is to gain information of how the RSM can be applied for a CCSSP.

In Chapter 5, a study of the evaluation in the Fatigue Limit State is presented. This done using the model described in Chapter 3 and the same cross section as in Chapter 4. The aim of this investigation is to find a suitable way to verity the CCSSP in FLS.

In Chapter 6, the created design program is presented. This done using the model described in Chapter 3 and the same cross section as in Chapter 4 and 5. The aim of this investigation is to test the design program on one cross section configuration.

In Chapter 7, the design program from Chapter 6 is used to perform a parametric study to investigate the impact of certain cross-section parameters on the URs of a CCSSP. The parametric study is divided into two parts. Part one is a Fractional Factorial Design and part two is an investigation regarding the influence of the weld width on the fatigue relevant stresses in the CCSSP.

In Chapter 8, a general discussion regarding the thesis is presented.

In Chapter 9, the final conclusions and future studies are presented.

2
Theory

2.1 Bridge decks

A bridge deck has two main purposes; to establish the roadway, enabling traffic to pass and to transfer all the loads to the supporting elements (Chen & Duan, 2014, p.352). The most commonly used construction materials for bridge decks are concrete, steel and timber, where concrete is the most common among them. Steel is a material well suited for bridge decks due to its high strength in relation to its weight (Chen & Duan, 2014, p.305). Timber is the oldest construction material used in bridges and its use is increasing (Chen & Duan, 2014, p.341). The advantage of using timber is that it emits the lowest amount of CO_2 out of the three materials mentioned above. Each material is utilized in different ways and solutions with a combination of the materials are also common. When choosing a solution and a material, important aspects to consider are the financial and environmental impacts.

2.1.1 Concrete bridge decks

A bridge deck in concrete is the most commonly used solution (Chen & Duan, 2014, p.271). Such a bridge deck can be either prefabricated or cast-in-situ. The advantages which have made concrete so widely used are mainly the ease of production and wide availability (Peck, 2006, p.9). On the other hand does the manufacturing of concrete, mainly the production of cement, emits high amounts of CO_2 (Peck, 2006, p.10). The most common solution when it comes to concrete bridge decks are simply supported or continuous, reinforced concrete decks. Concrete can be prestressed which increases the concrete's flexural performance, however using this method results in a more complex production.

2.1.2 Steel bridge decks

Another common bridge deck solution is orthotropic steel deck. Following World War II, over 40 bridges with different configurations of orthotropic steel decks have been built in Germany, Yoguslavia and Canada (Wolchuck, 1963, p.3). According to Wolchuck (1963, p.1), there are two main reasons for using steel decks in bridge construction: they are material efficient and light-weight structures.

The most common design of an orthotropic steel bridge deck is known as a stiffened plate and consists of a top plate with longitudinal and transverse stiffeners welded below it (Wolchuck, 1963, p.1-2). This type of design has a large orthotropy which

raises the stress levels in sensitive areas and results in several fatigue issues (Nilsson, 2015, p.1). In order to make most use of the material, the use of plate action in steel decks is a promising solution (Wolchuck, 1963, p.3). Steel Sandwich Panels (SSPs) have shown great potential (Nilsson, 2015, p.3-4). These plates are less orthotropic than the stiffened plates and plate action can be utilized, as illustrated in Figure 2.1.

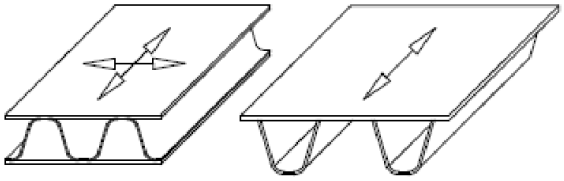

Figure 2.1: *Illustration of the actions of a sandwich panel (left) and a stiffened plate (right) (Nilsson, 2017, p.4)*

The SSPs can be designed in many different ways, using varying core configurations, with different stiffness properties as a result (Alwan & Järve, 2005, p.20). Alwan and Järve (2005, p.55) concluded that a sandwich panel using a corrugated core performs better than other studied configurations.

2.1.3 Timber bridge decks

Bridge decks can also be built in timber, although mostly for shorter spans (Pousette et al., 2017, p.10). Composite timber elements is a common design choice for timber bridge decks (Swedish Wood, 2016, p.293). In Sweden, the most common timber bridge deck design is a stress laminated timber bridge deck (Pousette et al., 2017, p.10). Stress laminated timber bridge decks consist of timber laminates (Pousette et al., 2017, p.10). They are held together by prestressing rods made of steel, which introduces friction force between the laminates and thereby plate action is achieved. It is also common for timber bridges to include other materials such as concrete (Pousette et al., 2017, p.10).

One of the most critical aspects of using timber in bridges or other outdoor structures is its sensitivity to moisture. Due to this, bridge decks made of timber must be well protected and maintained during its lifetime which affects both the design and total cost (Pousette et al., 2017, p.11-12).

2.2 Attributes of a Steel Sandwich Panel

Sandwich panels consist of two face plates surrounding some type of core. The face plates carry bending (Davies, 1993, p.179-181). The core carries shear and stiffens the face plates which leads to reduced risk for local buckling (Davies, 1993, p.180).

Thanks to the sandwich effect, the bending stiffness of a SSP is greatly increased compared to a conventional bridge deck (Nilsson, 2015, p.3). This is done by separating the face plates from each other by the core (Nilsson, 2015, p.3), which means that a higher core results in a higher bending stiffness. The core's ability to resist shear strains also increases the stiffness of the plate (Nilsson, 2015, p.3).

One of the positive aspects of the sandwich element is that it is possible to use a lightweight core in order to retrieve a high stiffness-to-weight ratio (Nilsson, 2015, p.4). This is thanks to the geometry of the core. However, the core is relatively flexible in shear in the weak direction which weakens the global behaviour of the plate (Davies, 1993, p.181).

A prominent aspect of SSPs is the reduced shear lag effect (Nilsson, 2015, p.37). Shear lag is an effect of varying membrane and in-plane shear stiffness when a structure is subjected to tensile stresses (Giroux & Easterling, 1993, p.77). The stress is higher at the areas connected to other members as these are stiffer. SSPs have a high in-plane shear stiffness which results in a less pronounced shear lag effect and compared to the conventional solution SSP provide a more effective beam (Nilsson, 2015, p.21). In turn, this means that very high stress peaks in the face plates can be avoided.

The Mindlin-Reissner plate theory is most appropriate for analysing sandwich plate because it allows for the cross section to rotate with respect to the centre line. This means that it accounts for the rotations due to shear which occur in sandwich plate (Persson, 2016, p.6).

Many different SSP configurations have been discussed in literature (e.g. by Romanoff and Varsta (2006)). Some of the most common configurations can be seen in Figure 2.2. The choice of core affects the stiffness properties of a sandwich plate (mainly the shear stiffness) and also the mass per square meter bridge deck.

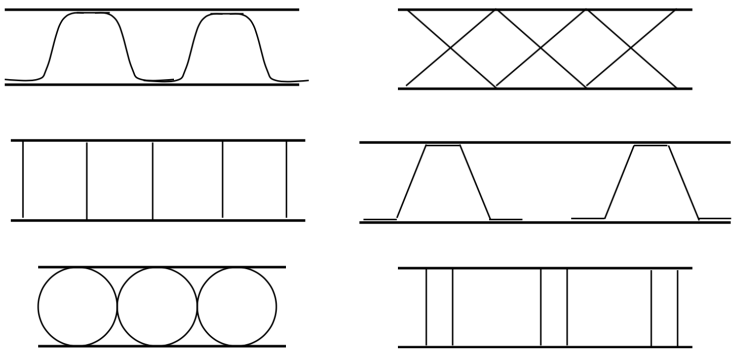

Figure 2.2: *Common configurations of cores in steel SSPs (created by authors, inspired by Romanoff and Varsta (2006))*

2.3 Attributes of Corrugated Core Steel Sandwich Panels

A Corrugated Core Steel Sandwich Panel (CCSSP) is a type of SSP with two face plates divided by a core of a corrugated steel plate, as seen in Figure 2.3. The panel can be produced by robotic welding (Nilsson, 2017, p.2). The different parts are welded together using a one sided welding technique forming a sandwich element (Nilsson, 2015, p.5). The solution sets very high demands on the welds in the structure, as for most configurations of steel bridge decks. A CCSSP has the general attributes of a SSP with some improvements thanks to the geometry of the core.

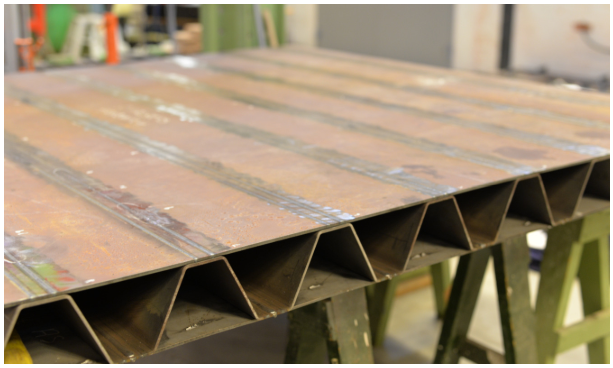

Figure 2.3: *Corrugated Core Steel Sandwich Panel (CCSSP) with double welds (Nilsson, 2017, p.4)*

Due to the angling of the corrugation of the core, the CCSSP has an increased transverse shear stiffness in the weak direction and the orthotropy of the sandwich panel is decreased compared to other configurations (Nilsson, 2015, p.17). Another attribute of a CCSSP is that it is two-way load carrying which increases the bending stiffness. In Figure 2.4 an illustration of the CCSSPs cross section parameters per cell is presented.

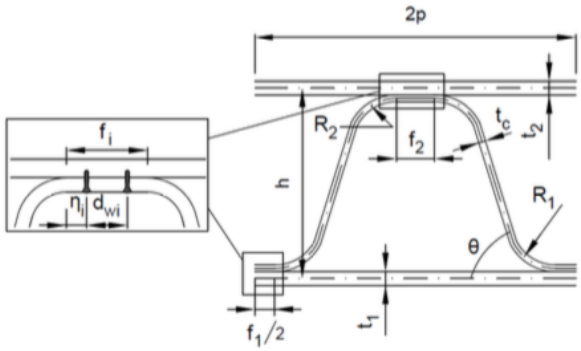

Figure 2.4: *Illustration of one cell in a CCSSP and its parameters (Nilsson, 2017, p.10)*

When comparing a CCSSP to the X-core or O-core configurations, it has been proven that the corrugated core configuration has a higher stiffness to weight ratio (Nilsson, 2015, p.16-17). The corrugated core also has a better production potential than for example the truss core or the sinusoidal core thanks to the width of the horizontal part of the core connecting to the face plates which makes the welding easier (Nilsson, 2015, p.17). Nilsson (2017, p.3) also concluded three main advantages of using a CCSSP as a bridge deck in an open cross section: increased bending stiffness both longitudinally and transversely of the deck as well as for the global structure due to decreased shear lag.

2.4 Welding of CCSSPs

CCSSPs can be designed with connections of either one or two weld lines per connection between the face plates and the core. In studies by Persson (2016) and Nilsson, Atashipour, and Al-Emrani (2019), it is concluded that using two weld lines both reduces the effective notch stress in the weld and increases the transverse shear stiffness of the cross section. The studies also conclude that using two weld lines will prolong the fatigue life of the plate.

The CCSSP solution is difficult to weld with ordinary techniques since it must be welded from one side (Nilsson, 2015, p.5). The use of laser welding techniques is an effective solution since it allows for the welding to be performed from one side. When using this technique, the welding is performed by robotics and the welds are therefore easy to monitor. A laser weld becomes reliable due to the fact that the core and the face plates form a metallic bond through the welded plates (Caccese & Yorulmaz, 2009, p.4). There are two different laser welding techniques suitable for a CCSSP: Laser welding and Hybrid Laser-Arc Welding (HLAW) (Nilsson, 2017, p.2).

2.4.1 Laser welding

The laser welding technique, is a high energy density process and it is shown to be up to ten times faster than ordinary welding (Caccese & Yorulmaz, 2009, p.2). Because the welding is performed by robotics, the geometrical imperfections decrease. As a result, a highly reliable weld with low distortion and low residual stresses is retrieved. However, the laser welding technique is expensive since it requires a lot of equipment (Wouters, 2005, p.3).

2.4.2 Hybrid laser-arc welding

HLAW is a technique which combines laser welding with arc welding. As a result, HLAW has the advantages of both methods (Wouters, 2005, p.5). HLAW results in a weld with high accuracy, good gap bridging and a good control over the geometry of the weld. It can also be done with a higher speed than ordinary laser welding (Wouters, 2005, p.5). Drawbacks of the technique is that there is a lack of guidelines for design of welds using HLAW (Wouters, 2005, p.10).

2.5 Fatigue problems in a CCSSP

Fatigue is a failure mechanism driven by cyclic loading and the critical fatigue load may be much below the maximum yield strength of the material. Causing fatigue damage is a process that requires time and repeated loading (Al-Emrani & Åkesson, 2013, p.152). The cyclic loading leads to the initiation of micro cracks in the material. These propagate with each loading cycle until a brittle failure occurs.

The prevention of fatigue related problems are of high importance for a laser welded steel deck (Caccese & Yorulmaz, 2009, p.1). The driving process for fatigue failure in a CCSSP bridge deck are the locally concentrated forces from the tandem loads (Nilsson, Atashipour, & Al-Emrani, 2019, p.3).

In a study by Nilsson (2017) critical positions were investigated for a CCSSP with respect to fatigue damage due to tensile axial stress. These are illustrated in Figure 2.5. The aim of the study was to investigate the impact of geometrical imperfections from the welding process on fatigue relevant stresses in these positions. In another study by Nilsson, Atashipour, and Al-Emrani (2019) critical cracking modes were investigated. The study found the critical cracking modes to be weld cracking and another crack mode that propagated through the face plate. These are both illustrated in Figure 2.6. The tests gave the critical stress of 70 MPa for the weld crack and 77 MPa for the other crack. When comparing test results from the weld crack with tests made by Fricke, Robert, Peters, and Sumpf (2016), Nilsson (2017) also concluded that an SN-curve of $\Delta\sigma_C = 57$ MPa with a constant slope of m=3 corresponds well to both tests.

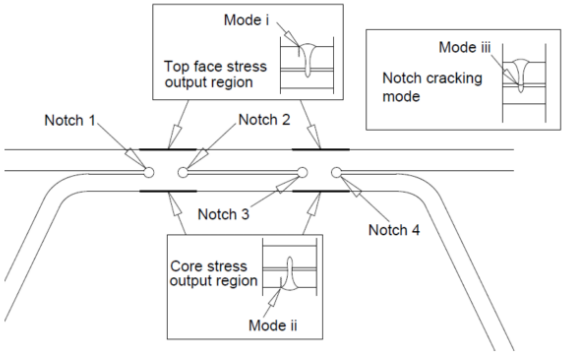

Figure 2.5: *Illustration of the critical positions related to fatigue included in the study by Nilsson (2017) (Nilsson, 2017, p.21)*

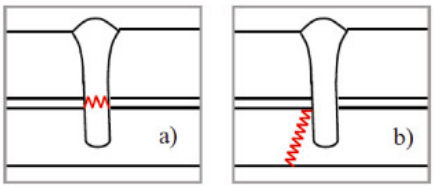

Figure 2.6: *Illustration of the critical positions related to fatigue cracking in a CCSSP (Nilsson, Atashipour, & Al-Emrani, 2019, p.3)*

2.6 Buckling

A CCSSP used as a bridge deck is subjected to loads that induce normal stresses which can cause buckling of the face plates. This can occur in different ways: Column-like buckling, plate-like buckling or a combination of both (Al-Emrani & Åkesson, 2013, p.116). Depending on the current situation, the reduction factor is affected. This is illustrated in Figure 2.7.

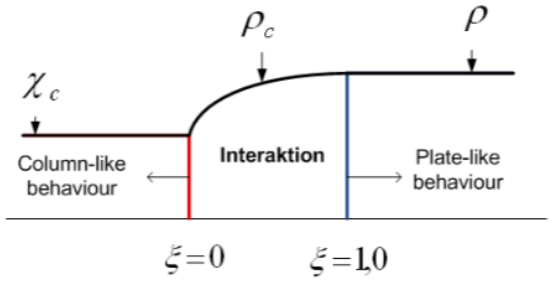

Figure 2.7: *Illustration of the interaction factor used for buckling behaviour of steel plates (Al-Emrani & Åkesson, 2013, p.116)*

2.6.1 Column-like buckling

A thin-walled plate which is supported only on two opposite edges can be described to buckle as a column, known as column-like buckling (Al-Emrani & Åkesson, 2013, p.56). This behaviour is illustrated in Figure 2.8. This can also occur in plates with a high height-to-width ratio, known as the slenderness ratio. The slenderness ratio is determined as the ratio between loaded width and thickness of the plate. In the case of column-like buckling of a plate, the critical buckling stress, σ_{cr}, is dependant on the length of the plate (see a in Figure 2.8). This is described in Equation 2.1. When column-like buckling occurs, the entire strength of the plate is utilized and it can not carry any more load.

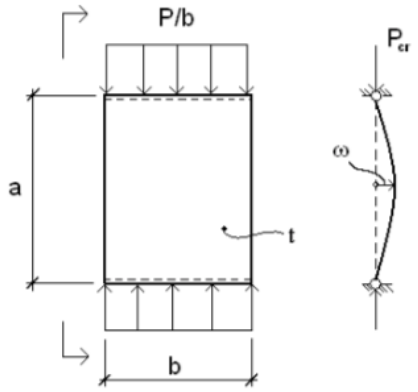

Figure 2.8: *Illustration of column-like buckling of an unstiffened plate (Al-Emrani & Åkesson, 2013, p.56)*

$$\sigma_{cr} = \frac{\pi^2 E}{12(1-\nu^2)(a/t)^2} \tag{2.1}$$

2.6.2 Plate-like buckling

Plate-like buckling occurs when a plate is supported on all four edges and happens suddenly out-of-plane (Al-Emrani & Åkesson, 2013, p.68) which is similar to column-like buckling. However, when plate-like buckling occurs, a stress field is created in the plate, as seen in Figure 2.9. In this case, the critical buckling stress, σ_{cr}, is dependant on the width of the plate rather than the length of the plate. This is described in Equation 2.2 where k is dependant on the support conditions. This plate-like behaviour means that the plate gets a post-critical strength reserve and the ultimate load is therefore larger than the elastic critical load (Zizza, 2016, p.5).

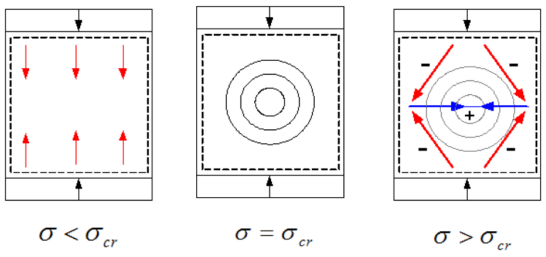

Figure 2.9: *Illustration of plate-like buckling of an unstiffened plate (Al-Emrani & Åkesson, 2013, p.67)*

$$\sigma_{cr} = k\frac{\pi^2 E}{12(1-\nu^2)(b/t)^2} \tag{2.2}$$

2.6.3 Buckling induced by biaxial stresses

Biaxial stresses is a common stress state for steel bridge decks and can cause local instability issues (Ndogmo, Mensinger, & Both, 2016, p.272). Research has also shown that it is common for orthotropic panels in ships and airplanes to experience biaxial membrane stresses (Araghi & Shanmugam, 2012, p.40). For a CCSSP, this can occur in the top plate field between welds under the tandem loads. In this position the combination of global bending effects and local effects from the tandems cause a biaxial stress state. This is illustrated in Figure 2.10.

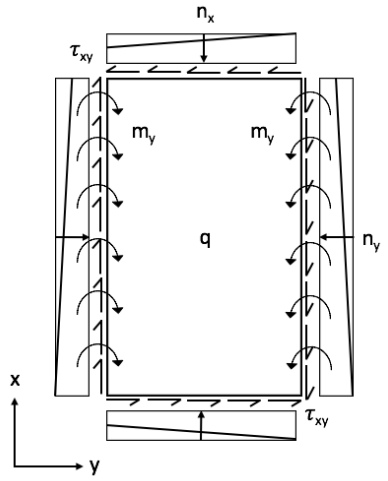

Figure 2.10: *Illustration of the biaxial stress state in the top plate of the CCSSP under patch loading (created by authors)*

2.7 Modelling of CCSSPs

Several modelling techniques are available for Finite Element (FE) analysis of a CCSSP. One of the determining factors when it comes to the choice of modelling technique is the time required to complete the analysis. If the run time becomes too long when using 3D solids or shells, an alternative sub-modelling approach can be used (Nilsson, Atashipour, & Al-Emrani, 2019, p.4).

2.7.1 3D solid model

FE-modelling using 3D solid elements is a versatile way to model problems in FE as it includes the material parameters in all directions. The response of a 3D solid element is described in the normal stresses and shear stresses in all three directions of space (Liu & Quek, 2014, p.249). However, when using solid elements the computational time becomes long and the meshing complex (Liu & Quek, 2014, p.250). Liu and Quek (2014, p.250) describes that a simplified modelling approach such as a beam or shell element should always be chosen when the results of those models are within an acceptable level. For CCSSPs which consist of thin steel plates in interaction, 3D solid elements are useful when modelling smaller details of the panel, such as the weld region (Persson, 2016, p.17).

2.7.2 3D shell model

The 3D shell element is commonly used when modelling elements with a very thin thickness, such as plates, compared to its other dimensions. Shell models are sometimes called membrane-bending elements as it better describes their response. Shell elements deal with membrane forces for in-plane load and bending and shear forces for out-of-plane load (Blaauwendraad, 2010, p.190). Shell models are more computationally efficient than solid elements (Liu & Quek, 2014, p.250). However, these models assume plane stress in the plane of the shell and will not capture the stress variation across the thickness of the elements (Difs & Ro, 2017, p.15).

In a 3D shell model, the elements can be modelled as triangular or quadrilateral and use either linear or second order shape functions (Liu & Quek, 2014, p.220-224). These are known as isoparametric elements. For a 3D shell element there are five Degrees of Freedom (DOFs) per node. Two in-plane displacement DOFs per node and three out-of-plane DOFs per node where two are rotational and one is an out-of-plane displacement DOF.

2.7.3 Sub-modelling technique

A subject of research regarding the CCSSPs is strategies to model these efficiently. A CCSSP consists of many structural details affecting the general behaviour which are of high importance to take into account in an FE-model. In Nilsson, Atashipour, and Al-Emrani (2019) a strategy is presented on how to model the CCSSPs using a deformation driven sub-modelling approach in order to save a lot of computational power. This includes three steps where each model uses the results from the previous model as input. The sub-models presented by Nilsson, Atashipour, and Al-Emrani (2019) are:

Homogenized Equivalent Single Layer-model
The first model in the sub-modelling technique is a homogenized Equivalent Single Layer (ESL) model. An ESL model uses homogenized equivalent stiffness parameters to model the CCSSP as a single layer orthotropic plate. This makes it possible to make a global model describing the hole system using a relatively coarse mesh that can be run in a reasonable time frame. This model is used to retrieve the global deformations in terms of the mid-line deflection. This is applied as boundary conditions on the next, smaller but more detailed, model. It is not possible to generate detailed results in the weld regions when using this modelling type.

Large sub-model with 3D shells
The second model in the sequence is a large 3D shell model where the cross section is modelled by 2D shell elements. This model uses a finer mesh compared to the previous step. Plane strain steel material parameters are used for all elements. The weld lines must be modelled by springs in order to get a realistic approximation of their behaviour. The requested outputs in this step are the deformations of the studied part which are applied as boundary conditions in the final step.

Small sub-model with 3D shells
The third model is similar to the previous one but in a smaller scale using an even finer mesh. It is also a 3D shell model which uses 2D planar elements to model the local behaviour of the entire cross section. From this model the detailed local stress distribution is studied.

2.7.4 Modelling of welds

The welds in a CCSSP can not be considered stiff. The real stiffness conditions for the weld region is somewhere between a rigid and a hinged connection (Nilsson, 2017, p.15). This is because during the welding process, a gap may form between the core and face plate, allowing for rotations in the weld region (Nilsson, Al-Emrani, & Atashipour, 2017a, p.2). However, contact between the core and the face plate increases the rigidity of the weld region. Nilsson et al. (2017a) have found a solution where the welds are modelled using springs. This modelling technique does not account for contact between the core and face plate. The technique uses three springs in x-, y- and z-direction and two rotational springs. Each weld node-pair has one connector from each plate with a small spring connecting them, as illustrated in Figure 2.11. This configuration is done in all nodes along each weld line.

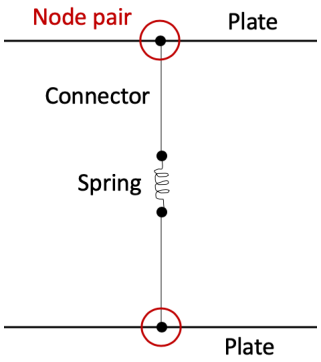

Figure 2.11: *Configuration of the weld modelling technique presented by Nilsson, Al-Emrani, and Atashipour (2017a) (created by author)*

Nilsson, Al-Emrani, and Atashipour (2017b, p.1814) conclude that by considering contact between the core and the face plate in the weld region of the CCSSP, the fatigue relevant stresses from locally applied loads are decreased by up to around 75% for local load in the plate field adjacent to the weld, if global action is restrained.

2.8 Stiffness parameters of CCSSPs

In order to correctly model CCSSPs, it is important to capture the stiffness of the different components of the panel. The different modelling approaches require stiffness properties that correspond well to the actual behaviour. In the following sections these are presented for a 3D solid model, a 3D shell model, an ESL-model and for the springs in the weld region of a CCSSP.

2.8.1 Stiffness parameters of a 3D solid and shell model

The 3D solid and 3D shell models consider the true stiffness parameters of the material. The stiffness parameters for steel with this modelling type are given in Eurocode 1993-1-1 (2005, p.28) as:

$E = 210$ MPa
$G = \frac{E}{2(1+\nu)} = 81$ MPa
$\nu = 0.3$

2.8.2 Homogenized stiffness parameters of the Equivalent Single Layer-model

In the sub-modelling method suggested by Nilsson, Atashipour, and Al-Emrani (2019), the ESL-model uses homogenized stiffness parameters presented by Libove and Hubka (1951). Because CCSSPs have an orthotropic behaviour, the stiffness properties are highly dependant on the direction of loading. In 1951, Libove and Hubka formulated equations describing these. In Figure 2.12 the directions of the equivalent stiffness parameters are illustrated and summarized in the list below.

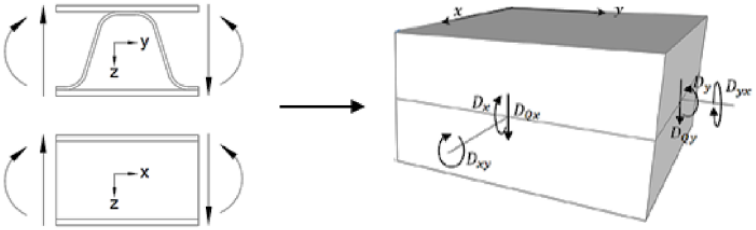

Figure 2.12: *Equivalent stiffness parameters of an ESL-model of a CCSSP (Nilsson, 2020, p.28)*

- D_x = Bending stiffness in the longitudinal direction in the model
- D_y = Bending stiffness in the the transverse direction in the model
- D_{xy} = Twisting stiffness in the xy-plane in the model
- D_{Qx} = Transverse shear stiffness in plane parallel to the corrugation axis in the model
- D_{Qy} = Transverse shear stiffness in the longitudinal direction in the model
- ν_x = Poisson's ratio in x-direction in the model
- ν_y = Poisson's ratio in y-direction in the model

The behaviour of the weld connections in a CCSSP highly affects the transverse shear stiffness of the panel, perpendicular to the core. In Libove and Hubka (1951, p.54) one weld is modelled as a rigid connection between the face sheets and the core. However, Nilsson (2017) presents a new method which better corresponds to the real behaviour of the core-to-weld interaction by using spring stiffnesses to calculate the contribution of the weld region to the homogenized stiffness of the CCSSP. This method is more suitable when two welds are used.

2.8.3 Rotational spring stiffness of the welds

The rotational spring stiffness (k_φ [kNm/rad]) of the springs used when modelling the welds in a CCSSP is calculated with an approximate closed form solution presented by Nilsson et al. (2017a, p.6-7) using Equation 2.3.

$$k_\varphi = \Lambda_g(\bar{h_g})\Lambda(\bar{t_1}, \bar{t_2})t_w^2 \tag{2.3}$$

Where $\Lambda_g(\bar{h_g})$ is calculated using Equation 2.4.

$$\Lambda_g(\bar{h_g}) = \alpha_1 + \alpha_2\bar{h_g} + \alpha_3\bar{h_g}^2 \tag{2.4}$$

And $\Lambda(\bar{t_1}, \bar{t_2})$ is calculated with Equation 2.5.

$$\Lambda(\bar{t_1}, \bar{t_2}) = (1 + \alpha_4 \cdot e^{-(\alpha_5\bar{t_1} - \alpha_6)})(1 + \alpha_4 \cdot e^{-(\alpha_5\bar{t_2} - \alpha_6)}) \tag{2.5}$$

With $\alpha_{1..5}$ according to Table 2.1.

Table 2.1: *Constant coefficients used to calculate the spring stiffness of a CCSSP weld region (Nilsson, Al-Emrani, & Atashipour, 2017a, p.6-7)*

α_1 [-]	α_2 [-]	α_3 [-]	α_4 [-]	α_5 [-]	α_6 [-]
22.86	-10.15	3.503	0.7768	2.392	0.4050

2.9 Loads

Eurocode 1991-2 (2003) describes four load models for ULS and SLS design and five load models for fatigue design which all apply to bridge design. Load Models 1 to 4 are traffic loads which determine ULS and SLS conditions. Fatigue Load Models 1 to 5 are used to determine the fatigue life of bridges. As this thesis is limited to Load Model 1 (LM1) and Fatigue Load Model 4 (FLM4), these are the only ones presented in this section.

2.9.1 Load Model 1

LM1 is presented in Eurocode 1991-2 (2003, p.35-38) and is a model that takes car and truck traffic into consideration. This is done by using both evenly distributed loads and tandem loads placed in the most unfavourable position on the bridge. The runway is divided into lanes (seen in Figure 2.13) and then the worst position of the

loads are determined. The load amplitudes are presented in Table 2.2. The reduction factors α_{Qi} and α_{qi} are decided based on expected traffic and road conditions. They are set to $\alpha_{Qi} = 0.9$ and in lane 1 $\alpha_{qi} = 0.8$ according to Transportstyrelsen (2018, p.36).

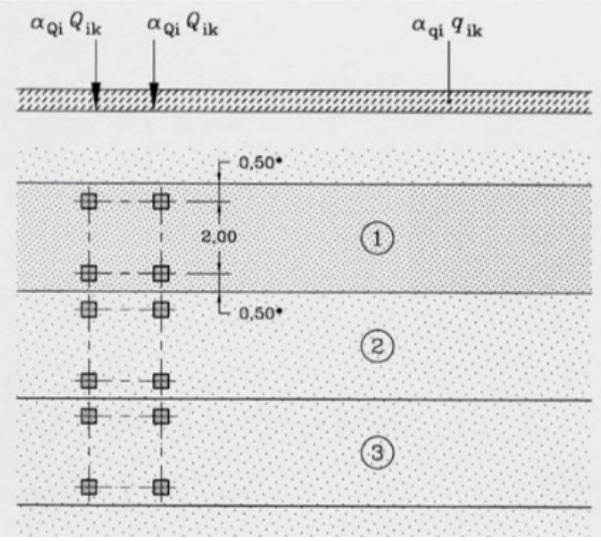

Figure 2.13: *Lane division in LM1 according to Eurocode 1991-2 (2003, p.37)*

Table 2.2: *Load magnitudes in LM1 according to Eurocode 1991-2 (2003, p.37)*

	Tandem load, Q_{ik} [kN]	Distributed load, q_{ik} [kN/m^2]
Lane 1	300	9
Lane 2	200	2.5
Lane 3	100	2.5
Remaining area	0	2.5

2.9.2 Fatigue Load Model 4

FLM4 is presented in Eurocode 1991-2 (2003, p.50-52). The model is meant to represent real traffic on road bridges and includes five lorry types, seen in Figure 2.14, with different combinations of three different kinds of wheel axles, seen in Figure 2.15. When each lorry passes the bridge it is the only vehicle on the bridge at that time (Eurocode 1991-2, 2003, p.52).

VEHICLE TYPE			TRAFFIC TYPE			
1	2	3	4	5	6	7
			Long distance	Medium distance	Local traffic	
LORRY	Axle spacing (m)	Equivalent axle loads (kN)	Lorry percentage	Lorry percentage	Lorry percentage	Wheel type
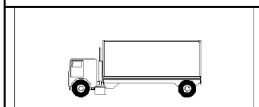	4,5	70 130	20,0	40,0	80,0	A B
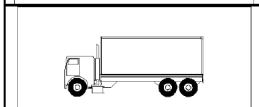	4,20 1,30	70 120 120	5,0	10,0	5,0	A B B
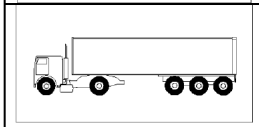	3,20 5,20 1,30 1,30	70 150 90 90 90	50,0	30,0	5,0	A B C C C
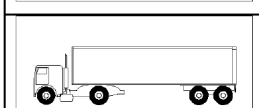	3,40 6,00 1,80	70 140 90 90	15,0	15,0	5,0	A B B B
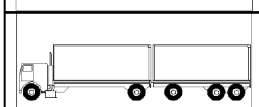	4,80 3,60 4,40 1,30	70 130 90 80 80	10,0	5,0	5,0	A B C C C

Figure 2.14: *Lorries included in FLM4 (Eurocode 1991-2, 2003, p.51)*

WHEEL/ AXLE TYPE	GEOMETRICAL DEFINITION
A	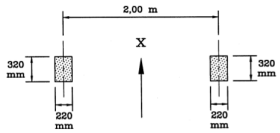
B	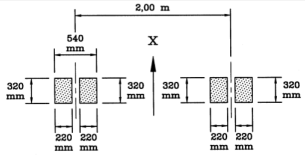
C	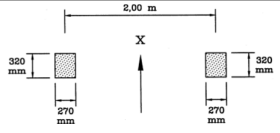

Figure 2.15: *Axles included in FLM4 (Eurocode 1991-2, 2003, p.52)*

When analysing global actions, the lorries in FLM4 are placed in lanes specified by Eurocode 1991-2 (2003). However, for analysis of local actions, the placement of the lanes where the lorries are applied is chosen for the specific case. In that case,

the transverse placement of the lorries is to be distributed according to Figure 2.16, based on the centre line of the chosen lane.

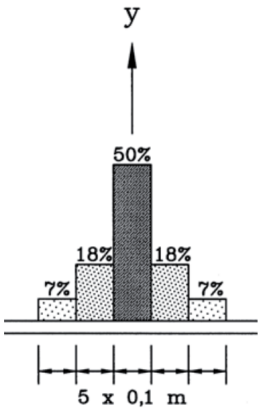

Figure 2.16: *Distribution of lorry placement in the transverse direction of the bridge lane, according to FLM4 (Eurocode 1991-2, 2003, p.47)*

The magnitude of each axle depends on the lorry type presented in Eurocode 1991-2 (2003). These can be seen in Table 2.3. The traffic type (long distance, medium distance or local traffic) decides the percentage of each lorry type which goes into the final load summation. Trafikverket (2016) recommends using regional traffic as the traffic type for bridges in Sweden.

Table 2.3: *Magnitude range of the axles in FLM4 (Eurocode 1991-2, 2003)*

Axle	Magnitudes [kN]
A	70
B	90 - 150
C	80 - 90

FLM4 includes a dynamic amplification factor, based on the distance, D, of the lorry to the expansion joint in the bridge (Eurocode 1991-2, 2003, p.47). This is given by Equation 2.6.

$$\Delta\phi_{fat} = 1.30\left(1 - \frac{D}{26}\right), \qquad \Delta\phi_{fat} \leq 1 \tag{2.6}$$

In FLM4, the number of cycles (N_{OBS}) of heavy traffic per year and lane depending on the road type is also specified (Eurocode 1991-2, 2003, p.46). This value is used to calculate the damage done to the bridge during its lifetime, according to Eurocode's Damage Accumulation Method (Eurocode 1993-1-9, 2005, p.10).

2.10 Load combinations

Eurocode 1990 (2002, p.42-44) specifies the load combinations used in bridge design, which are presented in Equations 2.7, 2.8 and 2.9. The Swedish National load factor γ_d has been added according to Transportstyrelsen (2018, tab 2.1) where Safety Class 2 is used for bridges with a span below 15m. The load combinations are applied to ULS (2.7 or 2.8) and SLS (2.9) (Transportstyrelsen, 2018, p.84). Equation 2.7 has the permanent load ($G_{k,j}$) as the main load and Equation 2.8 has the variable load ($Q_{k,1}$) as the main load. The load which is not the main load is reduced by a factor Ψ. The load P is the prestressing force for prestressed structures and the load $Q_{i,k}$ is the variable load in the lane which is not the main lane. Equation 2.9 is the frequent traffic load combination for SLS. The magnitudes of the reduction factors can be seen in Table 2.4.

$$\sum_{j>1} \gamma_d \gamma_{G,j} G_{k,j} + \gamma_d \gamma_P P + \gamma_d \gamma_{Q,1} \Psi_{1,1} Q_{k,1} + \sum_{i>1} \gamma_d \gamma_{Q,i} \Psi_{0,i} Q_{k,i} \tag{2.7}$$

$$\sum_{j>1} \xi_j \gamma_d \gamma_{G,j} G_{k,j} + \gamma_d \gamma_P P + \gamma_d \gamma_{Q,1} Q_{k,1} + \sum_{i>1} \gamma_d \gamma_{Q,i} \Psi_{0,i} Q_{k,i} \tag{2.8}$$

$$\sum_{j>1} G_{k,j} + P + \Psi_{1,1} Q_{k,1} + \sum_{i>1} \Psi_{2,i} Q_{k,i} \tag{2.9}$$

Table 2.4: *Safety factors for bridge load combinations*

Factor	Magnitude	Source
γ_d	0.91	Transportstyrelsen, 2018, §8
$\gamma_{G,j,sup}$	1.35	Eurocode 1990, 2002, tab. A2.4(B)
$\gamma_{G,j,inf}$	1.0	Eurocode 1990, 2002, tab. A2.4(B)
$\gamma_{Q,1}$	1.5	Transportstyrelsen, 2018, tab. 4.4
$\gamma_{Q,i}$	1.5	Transportstyrelsen, 2018, tab. 4.4
ξ_j	0.89	Transportstyrelsen, 2018, tab. 4.4
$\Psi_{0,i}$	0.75 or 0.40	Eurocode 1990, 2002, tab. A2.4(B)
$\Psi_{1,1}$	0.75 or 0.40	Eurocode 1990, 2002, tab. A2.4(B)
$\Psi_{2,i}$	0	Eurocode 1990, 2002, tab. A2.4(B)

2.11 Control of deflection in SLS

In SLS, the demands to fulfil for a steel bridge are related to the deflection. The maximum allowed deflection is chosen by the client with recommendations from Eurocode 1993-2 (2006, p.28). The deflection limit appropriate for a CCSSP-bridge deck is presented in Equation 2.10, where L is the bridge span.

$$\delta = \frac{L}{400} \tag{2.10}$$

2.12 Control of bending and shear in ULS

In ULS, the demands that must be fulfilled for a steel bridge are related to the stresses in the constituent parts. These are specified in Eurocode 1993-2 (2006, p.22) and are:

- Bending moment capacity in longitudinal and transverse direction (Equation 2.11)
- In plane shear capacity (Equation 2.12)

$$\frac{\sigma_{Ed}}{\sigma_{c,Rd}} \leq 1 \tag{2.11}$$

$$\frac{\tau_{Ed}}{\tau_{c,Rd}} \leq 1 \tag{2.12}$$

2.13 Control of buckling in ULS

There are some alternatives of methods to accurately perform controls related to biaxial bending of the plate. Eurocode 1993-1-5 (2006) states two different ways to perform the capacity check; The Effective Width Method and the Reduced Stress Method (RSM). An alternative approach presented here is a method stated by Det Norske Veritas (2002).

2.13.1 Effective Width Method

The Effective Width Method presented in Eurocode 1993-1-5 (2006, p.21) is a verification check considering both local buckling between stiffeners and global buckling of a slender plate. The capacity accounted for is reduced with the reduction factor ρ for plate buckling and χ_c for column buckling. In Equation 2.13, the interaction verification formula for a member subjected compression in one direction and bending around two axes is presented.

$$\eta_1 = \frac{N_{Ed}}{\frac{f_y A_{eff}}{\gamma_{M0}}} + \frac{M_{y,Ed} + N_{Ed} e_{y,N}}{\frac{f_y W_{y,eff}}{\gamma_{M0}}} + \frac{M_{z,Ed} + N_{Ed} e_{z,N}}{\frac{f_y W_{z,eff}}{\gamma_{M0}}} \leq 1.0 \tag{2.13}$$

The Effective Width Method that Eurocode 1993-1-5 (2006, p.21) suggests, considers stress redistribution between panels, which is one of its advantages. However, it does not include any rules regarding how to verify that the plate fulfills demands regarding multiaxial compression (Zizza, 2016, p.2).

2.13.2 Reduced Stress Method

The Reduced Stress Method (RSM) is presented in Eurocode 1993-1-5 (2006, p.40-42) and can be used to account for plate buckling due to biaxial stresses. This method accounts for normal stresses in two directions of the xz-plane and in-plane shear acting simultaneously. The principle of this method is that it assumes cross

section class 3 and allows for the use of the Von Mises yield criteria. The RSM assumes that the stress on the weakest member of the cross section determines the capacity of the entire cross section. This results in a more conservative assessment compared to the Effective Width Method (Mensinger et al., 2009, p.8). This is the biggest reason why it has not been used to a high extent in design in Sweden (Samvin & Skoglund, 2016, p.41).

The RSM is based on the criteria presented in Equation 2.14. If it is fulfilled then cross section class 3-parameters can be used in the capacity checks even if the cross section is in class 4. In turn, this means that the Von Mises stress criteria can be used to verify the capacity of the cross section, with the addition of the reduction factor ρ. This ρ can be decided in two ways, described in more detail below as alternatives I and II in Equations 2.25 and 2.26, respectively. These account for the interaction between shear force, bending moment, axial force and transverse load. The reduction factors in this verification use a special slenderness $\bar{\lambda}_p$, presented in Equation 2.20. The factors $\alpha_{ult,k}$ & α_{cr} account for the relationship between ultimate capacity and applied stress and critical buckling stress and applied stress, respectively. The factor γ_{M1} is equal to 1.1 (Eurocode 1993-2, 2006, p.19).

The rest of this section describes the principle of how the RSM is used and its constituent steps.

Basis of the Reduced Stress Method:
It is OK to assume CSC3 if

$$\frac{\rho\alpha_{ult,k}}{\gamma_{M1}} \geq 1 \tag{2.14}$$

Principle of the Reduced Stress Method according to Eurocode 1993-1-5 (2006, p.40-41):

1. Use load effect and buckling analysis to calculate α_{cr} & α_{ult}
2. Calculate the slenderness $\bar{\lambda}_p$
3. Use $\bar{\lambda}_p$ to calculate ρ_x, ρ_y & χ_w
4. Use the reduction factors to verify the capacity with respect to buckling

1. Calculate α_{cr} & α_{ult}

The factors $\alpha_{ult,k}$ & α_{cr} can be calculated using Equations 2.15 and 2.16. These are used to calculate the plate slenderness specific for the RSM.

Relationship between ultimate capacity and applied stress:

$$\frac{1}{\alpha_{ult,k}^2} = \left(\frac{\sigma_{x,Ed}}{f_y}\right)^2 + \left(\frac{\sigma_{z,Ed}}{f_y}\right)^2 - \left(\frac{\sigma_{x,Ed}}{f_y}\right)\left(\frac{\sigma_{z,Ed}}{f_y}\right) + 3\left(\frac{\tau_{Ed}}{f_y}\right)^2 \tag{2.15}$$

Relationship between critical buckling stress and applied stress:

$$\frac{1}{\alpha_{cr}} = \frac{1+\psi_x}{4\alpha_{cr,x}} + \frac{1+\psi_z}{4\alpha_{cr,z}} + \left[\left(\frac{1+\psi_x}{4\alpha_{cr,x}} + \frac{1+\psi_z}{4\alpha_{cr,z}} \right)^2 + \frac{1-\psi_x}{2\alpha_{cr,x}^2} + \frac{1-\psi_z}{2\alpha_{cr,z}^2} + \frac{1}{\alpha_{cr,\tau}^2} \right]^{\frac{1}{2}} \quad (2.16)$$

Unless α_{cr} of the entire plate field can be decided.

$$\begin{aligned} \alpha_{cr,x} &= \frac{\sigma_{cr,x}}{\sigma_{x,Ed}} \\ \alpha_{cr,z} &= \frac{\sigma_{cr,z}}{\sigma_{z,Ed}} \\ \alpha_{cr,\tau} &= \frac{\tau_{cr,\tau}}{\tau_{\tau,Ed}} \end{aligned} \quad (2.17)$$

According to Eurocode 1993-1-5 (2006, p.50), the factors $\alpha_{ult,k}$ and α_{cr} can be directly decided from their definitions as:

> $\alpha_{ult,k}$ - the smallest factor between the ultimate capacity and the applied stress without considering buckling and Lateral Torsional buckling
> α_{crit} - the smallest factor between the structure's critical stress and applied stress, considering buckling and Lateral Torsional buckling

This can be retrieved directly from an FE-analysis (Eurocode 1993-1-5, 2006, p.50) where λ_{eig} is the eigenvalue of the first buckling mode, which means that:

$$\alpha_{ult,k} = \frac{f_y}{\sigma_{VM}} \quad (2.18)$$

$$\alpha_{cr} = \frac{\sigma_{cr}}{\sigma_{Ed}} = \frac{\lambda_{eig} \cdot \sigma_{Ed}}{\sigma_{Ed}} = \lambda_{eig} \quad (2.19)$$

2. Calculate the slenderness $\bar{\lambda}_p$

The RSM uses a specific slenderness based on $\alpha_{ult,k}$ & α_{cr}. This is described in Equation 2.20.

Slenderness $\bar{\lambda}_p$:

$$\bar{\lambda}_p = \sqrt{\frac{\alpha_{ult,k}}{\alpha_{crit}}} \quad (2.20)$$

3. Calculate ρ_x, ρ_z & χ_w

The RSM slenderness, $\bar{\lambda}_p$, is used to calculate the reduction factors with respect to normal stress, ρ_x, ρ_z, and shear stress, χ_w. These are used to reduce the capacity as ρ in Equation 2.14.

The reduction factors for the normal stress is calculated according Equation 2.21 where ρ_c represents ρ_x and ρ_z depending on the current axis. ρ_c accounts for the interaction between column-like buckling and plate-like buckling using ξ, ρ & χ_c.

Reduction factor for σ:

$$\rho_c = (\rho - \chi_c)\xi(2 - \xi) + \chi_c \tag{2.21}$$

Which includes three components: ξ, ρ & χ_c

ξ is the aspect ratio between column-like buckling and plate-like buckling and is calculated as:

$$\begin{aligned} \xi &= \frac{\sigma_{cr,p}}{\sigma_{cr,c}} - 1 \\ \sigma_{cr,p} &= k_{\sigma,p}\sigma_E = 1 \cdot \frac{\pi^2 E t^2}{12(1-\nu^2)b^2} \\ \sigma_{cr,c} &= \frac{\pi^2 E t^2}{12(1-\nu^2)a^2} \end{aligned} \tag{2.22}$$

ρ is the reduction factor for plate-like buckling (internal compression members) and is calculated as:

$$\begin{aligned} \rho &= \frac{\bar{\lambda_p} - 0.055(3+\psi)}{\bar{\lambda_p}^2} \\ \psi &= \frac{\sigma_2}{\sigma_1} \end{aligned} \tag{2.23}$$

χ_c is the reduction factor for column-like buckling and is calculated as:

$$\begin{aligned} \chi_c &= \frac{1}{\Phi + \sqrt{\Phi^2 - \bar{\lambda_p}^2}} \leq 1.0 \\ \Phi &= 0.5\left[1 + \alpha\left(\bar{\lambda_p} - 0.2\right) + \bar{\lambda_p}^2\right] \end{aligned} \tag{2.24}$$

The reduction factor for the shear stress is χ_w. This is retrieved from Figure 2.17 (Eurocode 1993-1-5, 2006, p.24) using the specific slenderness for RSM, $\bar{\lambda_p}$.

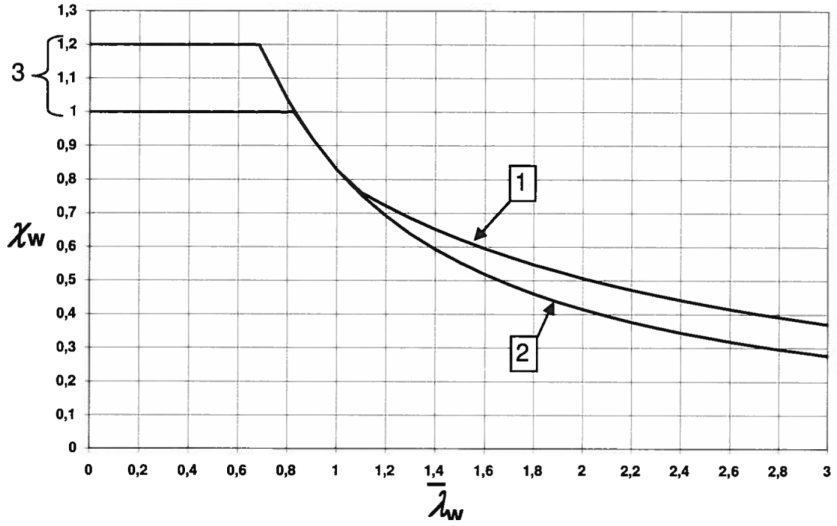

Figure 2.17: *Shear reduction factor χ_w from Eurocode 1993-1-5 (2006, p.24)*

4. Verification formula

There are two ways to verify the Reduced Stress Method for biaxial buckling of a plate in the xz-plane. These are both versions of Equation 2.14. Alternative I uses the minimum reduction factor out of the three calculated (ρ_x, ρ_z & χ_w). This one is described in Equation 2.25. Alternative II uses an interpolation of $\alpha_{ult,k}$ which gives the verification described in Equation 2.26

Verification formula, alternative I:

$$\left(\frac{\sigma_{x,Ed}}{f_y/\gamma_{M1}}\right)^2 + \left(\frac{\sigma_{z,Ed}}{f_y/\gamma_{M1}}\right)^2 - \left(\frac{\sigma_{x,Ed}}{f_y/\gamma_{M1}}\right)\left(\frac{\sigma_{z,Ed}}{f_y/\gamma_{M1}}\right) + 3\left(\frac{\tau_{Ed}}{f_y/\gamma_{M1}}\right)^2 \leq \rho^2 \quad (2.25)$$

Verification formula, alternative II:

$$\left(\frac{\sigma_{x,Ed}}{\rho_x f_y/\gamma_{M1}}\right)^2 + \left(\frac{\sigma_{z,Ed}}{\rho_z f_y/\gamma_{M1}}\right)^2 - \left(\frac{\sigma_{x,Ed}}{\rho_x f_y/\gamma_{M1}}\right)\left(\frac{\sigma_{z,Ed}}{\rho_z f_y/\gamma_{M1}}\right) + 3\left(\frac{\tau_{Ed}}{\chi_w f_y/\gamma_{M1}}\right)^2 \leq 1 \quad (2.26)$$

2.13.3 Capacity check according to Det Norske Veritas

An alternative procedure accounting for compression and biaxial bending is described by Det Norske Veritas (2002). Figure 2.18 illustrates a plate in the xy-plane, with a certain thickness, that is subjected to uniform lateral load and in-plane normal shear stresses which leads to a multiaxial stress state. In Equation 2.27, the

verification for this type of stress state according to Det Norske Veritas (2002) is presented.

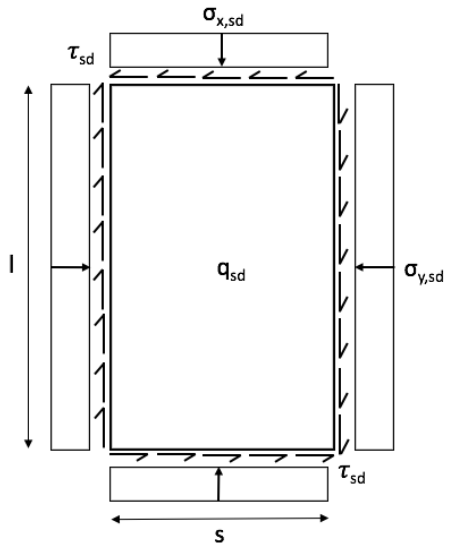

Figure 2.18: *Unstiffened plate with uniform lateral load and in-plane normal and shear stresses (created by author, inspired by Det Norske Veritas (2002, p.10))*

$$\left(\frac{\sigma_{x,Sd}}{\sigma_{x,Rd}}\right)^2 + \left(\frac{\sigma_{y,Sd}}{\sigma_{y,Rd}}\right)^2 - c_i \cdot \left(\frac{\sigma_{x,Sd}}{\sigma_{x,Rd}}\right) \cdot \left(\frac{\sigma_{x,Sd}}{\sigma_{x,Rd}}\right) + \left(\frac{\tau_{Sd}}{\tau_{Rd}}\right)^2 \leq 1.0 \tag{2.27}$$

$$\begin{aligned} c_i &= 1 - \frac{s}{120 \cdot t} \quad for \quad \frac{s}{t} \leq 120 \\ c_i &= 0 \quad for \quad \frac{s}{t} > 120 \end{aligned} \tag{2.28}$$

s = plate width [m]
t = plate thickness [m]

If any stress or both, $\sigma_{x,Sd}$ of $\sigma_{y,Sd}$, is negative and in tension then $c_i = 1.0$.

2.14 Capacity checks of welds

Welds in steel structures must be checked in two ways; static check in ULS and fatigue damage check in FLS.

2.14.1 Static checks

Static weld checks for steel structures are specified in Eurocode 1993-1-8 (2005, p.43). These consist of two equations, presented is Equation 2.29 and 2.30 with γ_{M2}=1.25 and β_w=0.9. They use the Von Mises stress in the welds, calculated according to Equation 2.31 where σ and τ are calculated according to Equations 2.32 & 2.33.

$$\sigma_{VM} \leq \frac{f_u}{\beta_w \gamma_{M2}} \tag{2.29}$$

$$\sigma_0 \leq \frac{0.9 f_u}{\gamma_{M2}} \tag{2.30}$$

$$\sigma_{VM} = \sqrt{\sigma_{90}^2 + 3\left(\tau_0^2 + \tau_{90}^2\right)} \tag{2.31}$$

$$\sigma = \frac{P}{A} + \frac{M}{W} \tag{2.32}$$

$$\tau = \frac{P}{A} \tag{2.33}$$

$P[N]$ and $M[Nm]$ are the load effects in the welds and $A[m^2]$ and $W[m^3]$ are the weld's geometric properties.

2.14.2 Control of fatigue life

Control of the structure in FLS is done in different ways depending on the Fatigue Load Model. FLM4 is to be used in conjunction with the Damage Accumulation Method (Eurocode 1993-2, 2006, p.45). This method compares the stress range from the applied load with the maximum allowed stress range for a certain detail. The fatigue damage, D is calculated using Equation 2.34. n_i represents the the number of cycles that the bridge is subjected to. N_i is calculated according to Equation 2.35 and represents the number of cycles the bridge can carry based on the applied stress range from the lorries in FLM4.

$$D = \sum_i \frac{n_i}{N_i} \leq 1.0 \tag{2.34}$$

$$N_i = 2 \cdot 10^6 \left(\frac{\Delta\sigma_C / \gamma_{Mf}}{\gamma_{Ff} \cdot \Delta\sigma_i} \right)^m \tag{2.35}$$

Where $m = 3$ for a CCSSP (Nilsson, Al-Emrani, & Atashipour, 2020, p.14) and $\gamma_{Mf} = \gamma_{Ff} = 1.0$ (Eurocode 1993-1-9, 2005, p.11).

2.15 Factorial design

Factorial design is a statistic approach used to design experiments where the aim is to investigate the impact of different independent variables on some dependent variables (Bickel et al., 2006, p.1-8). With this method, both main effects and interaction effects can be investigated between dependant and independent variables. The number of tests in a Full Factorial Design grows exponentially and often results in a vast amount of tests (Bickel et al., 2006, p.1-8).

2.15.1 Fractional Factorial Design

In a full factorial design, some of the performed experiments might not result in valuable information about certain effects of the studied case, such as the main effects. In a Fractional Factorial Design (FFD) process these are excluded from the process and only the most important experiments are performed (Bickel et al., 2006, p.1-8). Due to this, the number of tests are reduced. However it means that main effects and interaction effects between factors can be confounded and affect the results of the FFD.

The FFD is expressed as $I^{(k-p)}$, where I = number of levels of each parameter investigated, k = number of parameters and p = size of fraction in a full factorial design. The fraction determines the resolution of the FFD. Resolutions III, IV and V are the most common choices where resolution III generates the least amount of tests (NIST/SEMATECH, 2003). With resolution III, main effects are seen but are confounded by two-factor interaction. With resolution IV, all main effects are retrieved but two-factor interactions may be confounded by other two-factor interactions. With resolution V, main effects and two-factor interaction effects are retrieved but some of the two-factor interaction effects may be confounded by three-factor interaction effects (NIST/SEMATECH, 2003).

3
Model

This chapter describes the properties of the FE-model used in this thesis. The model is a 3D shell model of the entire bridge deck. A linear static analysis is performed in the FE-program BRIGADE/Plus using this model in order to gain information on the run time when using this model type. The linear static analysis using the described 3D shell model of this chapter shows a sufficiently short run time that it is used for all analyses in the thesis.

3.1 Cross section

The cross section of the model is illustrated in Figure 3.1. It consists of two edge beams with a number of cells between. The boundaries of one cell is marked in Figure 3.1. The edge beam measurements can be seen in Figure 3.1. The height of the edge beams exceed the plate height, h, with $50mm$ at the top and bottom. The number of cells can vary depending on the chosen cross section configuration for a certain width.

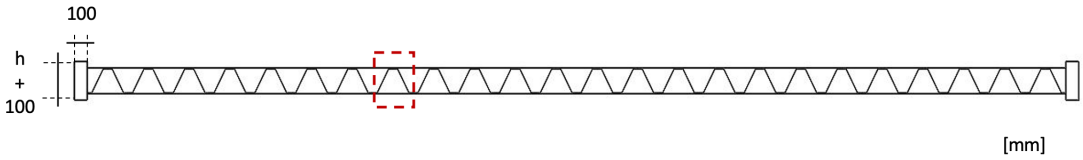

Figure 3.1: *Sketch of the cross section and the edge beams with one cell width marked in dashed lines*

3.2 Coordinate system

The cross section is sketched in the xy-plane. After assembling all the parts, the model is placed in the global coordinate system seen in Figure 3.2.

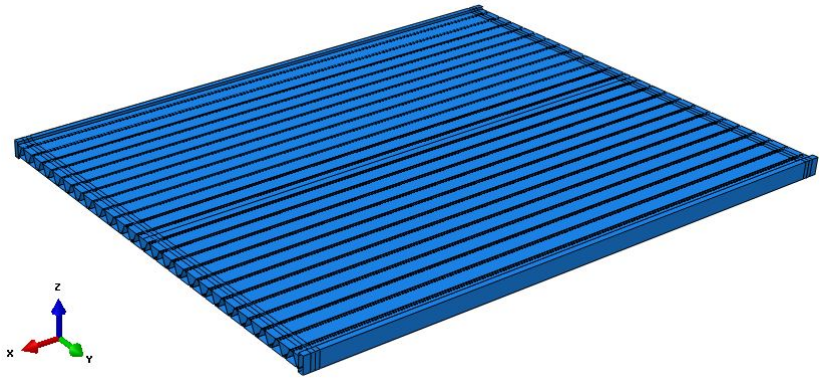

Figure 3.2: *Global coordinate system used for the model*

3.3 Boundary conditions

The deck is simply supported on two sides. The vertical supports prevent translation in the z-direciton and are applied at a distance dL from the edges of the deck, as seen in Figure 3.3. In order to prevent a mechanism, the model is also prohibited from moving in the xy-plane by preventing translation of two nodes in x-direction and two nodes in y-direction, as seen in Figure 3.4.

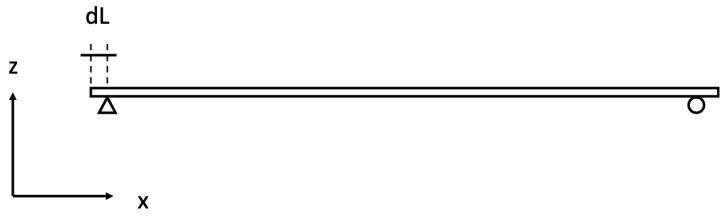

Figure 3.3: *Vertical boundary conditions used in the model*

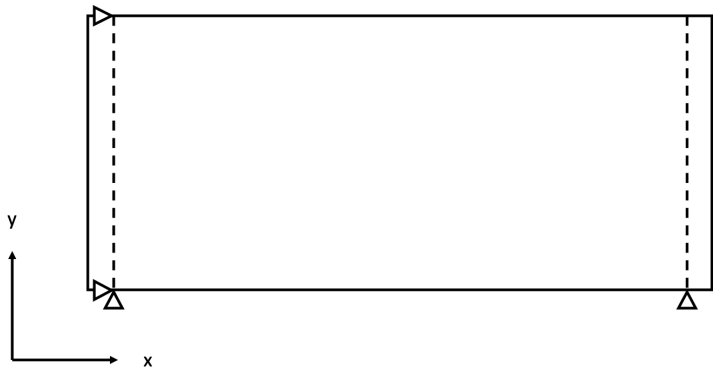

Figure 3.4: *In-plane boundary conditions used in the model*

3.4 Loads

The loads applied to the model vary depending on the analysis type. All applied loads are:

- **Self-weight**
  $\rho_{steel} = 7850$ kg/m^3 (Eurocode 1991-1-1, 2011, p.33) applied as a gravity load
- **Distributed load from surface pavement**
  $q_{coating} = 25$ kN/m^3 (Eurocode 1991-1-1, 2011, p.34) applied as pressure to the entire bridge
- **Distributed load from Eurocode's LM1**
  according to Section 2.9.1 with load combinations according to Section 2.10, applied as pressure in lanes according to Section 2.9.1.
- **Tandem loads from Eurocode's LM1**
  according to Section 2.9.1 with load combinations according to Section 2.10, applied as pressure on load plates corresponding to wheel pressure positions.
- **Tandem load plate from Eurocode's FLM4**
  according to Section 2.9.2 applied as pressure on load plates corresponding to wheel pressure positions.

On the load in the LM1-analyses of the model, the safety factors presented in Section 2.10 are applied. Which factors depend on the largest load combination of the current model and may thus change with each new geometry.

A 1:1 spread of the patch loads from the tandems in LM1 is assumed through the surface pavement. The pavement has a thickness of 50mm. This increases the application area of the tandem loads for LM1 and FLM4 by 100mm in each direction compared to their original sizes. The tandem loads are applied to the plate via additional plates with zero stiffness, seen in Figure 3.5. These are added and tied to the model one millimeter above the top plate. The actual load is applied to these plates instead of directly onto nodes in the top plate. This enables a simpler way of moving the patch loads. The measurements of the load plates in LM1 is presented in Table 3.1 and in FLM4 in Table 3.2.

Table 3.1: *Measurements of the load plates used in ULS and SLS*

	Length in x [mm]	Length in y [mm]
LM1	500	500

Table 3.2: *Measurements of the load plates used in FLS*

	Tandem type	Length in x [mm]	Length in y [mm]
FLM4	A	420	320
	B	420	640
	C	420	370

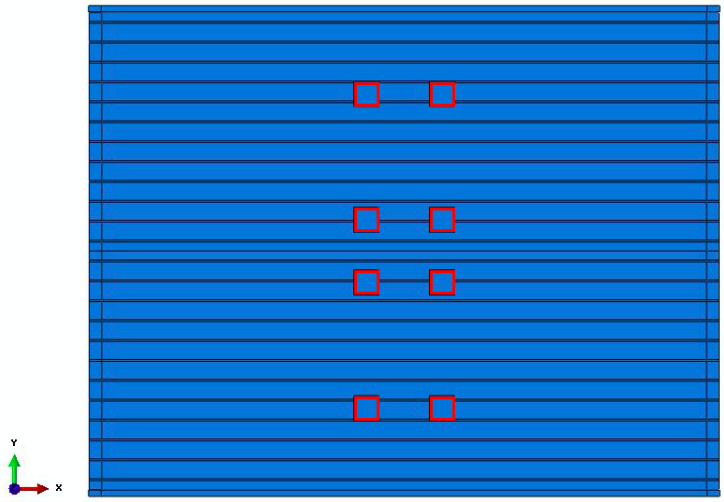

Figure 3.5: *Application of the tandem loads via load plates*

3.5 Element type

The model uses 8-noded quadrilateral 3D shell elements, as seen in Figure 3.6. Each node is evaluated with five integration points through the plate element thickness.

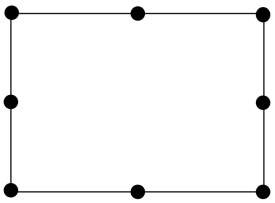

Figure 3.6: *8-noded quadrilateral shell elements*

3.6 Mesh and element size

The mesh size is chosen differently for different areas of the plate by seeding the edges of the cross section in different sizes. The dimensions of the mesh for different parts of the deck is presented in Table 3.3.

Table 3.3: *Mesh dimensions for the model*

Mesh parameter	Value	Unit	Description
elSize	78	mm	*Mesh size along bridge length*
LoadElSize	40	mm	*Mesh size on load application areas*
coreElSize	15	mm	*Mesh size mesh size in core*
plateElSize	40	mm	*Mesh size on surface plates*
edgeElSize	50	mm	*Mesh size on edge beams*

In order to retrieve results in points on a specific distance from the supports, partitions are created 75mm from the supports in both directions. This mimics a support width of 150mm and ensures that the mesh will supply nodes in these positions.

3.7 Material

Steel S355 with properties according to Table 3.4 is used in the modelling (Eurocode 1993-1-1, 2005, p.26-28).

Table 3.4: *Input data - material properties*

Material parameter	Value	Unit	Description
E_s	210	GPa	*Young's modulus for steel*
ν	0.3	-	*Poisson's ratio for steel*
f_y	355	MPa	*Yield stress for steel*
f_u	510	MPa	*Ultimate stress for steel*
ϵ_0	0	-	*Yield strain for steel*
ϵ_1	0.074	-	*Ultimate strain for steel*

3.8 Interaction of parts

The edge beams are connected to the top, bottom and core plates with a rigid connection. The welds are modelled as described in Section 2.7.4. The length of each spring is the smallest possible distance that BRIGADE/Plus allows which is $0.01mm$. The stiffness of the rotational springs are calculated for each case using Equation 2.3 presented in Section 2.8.3.

3.9 Verification of model

To determine that the mesh used in the analysis is fine enough to give accurate results, a convergence study is performed with respect to the Von Mises stress directly below the patch loads. The global behaviour of the model is verified by comparing the deflection of the FE-model with the deflection retrieved from hand-calculations. Finally, the local behaviour of the FE-model is verified by comparing the stresses beneath the patch loads when applying the load using load plates and with partitions in the top plate.

3.9.1 Convergence study

Two convergence studies are performed, one for the top and bottom plates and one for the core. These are illustrated in Figures 3.7 and 3.8.

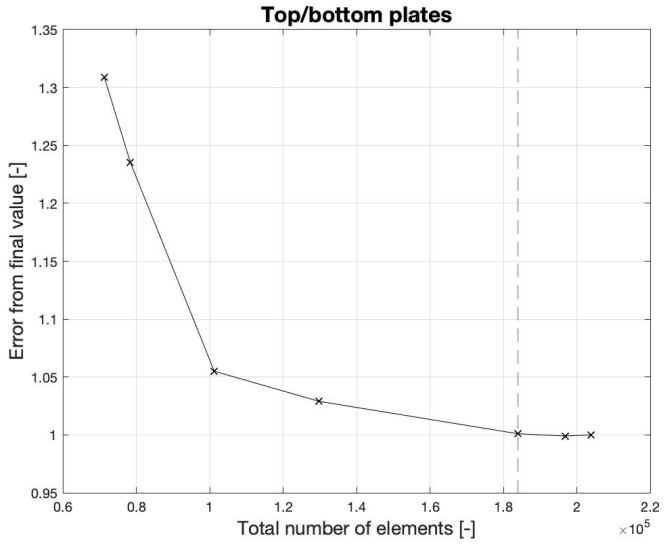

Figure 3.7: *Convergence study for the top and bottom plates (dashed line indicate chosen mesh)*

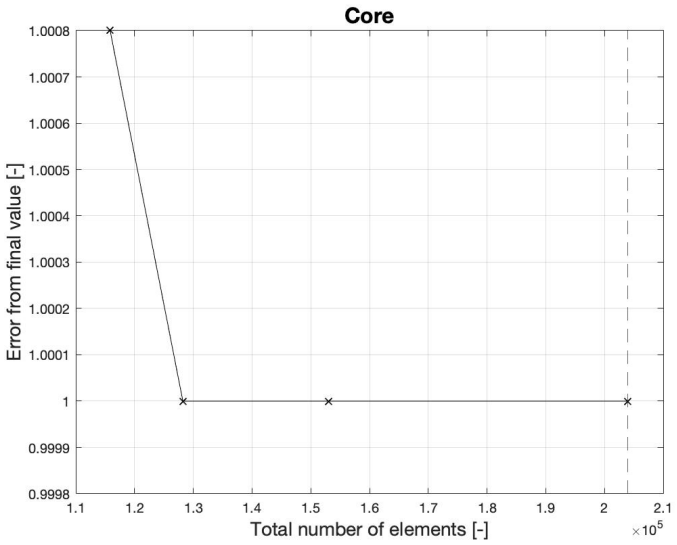

Figure 3.8: *Convergence study for the core (dashed line indicate chosen mesh)*

The results from the convergence studies can be seen in Table 3.5 where the dashed lines indicate the chosen mesh sizes. The chosen mesh size in the top and bottom plates give an error of less than 1%. In the core, the coarsest mesh tested also gives an error of less than 1%, however the chosen mesh size in the core is considered coarse enough to use. This results in an error very close to 0% in the core.

Table 3.5: *Result of mesh sizes according to the convergence studies*

Part	Mesh size (BxL) [mm]
Top & bottom plates	40x78
Core	15x78

3.9.2 Global verification of model

In the global verification, the deflection from the FE-analysis is compared with hand calculations, seen in Appendix A. The model used in this verification is loaded with one tandem load placed in the middle, uniform load from the most loaded lane according to LM1 and surface pavement. The welds in the comparison are modelled using tied connections instead of springs. The results are presented in Table 3.6 and the difference is small.

Table 3.6: *Comparison of deflection from hand calculations and FE-model to verify the global behaviour of the model*

Hand calculations [mm]	FE-analysis [mm]	Difference [%]
81	82	1

The conclusions from these verifications are that the model is globally responding well. The difference is small and conservative.

3.9.3 Local verification of model

In the local verification, the tandem loads are applied on load plates that are tied to the top plate in order to simulate the wheel pressure patch load. This method is used to make it simple to move the tandems along the bridge deck in the design program. The alternative is to partition the bridge deck in all the positions where the load is applied. Using partitions makes it more difficult to move the tandems in any position on the deck. To verify the use of load plates in the model these two methods are compared. In this verification the model is loaded with one load plate, and the partitions are created at the exact same positions. The comparison is done for the top plate using Von Mises stress. The result is presented in Table 3.7. The weld stresses are compared and presented in terms of normal stresses σ_{90} and maximum UR in the welds with respect to the Von Mises stress in the welds. These are seen in Table 3.8.

Table 3.7: *Comparison of plate stresses in the top plate when using load plates and partitions in the FE-model to verify the local behaviour of the FE-model*

	σ_{VM} [MPa]
Load plates	472
Partitions	475
Difference	**1%**

Table 3.8: *Comparison of weld stresses when using load plates and partitions in the FE-model to verify the local behaviour of the FE-model*

	σ_{90} [MPa]	Utilization [%]
Load plates	1945	530
Partitions	1981	539
Difference	**2%**	**2%**

The load plates result in a non-conservative behaviour. The difference is small, 2% which lead to the conclusion that this method can be used in the design program.

3.10 Conclusion of model type

A linear static analysis using the described 3D shell model shows a sufficiently short run time that this model is used for all analyses performed in this thesis. One analysis using the described mesh properties takes approximately 30 minutes to complete on one computer core.

The modelling properties in this chapter are used throughout the thesis. Different geometric input data is used in different investigations but the properties remain the same unless specified. The model in this chapter is also used in the design program created in this thesis.

4

Evaluation of the CCSSP with respect to biaxial stresses

The main aim of this chapter is to investigate the local behaviour of the panel under the tandem loads and the biaxial stress state which occurs here, as discussed in section 2.6.3. The focus is to verify the use of the RSM as a way to check the CCSSP bridge deck against buckling. This is done with linear static-, linear buckling- and nonlinear analyses using BRIGADE/Plus with calculations according to RSM.

4.1 Input data

The geometric data input of the cross section for the model is listed in Table 4.1 and is based on Figure 4.1. This input data is based on previous research by Nilsson, Hedegård, Al-Emrani, and Atashipour (2019, p.5) with some small modifications in order to make sure that the top plate of this cross section is in cross section class 4.

Table 4.1: *Geometric input data*

Geometric parameter	Value	Unit	Description
L	10	m	*Bridge length*
nCells	24	-	*Width of the bridge in number of cells*
t_1	5	mm	*Thickness of bottom plate*
t_2	8	mm	*Thickness of top plate*
t_c	8	mm	*Thickness of core plate*
t_e	10	mm	*Thickness of edge beam plate*
h	200	mm	*Height of the bridge deck*
f_1	60	mm	*Horizontal part of core at bottom*
f_2	60	mm	*Horizontal part of core at top*
dw_1	30	mm	*Distance between bottom welds*
dw_2	30	mm	*Distance between top welds*
Θ	64.4	°	*Corrugation angle*
R_1	7.4	mm	*Bottom radius of curvature*
R_2	7.4	mm	*Top radius of curvature*
a	2	mm	*Weld thickness*

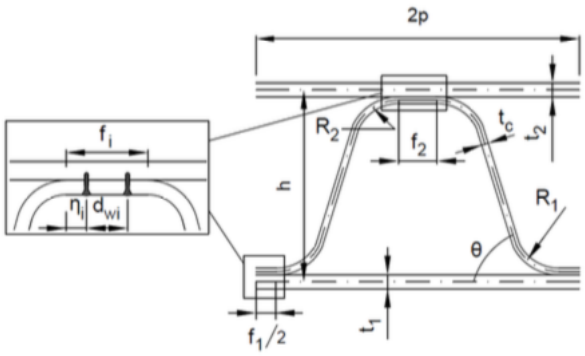

Figure 4.1: *Cross section of one cell of the bridge deck and its parameters (Nilsson, 2017, p.10)*

4.2 Model

In the performed evaluation a 3D shell model is used, as described in Chapter 3, with some modifications. The welds are modelled as tied connections instead of the solution described in Section 3.8. The ties affect the stresses in the weld positions but do not change the overall behaviour of the panel. This choice shortens the run-time for all the analyses performed but is still representative and can be used to draw conclusions related to the ULS design of the constituent plates of the cross section. The applied loads are only the tandem loads from LM1 placed at L/2, as these induce the most critical stress state in the panel with respect to biaxial stresses.

4.3 Results from FE-analyses

A linear static analysis is performed in order to investigate how a CCSSP acts as a simply supported bridge deck. The Von Mises stress distribution in the top plate, in the top integration point is visualized in Figure 4.2. The result shows that there are large local stresses in the top plate directly beneath the tandem load's application areas.

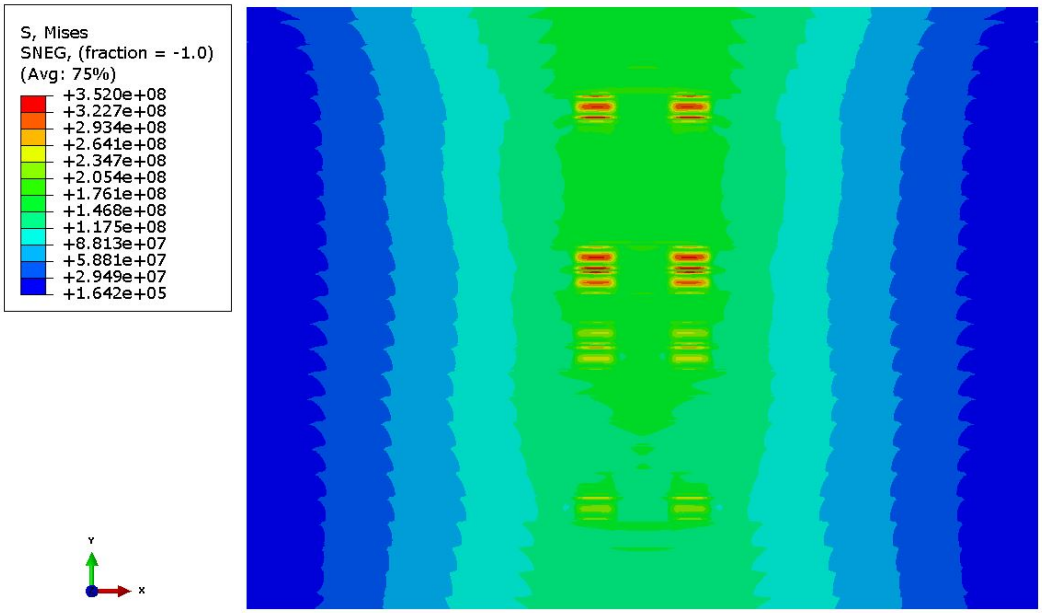

Figure 4.2: *Von Mises stress distribution in the top plate (σ_{VM} [Pa])*

The first eigenmode from the normal stress buckling analysis can be seen in Figure 4.3 and occurs in the top plate beneath the tandem loads. The eigenvalue of the first buckling mode is 4.35.

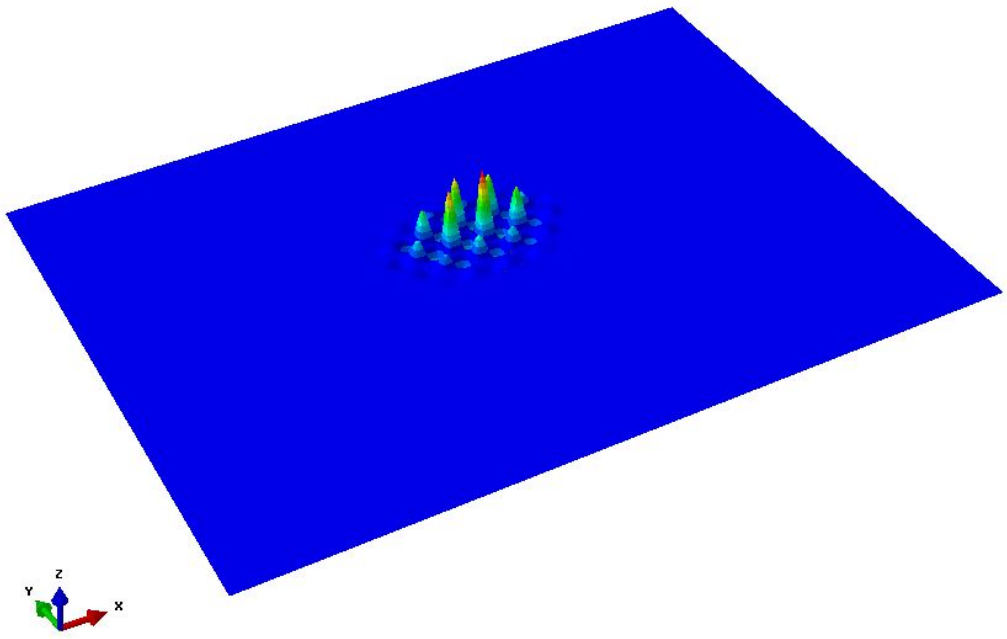

Figure 4.3: *First buckling mode λ_{eig}=4.35*

4.4 Biaxial compression in the CCSSP

The linear static- and linear buckling analyses show that the critical position with respect to biaxial stresses in the top plate is directly below the tandem loads. The load effects on the plate in this position can be seen in Figure 4.4 and they are:

- Normal stress in both directions of the xy-plane due to the global bending moment (n_x & n_y)
- In-plane shear due to global load effects (τ_{xy})
- Local bending moment along the welds (m_y) due to the local load effect from the patch load (q)

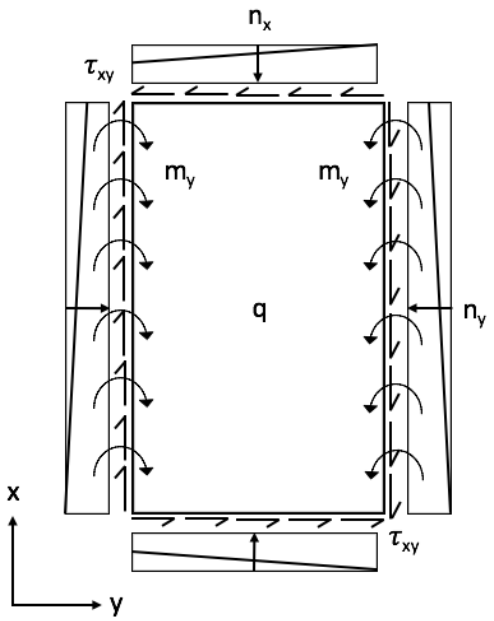

Figure 4.4: *Illustration of the biaxial stress state in the top plate of the CCSSP under patch loading*

4.4.1 Methods to evaluate biaxial compression

To evaluate the effect of biaxial stresses in the CCSSP, three methods are presented; the Effective width method, the Reduced Stress Method (both presented in Eurocode 1993-1-5) and a method presented by Det Norske Veritas (2002).

The Effective width method is not suitable in this specific case because it does not account for multiaxial stress states. The other methods both use the Von Mises yield criterion in its assessment, but because the RSM is included in Eurocode 1993-1-5 it is used here in the ULS design to verify the biaxial stress state.

4.4.2 Investigation of the Reduced Stress Method

This section evaluates the capacity of the CCSSP bridge deck using the RSM and compares it to a nonlinear analysis. The investigation is only done for the top plate. The bottom plate is in tension and is not subjected to buckling loads. Column buckling in the core can occur, but as the buckling analysis shows it is not a problem for this case. To prevent core buckling for other cross section configurations, a minimum core thickness is calculated. For the current case, t_c is calculated to a minimum of 5mm. This calculation is found in Appendix B.

Before an RSM evaluation is performed, the theoretical buckling stress is calculated in each direction and it is used to evaluate ξ. These calculations can be found in Appendix C. The ξ-value is the relationship between plate-like buckling and column-like buckling. By looking at the ξ-value for the studied case, the following conclusions are drawn:

- Plate-like buckling dominates in the x-direction. The calculated ξ-value becomes very large and ρ_x is equal to ρ (reduction factor for plate buckling)
- Column-like bucking dominates in the y-direction. The calculated ξ-value becomes very small and ρ_z is equal to χ_c (reduction factor for column buckling)

The RSM calculation is performed for a path in the top plate, directly below the tandem loads. The position of the path can be seen in Figure 4.5. α_u is received from the linear static analysis and α_{cr} is received from the linear buckling analysis, as described in Section 2.13.2. The reduction factors are presented in Table 4.2. The UR for the RSM evaluation in the top plate can be seen in Figure 4.6.

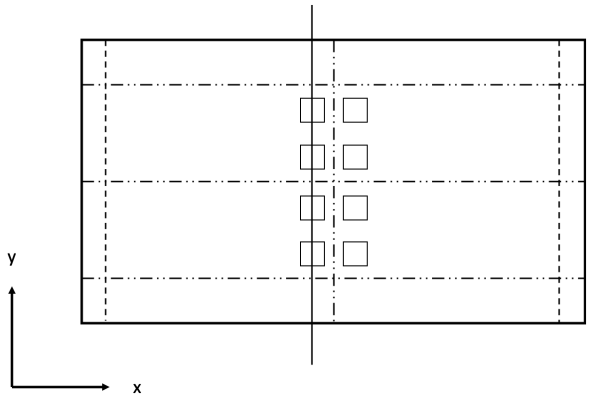

Figure 4.5: *Position of the path used in the RSM assessment of the CCSSP bridge deck*

Table 4.2: *Reduction factors for RSM in the top plate from the FE-analysis*

Top	
ρ	1.0
χ_c	0.85
χ_w	1.0

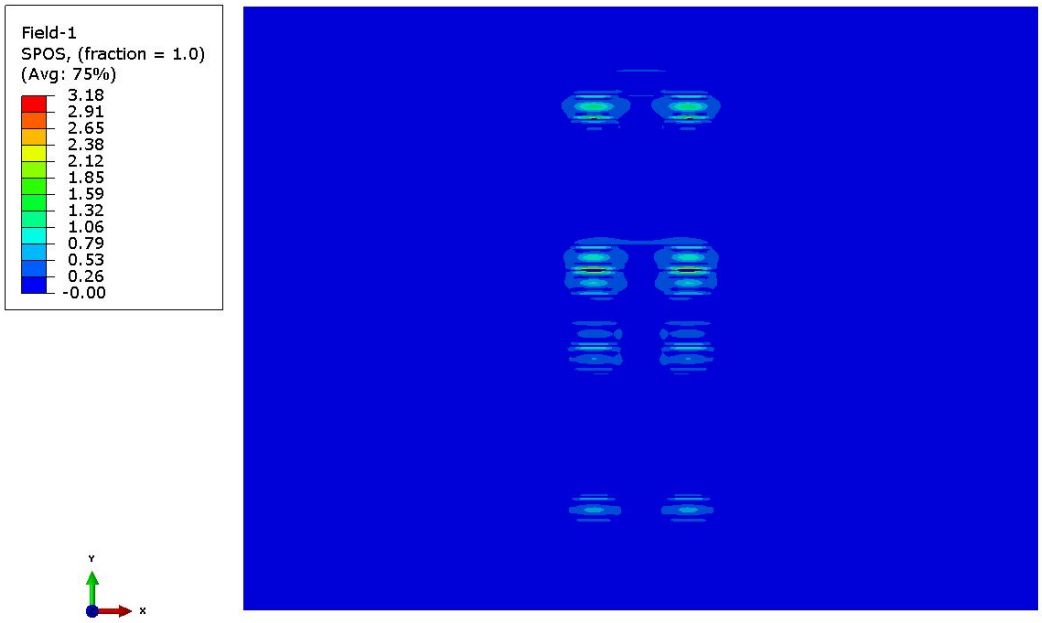

Figure 4.6: *Result of RSM in the top plate. Maximum UR: 318 %*

To investigate the applicability of RSM for CCSSPs a comparison with a full non-linear analysis is performed. This is done by adding elastic-plastic behaviour according to the material parameters described in Chapter 3. The nonlinear analysis includes initial imperfections according to Equation 4.1 from Eurocode 1993-1-5.

$$e_0 = L/200 \tag{4.1}$$

From the nonlinear analysis, a Load Proportionality Factor (LPF) is retrieved. This factor shows how much the design-load should be increased in order to reach the ultimate (plastic) capacity of the material. The LPF from this analysis is shown in Figure 4.7. The plastic capacity, f_y, corresponds to the LPF-value of 1.78. This is where the plate is not behaving elastically any more. From the LPF, the UR of the CCSSP in ULS can be calculated as $\eta = 1/LPF$. A comparison between the result from the non-linear analysis and the RSM can be seen in Table 4.3.

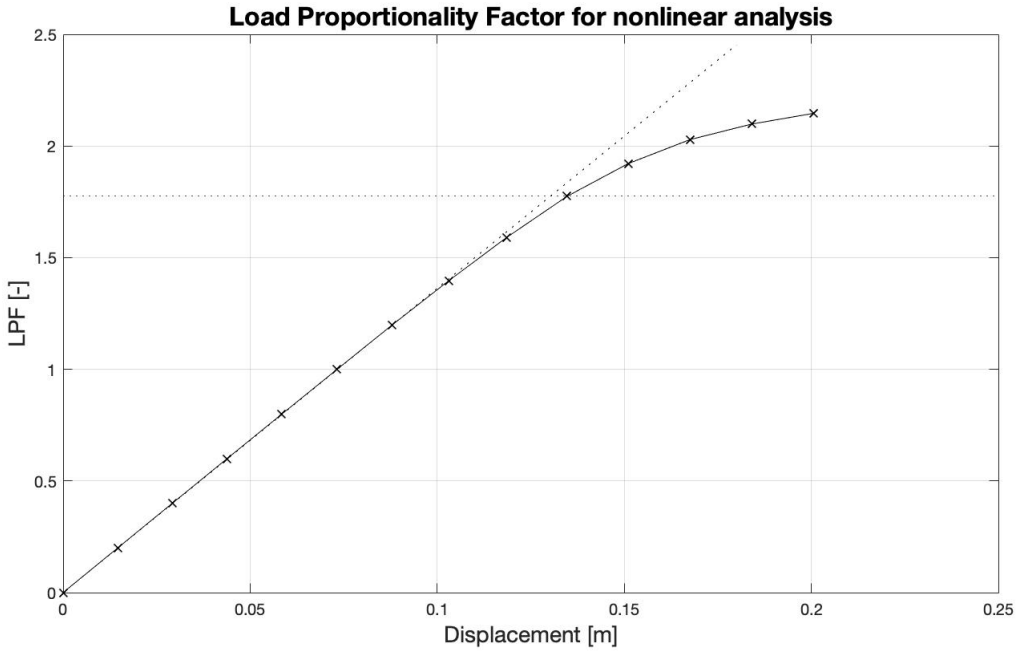

Figure 4.7: *Load proportionality factor versus displacement in z for a position between the welds directly under one of the tandem loads*

Table 4.3: *Comparison between the maximum UR for RSM and nonlinear analysis directly under one of the tandem loads*

Reduced Stress Method [%]	Nonlinear analysis [%]
318	56

4.5 Discussion

The results of the linear static analysis show that there are large concentrated stresses in the top plate directly beneath the patch loads in the tested case. The buckling analysis shows that the tested case buckles in the top plate in the same positions as the largest patch loads. This means that in the tested case, the top plate is critical with respect to biaxial compression. The concentration of the stresses in the top plate also shows that the local action is by far more critical than the global action for the CCSSP bridge deck.

Using the RSM for a CCSSP shows that plate action dominates in the longitudinal direction and column action dominates in the transverse direction of the top plate. This is because of the location of the weld lines which create a constraint of the plate fields in the top plate in the transverse direction. In turn, this means that the edges of the plate field in the longitudinal direction are constrained but in the transverse direction they are free. This effect is illustrated in figure 4.8.

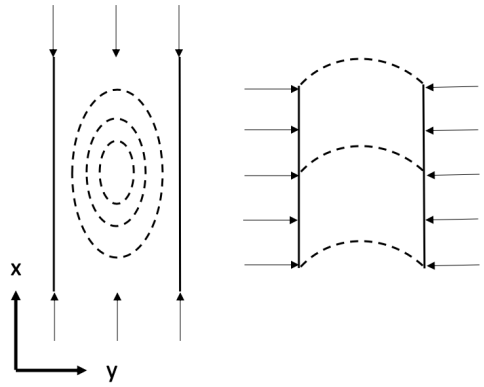

Figure 4.8: *Plate buckling (left) and column buckling (right) in the CCSSP top plate field*

As expected, the UR is high directly beneath the patch loads. In the rest of the plate, the UR is low. In the studied case the welds are modelled as tied connections, which gives increased stresses in the direct vicinity of the welds compared to when the welds are modelled as springs.

According to the RSM, each part of the cross section must be investigated with the correct boundary conditions and interaction between the constituent parts can not be accounted for. Due to this, the top plate is possible to evaluate with RSM using the model created. The core is difficult to model without accounting for the influence of the face plates and is excluded from the assessment of the CCSSP with respect to the RSM, as described in Section 4.4.2. The column buckling check used in Appendix B is a way to ensure that there is no risk of core buckling.

The investigations in this thesis show that there is a large difference in the results between the RSM and the full nonlinear analysis. The RSM uses the reduction factors ρ, χ_c and χ_w. These are based on the stresses in the top plate which come from membrane stresses and bending stresses. The RSM is meant to include the membrane stresses when reducing the capacity of the plate against buckling as these stresses are the ones contributing to the risk of buckling. However, the FE-analysis does not separate membrane stresses from bending stresses. As the FE-analysis is used to reduce the capacity of the CCSSP with respect to the RSM, this leads to an increased reduction factor due to higher stresses. Another factor that explains the difference is that the full nonlinear analysis accounts for plastic redistribution of stresses while the RSM does not consider this. Because of this, the UR for the nonlinear analysis is calculated with the yield stress f_y, which is marked in Figure 4.7. The UR for the RSM also includes the partial safety factor γ_{M1} which reduces the yield stress in this method.

4.6 Conclusion

The investigations of the RSM leads to the conclusion that it is a conservative method, as predicted. Because it is conservative, it can be used in the design program to check the capacity of a CCSSP with respect to buckling of the top plate. In order to prevent the core from buckling, a column buckling check of the core is used in the design program.

5
FLS design approach

The aim of this chapter is to present how to apply Eurocode's FLM4 in FLS controls to a CCSSP used as a bridge deck for simply supported, short-span bridges and verify simplifications made related to these controls. This is done through investigations using FE-model with loads from FLM4 as described in Section 2.9.2 and with the checks described in Section 2.14.2.

5.1 Simplifications

The simplifications that are done regarding the design calculations related to the fatigue life of the CCSSP bridge deck are:

1. The vertical normal stress σ_{90} along the weld line is the decisive stress component with respect to fatigue failure in the welds.
2. The distribution of the vertical normal stress σ_{90} along the weld line is such that:
   - Each tandem can be seen as one load cycle.
   - Each weld is only affected by load in the near vicinity of the weld.
3. Tandem type C from FLM4 can be modelled as tandem type A. This is conservative because tandem type A gives a more concentrated load on the welds.
4. The wheel pairs of tandem type B is modelled as one patch load so that tandem type B consists of two large plates. This is realistic because of the spread of the load through the pavement.

Because simplifications number 2-4 are either true or conservative, the simplification which needs verification is simplification number 1. This is done in Section 5.3.

5.2 Input data

The geometric input data for the model used in this chapter is described in Section 4.1. In this chapter, the springs related to the weld region deformability are modelled as described in Chapter 2.7.4. The spring stiffness is presented in Table 5.1.

Table 5.1: *Rotational spring stiffness for the specific case*

$k_{\varphi 1}$	108	*Rotational spring stiffness top plate [kNm/rad]*
$k_{\varphi 2}$	153	*Rotational spring stiffness bottom plate [kNm/rad]*
k_{φ}	10^{11}	*Spring stiffness in all the other springs [kNm/rad]*

The magnitudes of the patch loads used in all models with FLM4 are specified in Table 5.2. The magnitudes describe the total magnitude of one patch load of that type.

Table 5.2: *Magnitudes of the patch loads in FLM4 as they are applied in this thesis*

Patch load type	Magnitude [kN]
A	45
B	75

5.3 Verification of simplifications

Simplification 1 of the design calculations related to the fatigue life of the CCSSP bridge deck is verified using FE-analysis with the following model:

(1) Model performing linear static analysis with FLM4, wheel pressure type A with load placed at L/2

Model (1) performs a linear static analysis with loads according to FLM4, tandem type A. The modelling conditions are the same as described in Chapter 3. Because it is assumed that σ_{90} is the decisive stress component and it is assumed that each weld is only affected by a load close to it, the model used in the FLS design includes only one patch load, as seen in Figure 5.1.

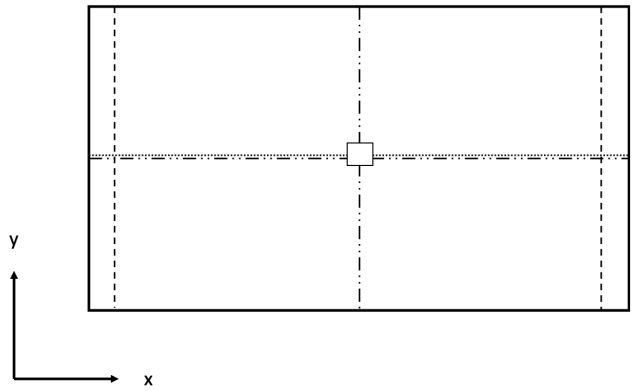

Figure 5.1: *Load position in model (1) placed above weld 26*

The required output from model (1) is the forces and moment in the springs used to model the welds. These are P_x, P_y, P_z & M_x and are transformed to weld stresses with a set of equations. Equation 5.1 is used to transform the force, P, in each spring ([N]) to the force per element ([N/m]) along each weld. This is done with the forces from all three nodes of each element, as seen in Figure 5.2. The same procedure is used to transform the bending moment, M_x ([Nm]), in the springs to moment in each element ([Nm/m]) as seen in Equation 5.2. The average force and moment per element are then used to calculate the stresses σ_{90}, τ_0 & τ_{90} using Equations 5.3-5.5.

$$P_{norm,k} = \frac{\frac{P_{j-1}}{2} + P_j + \frac{P_{j+1}}{2}}{elSize_k} \quad [N/m] \tag{5.1}$$

$$M_{norm,k} = \frac{\frac{M_{j-1}}{2} + M_j + \frac{M_{j+1}}{2}}{elSize_k} \quad [Nm/m] \tag{5.2}$$

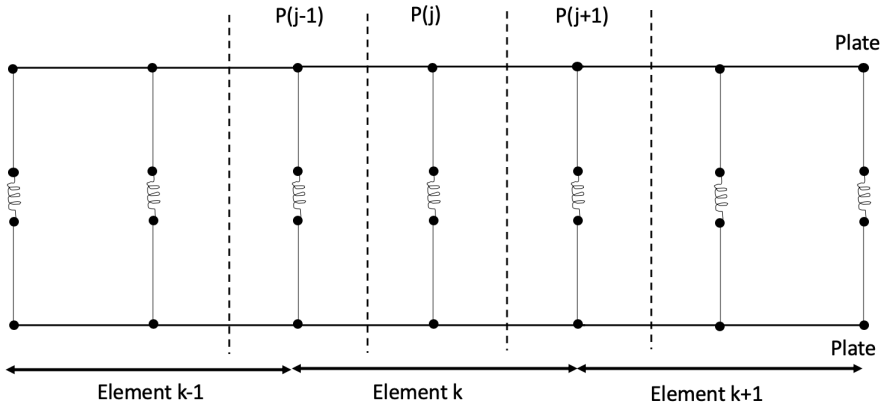

Figure 5.2: *Illustration of how the spring forces are calculated per meter in each element*

$$\sigma_{90} = \frac{P_z}{A} + \frac{M_x}{W} \tag{5.3}$$

$$\tau_0 = \frac{P_x}{A} \tag{5.4}$$

$$\tau_{90} = \frac{P_y}{A} \tag{5.5}$$

A comparison of the magnitudes of σ_{90}, τ_0 & τ_{90} can be seen in Figure 5.3. The result clearly shows that σ_{90} is the critical stress. Figure 5.4 also shows that σ_{90} is mainly influenced by the contribution from the bending moment, M_x, in the welds.

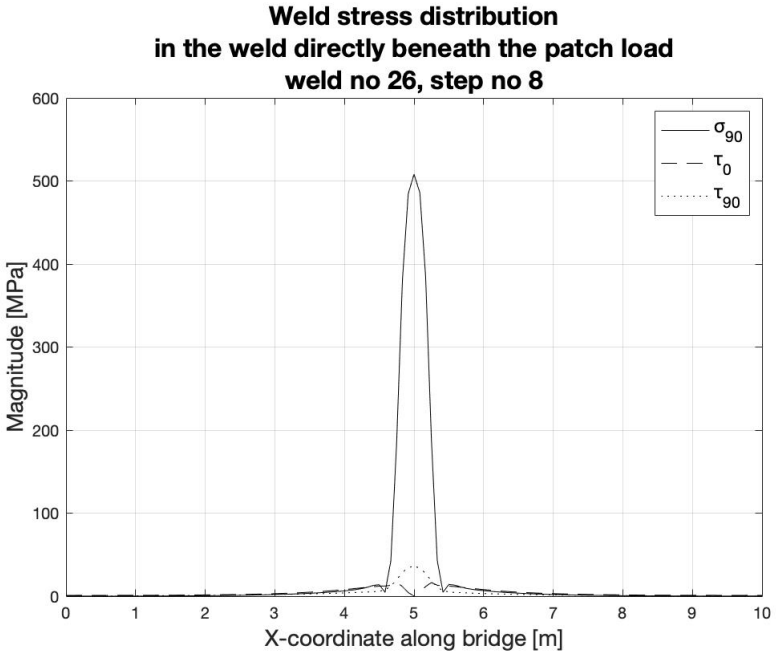

Figure 5.3: *σ_{90}, τ_0 & τ_{90} in model (1) in the weld directly below the patch load*

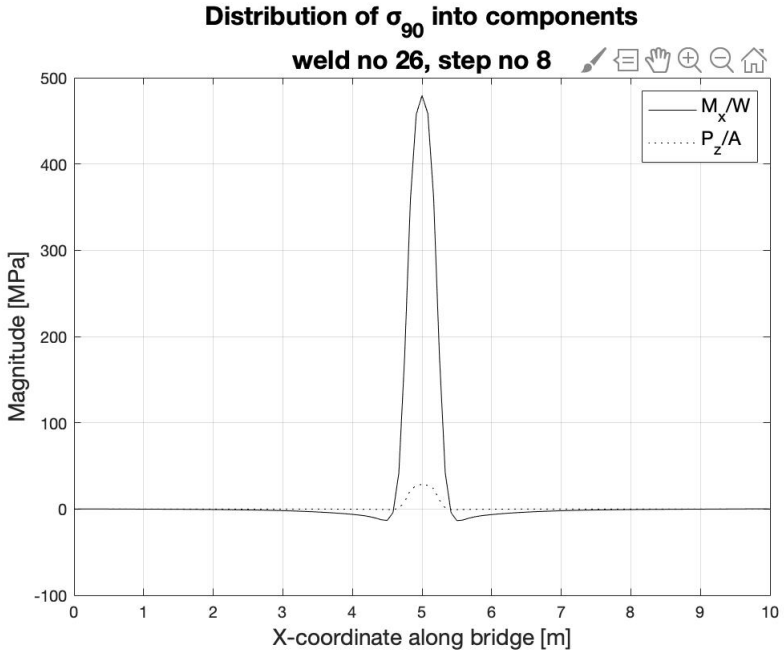

Figure 5.4: *Distribution of σ_{90} into components in model (1) in the weld directly below the patch load*

5.4 Investigation of worst load position

To find the worst load position, two models with different load placement are tested. These are:

(1) Model performing linear static analysis with FLM4, tandem type A with load placed in mid span, at L/2
(2) Model performing linear static analysis with FLM4, tandem type A with load placed by the support, at 0.1·L

Model (1) and model (2) are used to perform a linear static analysis with loads according to FLM4, tandem type A. The modelling conditions are the same as described in Chapter 3. The models are run in 15 steps each to capture the stress peak. The load applied in all steps is one patch load of one tandem of type A, according to FLM4. In each step, the load plate is moved 100mm in the y-direction of the bridge. The positioning of the load plate in step number 8 can be seen in Figure 5.5 for both models. In this step, there is a weld directly centered below the load plate. The required outputs from model (1) and (2) are the spring forces P_z and M_x. The stress σ_{90} is calculated in each weld, according to Section 2.14.

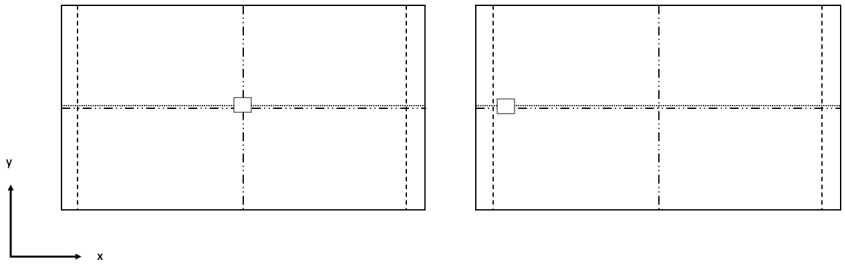

Figure 5.5: *Load position in model (1) (left) and model (2) (right)*

The results from the analyses can be seen in Figure 5.6 which shows the most stressed weld in all steps. In this case the critical loading position is when the wheel pressure is placed in the middle of the span, as in model (1). However, the results are very similar. To get an indication of the damage, it is possible to use either of the load positions. The loading position L/2 is therefore used in the FLS evaluation for both tandem type A and B in this chapter. It is also the position used in the rest of the thesis as the stresses are very similar for both positions. However, when performing a final design of the bridge it is necessary to check for the most critical position in each individual case.

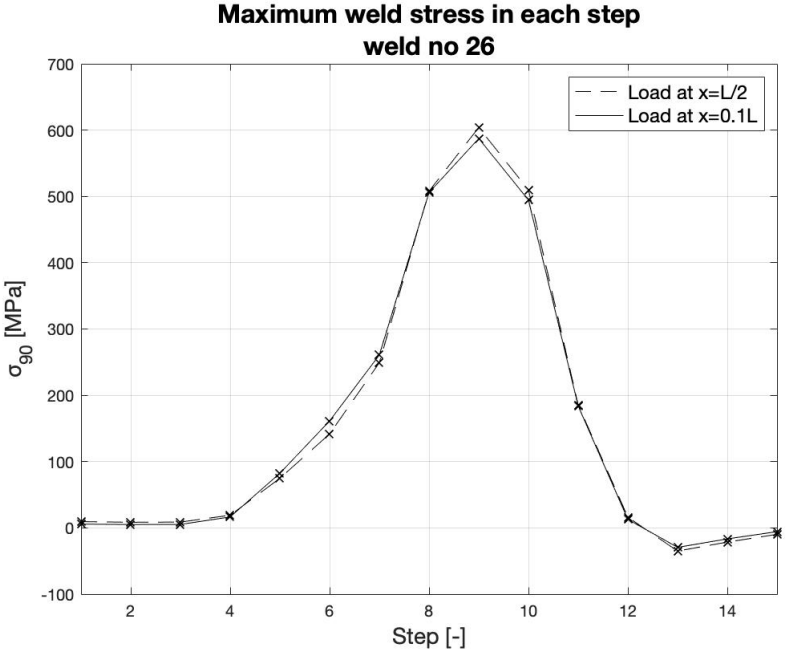

Figure 5.6: *Stress in weld number 26 where the load plates are centered above the weld in step number 8*

5.5 Fatigue assessment

The fatigue assessment in this thesis is based on Eurocode's Damage Accumulation Method as described in Section 2.14.2. The loads are applied according to FLM4 as described in Section 2.9.2 with modifications based on the assumptions made in Section 5.1.

The basis of the evaluation is comparing number of cycles in design and capacity: n_i and N_i, respectively. n_i is the applied number of cycles of each tandem type and position during the bridge's lifetime. N_i is the maximum number of cycles that the bridge can withstand for a specific stress range. It is calculated based on the stress range for each position and each tandem type. The total damage is calculated according to Equation 5.6.

$$D = \sum_i \frac{n_i}{N_i} \leq 1.0 \tag{5.6}$$

5.5.1 Design life

The design life of the bridge considering fatigue life is formulated as the number of cycles that the bridge is subjected to during its lifetime. It is based on the number of heavy vehicles passing over the bridge per year, N_{OBS}.

The chosen traffic category for the fatigue analysis in this thesis is traffic category 2; *Roads and motorways with medium flow rates of lorries* as this is recommended by the according to the National Annex, *Krav Brobyggande* (Trafikverket, 2016, p.76), for smaller road bridges in Sweden. This gives N_{OBS} as below for the CCSSP bridge deck (Eurocode 1991-2, 2003, p.42).

$$N_{OBS} = 0.5 \cdot 10^6 \qquad [cycles/year]$$

The traffic type is chosen as *Regional*, according to the National Annex, *Krav Brobyggande* (Trafikverket, 2016, p.76). This affects the percentage of each lorry type on the bridge.

The distribution of the applied number of cycles, n_i, is based on:

- Percentage of N_{OBS} of each lorry type (40%/10%/30%/15%/5%)
- Percentage of vehicles in each position along the bridge width (7%/18%/50%, as in Figure 2.16)

Finally each position of each tandem type of each lorry type, gets a number of cycles which the capacity must exceed. This results in a total number of load-cycles during the bridge's entire lifetime (100 years).

5.5.2 Capacity

The fatigue capacity is calculated using the worst load case from Section 5.4 for all tandem types. This means that model (1) from Section 5.4 is run in two versions: one using tandem type A from FLM4 and one using tandem type B from FLM4, seen in Figure 5.7. The load applied to each model is described in Table 5.2.

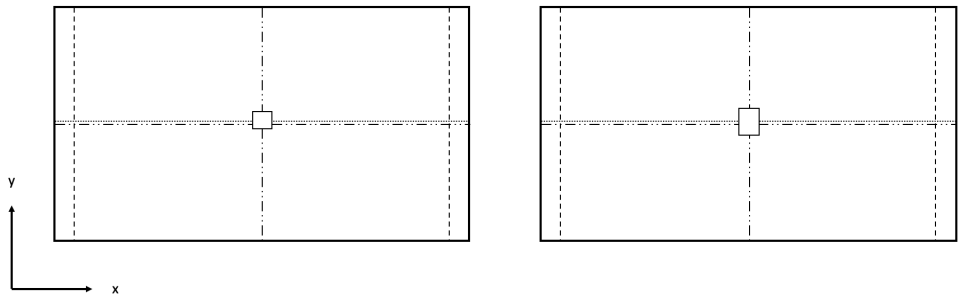

Figure 5.7: *Models used to assess fatigue life with tandem type A (left) and B (right)*

The required output from both models is the spring force P_z and the spring moment M_x used to calculate σ_{90}. The procedure to go from forces to stress described in

Section 5.3 applies. σ_{90} for each tandem type is used as $\Delta\sigma_i$ in Equation 5.9. Because the tandem loads in FLM4 have different magnitudes depending on the lorry type, as described in Figure 2.14, the stress, $\Delta\sigma_i$, is scaled based on the lorry- and tandem type of each cycle.

The load effect from each lorry is divided proportionally between the different positions in transverse direction of the bridge, in accordance with Figure 2.16 in Section 2.9.2. This distribution is seen in Figure 5.8 for model (1) with tandem type A where the middle position with 50% of the lorries is placed at the position of the maximum stress to create the worst possible load situation. This position varies with each cross section and it is important to include enough steps in the transverse direction of the bridge to cover the maximum position and the adjacent percentages, as seen in Figure 5.8.

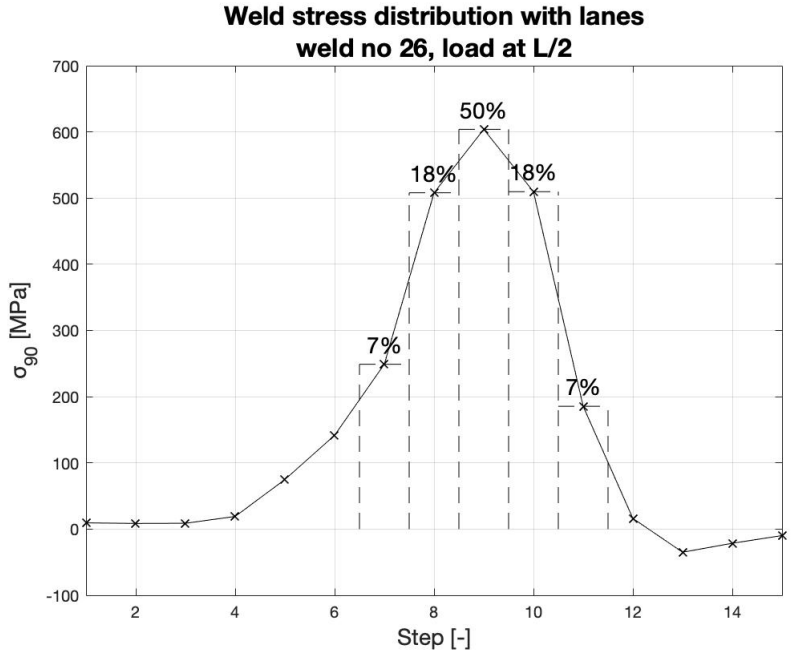

Figure 5.8: *Distribution of percent of lorries in the transverse direction of the bridge with tandem type A*

Based on the detail category, $\Delta\sigma_C = 57MPa$, for weld cracking of a CCSSP (as presented in Section 2.5), the SN-curve is calculated and can be seen in Figure 5.9.

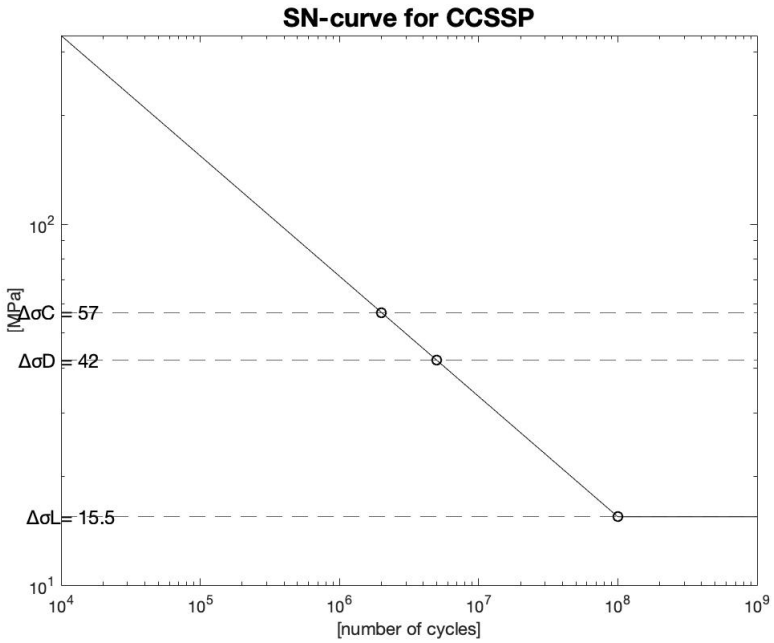

Figure 5.9: *SN-curve for weld cracking of a CCSSP*

$\Delta\sigma_D$ and $\Delta\sigma_L$ are retrieved from Eurocode 1993-1-9 as:

$$\Delta\sigma_D = 0.737\Delta\sigma_C = 42MPa \tag{5.7}$$

$$\Delta\sigma_L = \frac{\Delta\sigma_C}{\left(\frac{10^8}{2\cdot10^6}\right)^{1/3}} = 15.5MPa \tag{5.8}$$

This gives the capacity of each tandem type according to Equation 5.9.

$$N_i = 2 \cdot 10^6 \left(\frac{\Delta\sigma_C/\gamma_{Mf}}{\gamma_{Ff} \cdot \Delta\sigma_i}\right)^3 \tag{5.9}$$

5.5.3 Result of fatigue life

The total fatigue damage done to the bridge during its lifetime is the sum of D_i. If the sum is lower than 1, the fatigue life check is passed. The calculations for this case result in a damage of $D = 51844$ for the most critical weld.

5.6 Discussion

The FLS evaluation is done in a simplified conservative manner to enable the evaluation and to save computational time. The number of cycles that the bridge deck is subjected to during its lifetime has a large impact on the damage, D, and the damage in the tested case becomes large. Because of the significant impact of the number of load cycles on the fatigue damage, simplification 2 has a great impact on

the fatigue damage and makes the tested method conservative.

The results from Section 5.3 showed that σ_{90} is the dominant stress component which verifies simplification 1. It is very concentrated which indicates that simplification 2 is true. This can be related to the results from the linear analysis in Chapter 4.3 which show that the local effects are dominant with respect to the Von Mises stress in the top plate. This shows that the local effects are dominant in both the top plate and the welds in the top plate.

The two tested load cases result in similar stresses which means that it is difficult to predict which load position is critical for other cross section geometries. In turn, both load positions must be tested for each cross section configuration to be sure to capture the fatigue life determinant case.

5.7 Conclusion

The method presented to evaluate FLS is possible to use. The assumptions are verified and the local effects are highly dominant. The method is possible to use in a design program with the simplifications made and will give a conservative result.

6
Design program

In this thesis a design program for a CCSSP is created using Python scripts executed in the software BRIGADE/Plus. The program creates models based on chosen input-parameters and evaluates the CCSSP bridge deck based on the demands stated in Eurocode in SLS, ULS and FLS. The RSM from Chapter 4 is used to evaluate the CCSSP in biaxial compression and the fatigue life is evaluated according to Chapter 5. An outline of the design program can be seen in Figure 6.1. Appendix D shows an overview of all scripts created for the design program. In this chapter the design program is tested on one cross section configuration. This cross section is the same as the one used in Chapters 4 & 5.

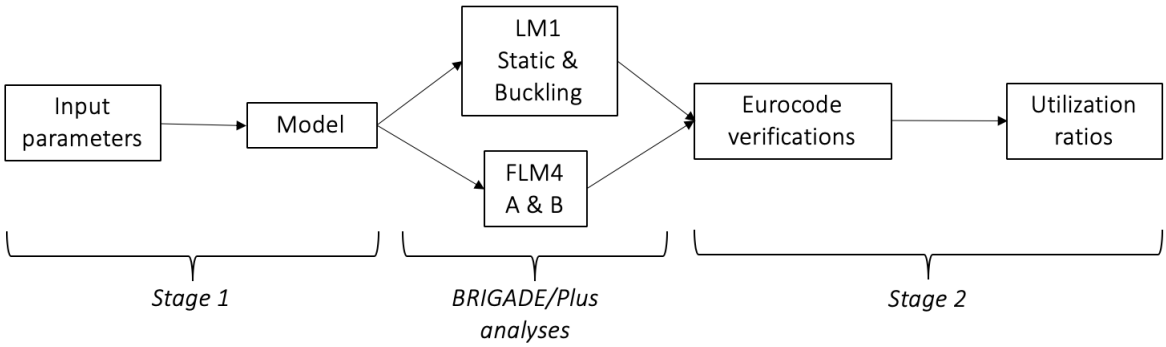

Figure 6.1: *Outline of the design program*

6.1 Input data

The input data for the model is presented in Section 4.1. The springs are modelled as described in Chapter 2.7.4 and presented in Table 6.1.

Table 6.1: *Rotational spring stiffness for the specific case*

$k_{\varphi 1}$	108	*Rotational spring stiffness top plate [kNm/rad]*
$k_{\varphi 2}$	153	*Rotational spring stiffness bottom plate [kNm/rad]*
k_{φ}	10^{11}	*Spring stiffness in all the other springs [kNm/rad]*

6.2 Models and analyses

Four different models are run in the design program. These are:

(1) Model performing linear static analysis with LM1
(2) Model performing linear buckling analysis with LM1
(3) Model performing linear static analysis with FLM4, tandem type A
(4) Model performing linear static analysis with FLM4, tandem type B

Two load positions in the longitudinal direction of the bridge are tested in each model; when the patch loads are centered around the x-coordinate 0.1L and when the patch loads are centered around the x-coordinate L/2. As described in Chapter 4, the local effects dominate the stresses in the CCSSP. Due to this, these two load positions are most relevant. Each of the models above is used to retrieve certain results in order to perform all relevant design-checks according to Eurocode. A summary of all equations used to perform the capacity checks can be found in Appendix E.

6.2.1 Model (1)

Model (1) is used to perform a linear static analysis with loads according to LM1. The modelling conditions of model (1) are the same as described in Chapter 3. There are three steps in model (1).

Step 1 is used to check the capacity of the bridge in ULS. It includes load from surface pavement and traffic load according to LM1 with ULS load combination. The required outputs of this step are:

- Normal stress in all plates
- Shear stress in all plates
- Von Mises stress in all plates
- Weld stresses in the form of spring forces in the springs

The plate stresses are checked using the maximum respective stress in paths I, II and III in Figure 6.2, according to Section 2.12. The top plate of the cross section in case study III is in cross section class 4 and is checked according to the RSM rather than the Von Mises stress. This is done using the stresses from this analysis with the eigenvalue received from model (2), according to Section 2.13.2. The welds are checked with results from step 1 using the maximum stress in each weld. The weld stresses are calculated from the spring forces, and checked according to Section 2.14.

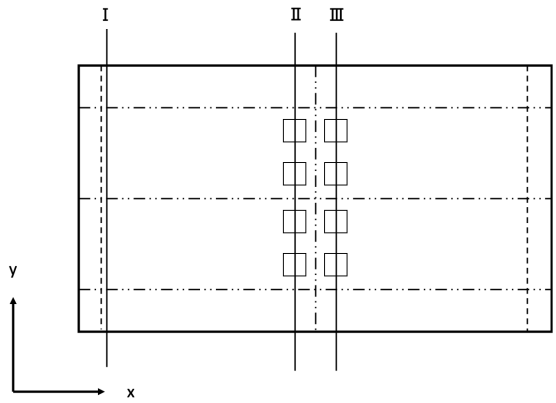

Figure 6.2: *Placement of tandem loads from LM1 in step 1*

Step 2 of model (1) is also used to check the capacity of the bridge in ULS. The same calculations are performed as described for step 1 with the exception that the results of the plate stresses are retrieved in the paths seen in Figure 6.3.

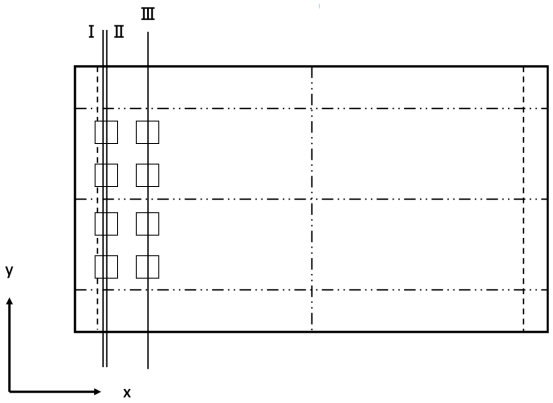

Figure 6.3: *Placement of tandem loads from LM1 in step 2*

Step 3 of model (1) is used to check the capacity of the bridge in SLS. This is done by retrieving the deflection in z-direction of the bottom plate in path I of Figure 6.4. Path II is then created at the position of the maximum deflection in path I. The maximum deflection of the bottom plate in this path is the one used to check the bridge's capacity in SLS according to Section 2.11.

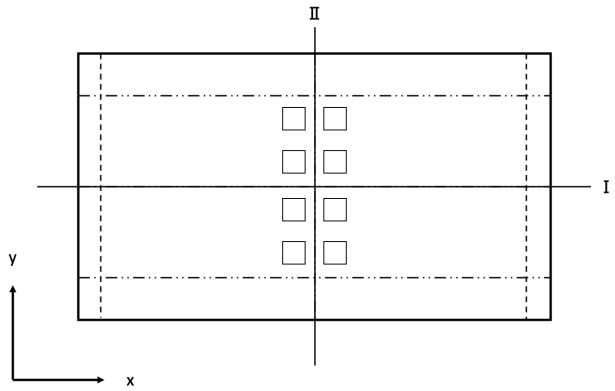

Figure 6.4: *Placement of tandem loads from LM1 in step 3*

6.2.2 Model (2)

Model (2) is used to perform a linear buckling analysis with loads according to LM1. The modelling conditions for model (2) are the same as described in Chapter 3 except for the welds which are modelled as tied. This is done to minimize the run time and result in a conservative value on the eigenvalue λ_{eig}.

Model (2) is run in two steps where the same loads are applied as in steps 1 and 2 in model (1). The output of both steps in model (2) is the eigenvalue (λ_{eig}) of the first eigenmode in each step. This is used to check the capacity of the top plate with respect to the RSM, according to Section 2.13.2.

6.2.3 Model (3)

Model (3) is used to perform a linear static analysis with loads according to FLM4, tandem type A. The modelling conditions of model (3) are the same as described in Chapter 3. Model (3) is run in 15 steps as described in Chapter 5.

The required output from model (3) are the spring forces P_z and M_x in the springs used to model the welds. These give the stress σ_{90} in each weld, according to Section 2.14. This stress is used in combination with model (4) to calculate the fatigue damage in each weld in the top plate.

6.2.4 Model (4)

Model (4) is used to perform a linear static analysis with loads according to FLM4, tandem type B. The modelling conditions of model (4) are the same as described in Chapter 3. Model (4) is run in 15 steps with the same required output as model (3). The output is used in the same way as for model (3) to find the fatigue damage in each weld in the top plate.

6.3 Results from the evaluated case used to test the Design Program

The results for the evaluated configuration used to test the design program in this chapter is presented in terms of URs and fatigue damage for the tested bridge deck. The result of the SLS evaluation can be seen in Table 6.2. Results from the weld checks is illustrated in Figure 6.5 and listed in Table 6.3 and 6.4. Only the top plate welds are presented as they are the only welds with URs over 100%. The fatigue evaluation is done with the load positioned at L/2 as this was the worst position for this configuration as Figure 5.6 illustrates. Finally, the stresses and corresponding URs in the top plate, bottom plate and the core can be seen in Tables 6.5 and 6.6.

Table 6.2: *Result from the SLS evaluation*

Deflection [mm]	η [%]
4.5	186

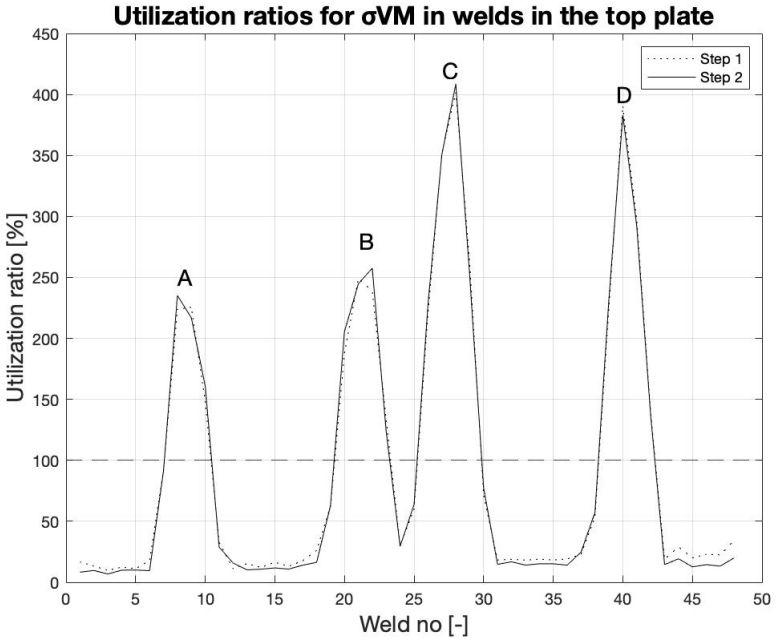

Figure 6.5: *URs for welds in the top plate in step 1 and step 2 of model (1) (A-D represent the patch loads in the transverse direction of the bridge)*

Table 6.3: *Weld URs over 100% in the top plate*

Patch load	Weld no	η [%]	
		Step 1	Step 2
A	7	223	234
	8	226	217
	9	148	161
B	19	188	205
	20	249	245
	21	239	258
	22	133	124
C	25	220	227
	26	354	350
	27	401	409
	28	261	251
D	38	226	232
	39	390	383
	40	297	292
	41	139	137

Table 6.4: *Damage in welds where fatigue life is not 0.0*

Weld no	D [-]
21	0.1
22	3
23	207
24	5569
25	21172
26	51844
27	42174
28	9124
29	1463
30	31
31	0.96

Table 6.5: *URs for the tested bridge in ULS with load placement 1 (centre)*

		Description	Magnitude [MPa]	Ratio [%]
Top plate	Path I	σ_x	15	4
		σ_y	41	11
		τ	18	9
		RSM	-	12
	Path II	σ_x	338	95
		σ_y	400	113
		τ	47	23
		RSM	-	160
	Path III	σ_x	339	95
		σ_y	400	113
		τ	55	27
		RSM	-	163
Bottom plate	Path I	σ_x	98	28
		σ_y	180	51
		τ	76	37
		σ_{VM}	201	57
	Path II	σ_x	275	78
		σ_y	123	35
		τ	13	6
		σ_{VM}	251	71
	Path III	σ_x	276	78
		σ_y	122	34
		τ	19	9
		σ_{VM}	250	71
Core	Path I	σ_x	118	33
		σ_y	82	23
		τ	62	30
		σ_{VM}	132	37
	Path II	σ_x	282	79
		σ_y	277	78
		τ	50	24
		σ_{VM}	313	88
	Path III	σ_x	283	80
		σ_y	271	76
		τ	51	25
		σ_{VM}	313	88

Table 6.6: *URs for the tested bridge in ULS with load placement 2 (at support)*

		Description	Magnitude [MPa]	Ratio [%]
Top plate	Path I	σ_x	136	38
		σ_y	434	122
		τ	38	19
		RSM	-	158
	Path II	σ_x	128	36
		σ_y	457	129
		τ	27	13
		RSM	-	273
	Path III	σ_x	208	59
		σ_y	441	124
		τ	31	15
		RSM	-	153
Bottom plate	Path I	σ_x	270	76
		σ_y	177	50
		τ	109	53
		σ_{VM}	242	68
	Path II	σ_x	40	11
		σ_y	42	12
		τ	30	14
		σ_{VM}	59	17
	Path III	σ_x	124	35
		σ_y	81	23
		τ	18	9
		σ_{VM}	112	32
Core	Path I	σ_x	358	101
		σ_y	232	65
		τ	205	100
		σ_{VM}	387	109
	Path II	σ_x	95	27
		σ_y	252	71
		τ	41	20
		σ_{VM}	231	65
	Path III	σ_x	166	47
		σ_y	265	75
		τ	31	15
		σ_{VM}	238	67

6.4 Discussion

The results from the evaluation of a CCSSP show that the URs for the tested cross section are high when it comes to weld stresses in ULS and FLS, especially in FLS. The RSM also gives high URs in the top plate, which is expected as the method is conservative.

The design program enables a full capacity check of a CCSSP used as a simply supported bridge deck as requested. This program can be used to perform an optimization of this type of bridge. To enable the optimization, it is important that the parameters included in this type of study as possible cross section dimensions are close to a solution that actually fulfils all the demands. A parametric study is a useful way to gain understanding about how the cross section parameters influence the URs calculated in the design program and in turn find a solution closer to fulfilling all the demands. Based on this case, it is especially interesting to investigate the influence of the different cross section parameters on the weld stresses in order to understand what influences the fatigue life of the CCSSP bridge deck.

6.5 Conclusion

A full capacity check can be performed with the created design program. However, the tested case has very high URs in some areas. A parametric study is beneficial for better understanding of the influence of the different cross section parameters. Especially the weld stress is an interesting parameter to study.

7
Parametric study

The design program finalized in Chapter 6 is used to perform a parametric study of the CCSSP used as a simply supported bridge deck. The aim of the parametric study is to gain knowledge about how different parameters impact the response of a CCSSP. The focus of the study is to evaluate how to reduce the weld stresses. This is important to enable an optimization of a CCSSP in the future.

7.1 Fractional Factorial Design

Resolution IV Fractional Factorial Design, described in Section 2.15.1, is used to perform a parametric study in order to gain knowledge regarding how different independent parameters impact the response of a CCSSP with respect to some dependent parameters. In the FFD, the weld width is kept to $a = 2mm$ and the horizontal part of the core, f_1 & f_2 are kept to:

$$f_1 = dw_1 + 2 \cdot 0.015m$$

$$f_2 = dw_2 + 2 \cdot 0.015m$$

7.1.1 Independent parameters

The following parameters are included in the FFD:

- t_1 - Thickness of bottom plate
- t_2 - Thickness of top plate
- t_c - Thickness of core plate
- h - Height of the bridge deck
- Θ - Corrugation angle
- dw_1 - Distance between welds bottom plate
- dw_2 - Distance between welds top plate
- R - Radius of corrugation ($R_1 = R_2 = R$)

The values used for the independent parameters are presented in Table 7.1. The mid value is used as a start value and the low/high are ± 20% from that value. Resolution IV FFD with 8 independent parameters of two levels per parameter (low/high) generates a matrix which specifies 16 different cross section configurations. These are presented in Table 7.2. All models have a length of $10m$, a span of $L = 9.6m$ and a width $B \approx 7m$ depending on the cell width of each model.

Table 7.1: *Independent parameters included in the FFD and their low/high values*

Parameter	Low (-1)	Mid	High (1)
t_1 [mm]	4	6	8
t_2 [mm]	8	10	12
t_c [mm]	4	6	8
h [mm]	240	300	360
Θ [°]	60	75	90
dw_1 [mm]	24	30	36
dw_2 [mm]	24	30	26
R [mm]	13	16	19

Table 7.2: *Models included in the FFD of resolution IV*

Model	t_1 [mm]	t_2 [mm]	t_c [mm]	h [mm]	Θ [°]	dw_1 [mm]	dw_2 [mm]	R [mm]
1	4	8	8	240	60	24	24	13
2	4	8	8	360	90	36	36	13
3	4	8	10	240	90	36	24	19
4	4	8	10	360	60	24	36	19
5	4	12	8	240	90	24	36	19
6	4	12	8	360	60	36	24	19
7	4	12	10	240	60	36	36	13
8	4	12	10	360	90	24	24	13
9	6	8	8	240	60	36	36	19
10	6	8	8	360	90	24	24	19
11	6	8	10	240	90	24	36	13
12	6	8	10	360	60	36	24	13
13	6	12	8	240	90	36	24	13
14	6	12	8	360	60	24	36	13
15	6	12	10	240	60	24	24	19
16	6	12	10	360	90	36	36	19

7.1.2 Dependent parameters

The dependent parameters in the FFD are the UR for the deflection in SLS and the UR of the most stressed weld in ULS. The UR in SLS is mainly influenced by the global behaviour of the CCSSP bridge deck. The weld- and plate stresses in ULS are mainly influenced by the local behaviour of the CCSSP bridge deck.

7.1.3 Result from FFD

The result from the analyses of the 16 runs included in the FFD are presented in this section. In Table 7.3 the URs for the dependant parameters are presented for each run. Figures 7.1, 7.2 and 7.3 show the influence of the independent parameters on the dependent parameters. The independent parameters with a steeper slope has a larger influence on the dependent parameters than those with a slope closer to zero. If the slope is positive, it means that increasing the independent parameter increases the UR. If the slope is negative it means that increasing the independent parameter reduces the UR.

Table 7.3: *Dependent parameters: URs for each model*

Model	SLS [%]	Top weld [%]	Bottom weld [%]
1	143	469	92
2	56	178	92
3	114	138	67
4	66	989	152
5	115	137	76
6	65	522	249
7	123	332	91
8	44	60	39
9	132	766	200
10	53	169	93
11	105	120	31
12	57	746	175
13	103	86	73
14	54	544	154
15	114	280	72
16	44	119	90

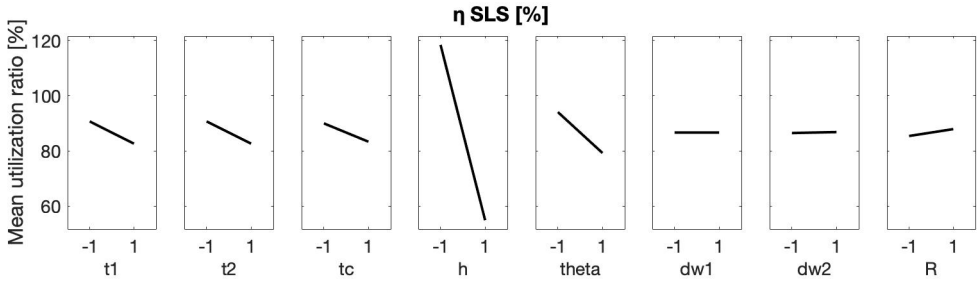

Figure 7.1: *Influence of tested parameters on the UR of the deflection in SLS due to main effects*

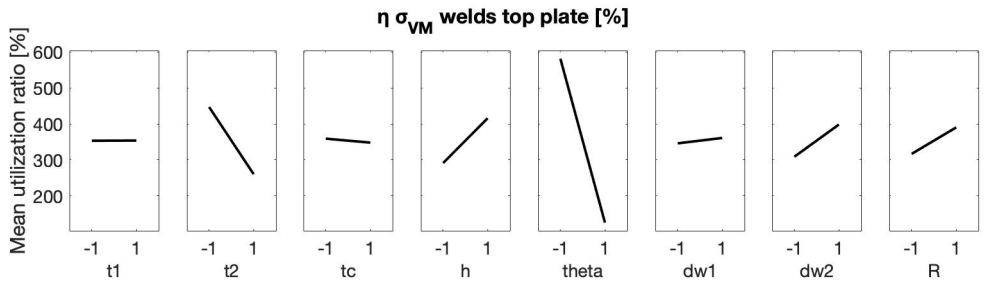

Figure 7.2: *Influence of tested parameters on the UR of the Von Mises stress in the welds in the top plate to core due to main effects*

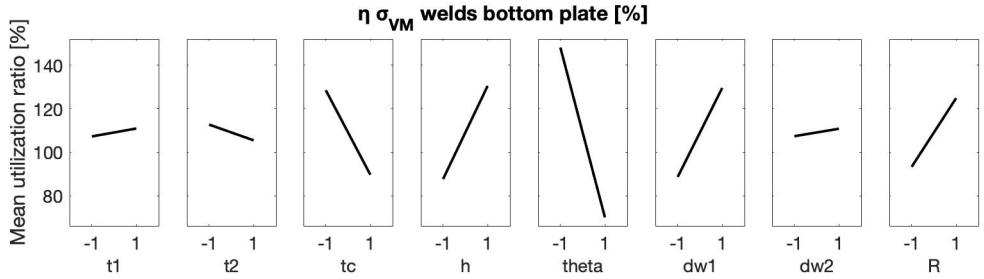

Figure 7.3: *Influence of tested parameters on the UR of the Von Mises stress in the welds in the bottom plate to core due to main effects*

7.2 Study of fatigue damage

As seen in the result from the FFD, solution number 8 has URs below 100% in the three dependent parameters. Solution number 8 is therefore modified using the knowledge of how certain parameters impact the response of the CCSSP, which results in three new solutions that are presented in Table 7.4. The aim of these solutions is to find a configuration that results in lower fatigue damage. This is done by increasing the plate thicknesses and/or reducing the cell width, $2p$, which places more welds beneath the load plates and distributes the load. The cell width, $2p$, can be reduced either by reducing the height of the cross section or by increasing the angle of the corrugation. When the height is reduced, the bending stiffness of the plate decreases. This is compensated by increasing the plate thicknesses. An additional parameter that is investigated is the influence of the weld width which has previously been set to 2mm in all models.

Table 7.4: *Configurations of the modified cross section solutions*

Model	t_1 [mm]	t_2 [mm]	t_c [mm]	h [mm]	Θ [°]	dw_1 [mm]	dw_2 [mm]	R [mm]	$2p$ [mm]
1	4	14	10	300	85	24	24	13	205
2	6	16	10	280	80	24	24	13	243
3	10	16	6	240	80	24	24	12	226

7.2.1 Fatigue life of the modified cross section solutions

The fatigue life is calculated for each modified solution the results are presented in Table 7.5. For this investigation the loads are placed at L/2. The results show that the fatigue damage is still high.

Table 7.5: *Maximum fatigue damage for each of the models in Table 7.4*

Model	D [-]
1	409
2	525
3	2545

The final investigation in the parametric study is to modify the weld width from 2mm to 4mm and 6mm. This is done for Model 1, illustrated in Figure 7.4, with the lowest damage out of the three modified cross section solutions and a total weight of approximately 30 tons. The results are presented in Table 7.6 and shown in Figure 7.5.

Figure 7.4: *Illustration of the cross section configuration of Model 1*

Table 7.6: *Maximum fatigue damage for Model 1 in Table 7.4 after changing the weld width to 4mm and 6mm*

Weld width [mm]	D [-]
2	409
4	28
6	15

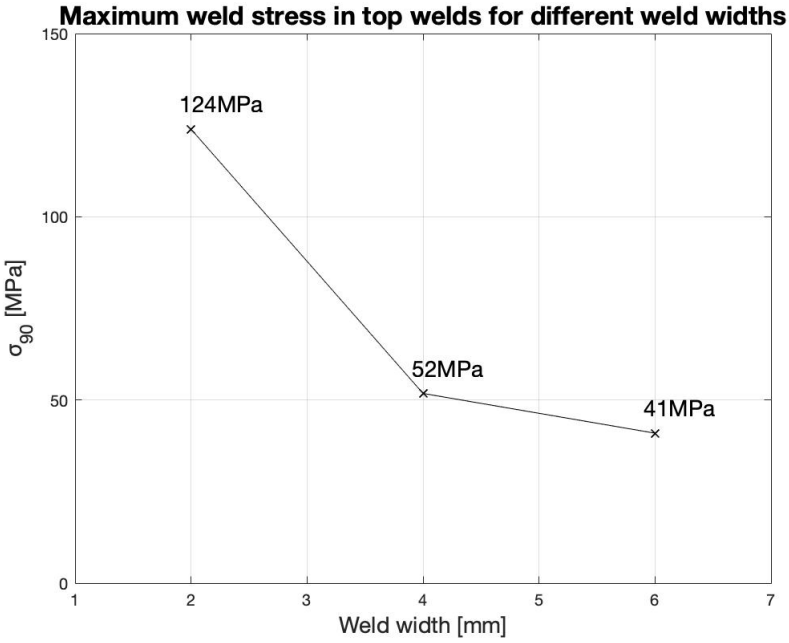

Figure 7.5: *Maximum stress, σ_{90}, in any weld at the three tested weld widths*

7.2.2 Scaling of the fatigue stress

Figure 7.5 shows that reducing the weld width to 4mm has a large influence on the fatigue damage of the CCSSP bridge deck. However, the damage is still higher than allowed. An investigation is performed to find out how much the applied stress in the weld, $\Delta\sigma_i$, must be reduced in order to get a fatigue damage below 1. This investigation is performed using Equation 7.1 on the results from the FE-analysis performed for the actual case using a 4mm wide weld, which gives a damage of 2 when unscaled.

$$(1 - \beta) \cdot \Delta\sigma_i \tag{7.1}$$

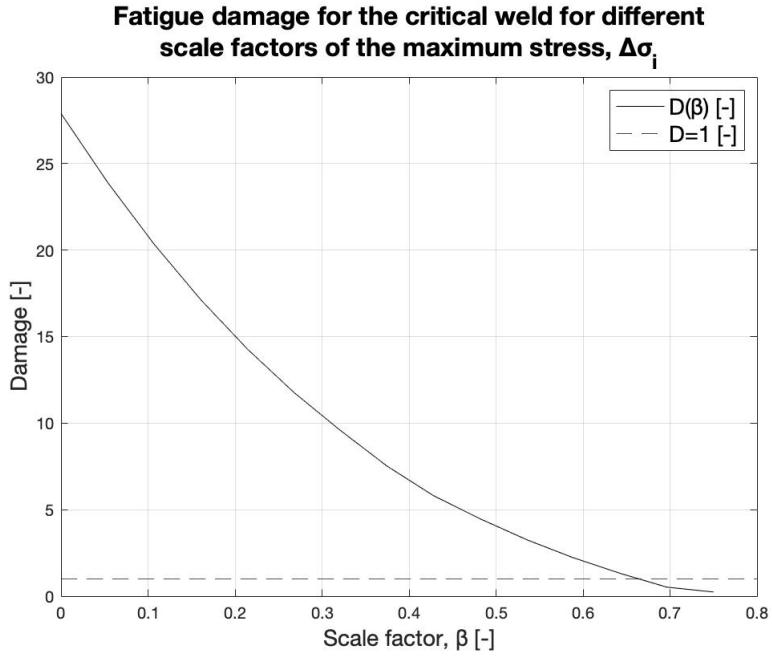

Figure 7.6: *Maximum stress, σ_{90}, in any weld at the three tested weld widths*

As Figure 7.6 shows, the applied fatigue stress in the critical weld when using a weld width of 4mm must be reduced with 67% in order to retrieve a damage below 1.

7.3 Discussion

The parametric study gives an indication of how certain parameters affect the response of a CCSSP for the studied cases.

7.3.1 SLS response

The UR in SLS is calculated from the deflection of the CCSSP bridge deck. The deflection is influenced by the bending stiffness of the CCSSP which in turn is influenced by the moment of inertia of the cross section.

Figure 7.1 shows that the most influential parameter with respect to the UR in SLS is the height of the cross section. An increased height, result in an increased distance from the center of gravity of the top and bottom plate, it also result in a higher core. This increases the moment of inertia for the cross-section. Figure 7.1 also shows that the thicknesses of the plates have an influence on the UR in SLS. This is because thicker plates result in an increased moment of inertia and in turn reduces the UR.

The core angle and the core radius have some influence on the UR in SLS while the weld distances, dw_1 & dw_2, do not influence the UR in SLS at all. A reduced cell width, $2p$, results in more cells in the cross section of the CCSSP for the same bridge deck width. In turn this results in a higher number of angled parts in the

core which contributes to the moment of inertia and increases the bending stiffness. The cell width is decreased by choosing a higher angle, Θ, decreasing the radius R and decreasing the weld distance dw_1 and dw_2. However, the weld distances do not influence the UR in SLS according to Figure 7.1. This is likely because an increased weld distance also increases the horizontal part of the cross section which in itself also contributes to the bending stiffness.

7.3.2 ULS response in the welds

The URs of the welds in ULS are calculated by comparing the Von Mises stress in the weld with its capacity, f_u. The Von Mises stress in a weld is calculated from σ_{90}, τ_{90} and τ_0. These components are influenced by two main parameters; the stiffness of the weld, calculated for each case using Equation 2.3 described in Section 2.7.4, and the magnitude of the bending moment over the welds, which is the dominant load effect. The spring stiffness depends on the thickness of the top- and bottom plates, the weld width and the gap height (distance between the center position of the top/bottom plate to the center of the core plate). The bending moment over the welds is influenced by the local span length in the top plate, which in turn is influenced by the width of the cells, $2p$.

Figures 7.2 and 7.3 show that the parameter that influences the Von Mises stress the most in both the top and bottom welds is the corrugation angle, θ. A higher θ, results in a smaller cell width, $2p$, which results in a shorter span beneath the load plates. A lower height also reduces the UR in the welds in ULS. This is because a lower height reduces the width of the angled part of the core and in turn the cell width. The parameters dw_1, dw_2 and R also influence the weld stress by influencing the cell width.

There is a difference in the influence of the different parameters on the URs of the welds in the top and bottom plates. Note that the scale in Figure 7.2 and 7.3 is different. In general, the UR in the bottom plate is less influenced by all parameters than the utilization ratio in the top plate. This is because the UR of the welds is mostly affected by the local effects from the patch loads which are applied to the top plate. The weld distance dw_1 has a larger influence on the UR of the welds in the bottom plate than the weld distance dw_2 has on the UR of the welds in the top plate, in relation to the other parameters. The reason is likely because the bending moment over the weld pair in the bottom plate is more increased with an increased weld distance in the bottom plate than in the top plate because the bottom plate generally has a lower thickness than the top plate.

7.3.3 Fatigue life investigation

From the FFD, it is concluded that the cell width, $2p$, has a large influence on the weld stresses and a lower cell width gives lower URs in the welds in ULS. This is used when choosing the modified cross sections and calculating their fatigue damage based on the assumption that the weld stress in ULS and FLS are influenced

in a similar way. The fatigue damage is hard to predict since it is not based on a maximum stress in a weld, but a sum based on every stress above the cut-off-limit. A large difference in the damage does not always correlate to much higher stresses when comparing two cases. It is a combination of every stress above the cut-off-limit per cycle and the magnitude of those stresses that give the final damage. Because the fatigue damage is a summation of the damages of all cycles, it is sensitive to small changes in the stress of each cycle.

An aspect to consider when comparing the UR of the welds in ULS with the fatigue damage in FLS is that the ULS control uses the Von Mises stress with all three stress components, σ_{90}, τ_0 and τ_{90} (where σ_{90} is dominant) while the FLS control only considers σ_{90}. As seen in Chapter 5 in Figure 5.4, σ_{90} in the fatigue model is mainly influenced by the bending moment M_x in the springs. Both τ_0 and τ_{90}, however, are calculated only with the spring forces in x- and y-direction. This means that parameters which have a high impact on the bending moment in the springs have a greater effect on the fatigue damage than on the UR in the welds in ULS.

As the results in Table 7.6 indicate, the weld width has a large impact on the fatigue life. The damage is significantly reduced when increasing the width from 2mm-4mm. With an increase from 4mm-6mm the impact is smaller. When the weld width is increased, the rotational spring stiffness in the FE-model is increased. An increase in the rotational spring stiffness results in higher forces in the spring. In turn this results in a higher risk for fatigue damage. On the other hand, the area, A_{weld} of the weld and the section modulus of the weld, W_{weld} is increased when the weld width is increased. This results in lower stresses than for smaller welds, which is positive with respect to the fatigue damage.

Another indication from Table 7.6 and Figure 7.5 is that it is more efficient to change the weld width from 2mm to 4mm than from 4mm to 6mm. Both the weld stress and damage is reduced more between 2mm to 4mm than between 4mm and 6mm. Because laser welding is a high energy density process, it can also be difficult to increase the weld width above certain widths as it requires vast amounts of energy. Therefore, it is more relevant to look at the weld stresses and fatigue damage when the weld width of 4mm is used. Figure 7.6 shows that in order to achieve a damage below 1 for model 1 in Table 7.4 with a weld width of 4mm it is necessary to reduce the weld stresses by 67%.

Another aspect to consider in terms of the welded areas is whether or not to include contact between the top/bottom plates and the core. In this thesis contact is not considered which has an impact on the weld stresses, as mentioned in Section 2.7.4. Based on the conclusions made by Nilsson et al. (2017b) contact yields a significant stress decrease in the weld, as mentioned in Section 2.7.4. This stress decrease is high enough to reduce the stress by the 67% necessary in this case.

7.4 Conclusions

The parametric study shows that parameters which influence the cell width, $2p$, have a large influence on both the UR in SLS and on the UR of the Von Mises stress in the welds in ULS. In general, a lower cell width results in lower URs. In SLS, a larger cross section height contributes most to reducing the UR out of all the tested parameters. For the weld stresses in ULS, thicker plates generally result in lower UR. In FLS, the weld width highly affects the damage in the welds. A wider weld results in a smaller damage D.

8

Discussion

The investigations in this thesis show that the tested cross sections of the CCSSP bridge deck fulfill most of the controls according to Eurocode. The tested cross sections have geometries that are realistic to use as bridge decks, such as a relatively low height. It is shown that the necessary reduction of the fatigue relevant stresses can be achieved by considering contact in the weld region. The studied cases in the thesis have a total length of 10 meters. However, shorter lengths would reduce all URs. In summation, this indicates that the CCSSP is a potential solution for a bridge deck.

As the investigations for the specific cases in Chapter 7 show, the welds width and plate thicknesses influence the fatigue life. When performing the investigations in this thesis, the measurements for these parameters have been kept as realistic values which are possible to produce. There is a possibility that increasing these values even more can facilitate lighter decks. When doing this it is important to keep in mind that the welding process of the CCSSP limits the thickness of both the welds and the plates. In order for the CCSSP to be a potential solution for a bridge deck, it is crucial that the controls can be fulfilled within these limits.

This thesis does not consider contact in the weld region. This is because it is difficult to ensure that there is no gap between the face plates and the core, when producing the CCSSP. Research has shown, however, that considering contact can reduce the fatigue relevant stresses significantly. As these stresses are shown to be critical in this thesis, it is of high relevance to investigate a possible way to account for contact in the design program.

8.1 Impact of modelling conditions on the results

When using a FE-software such as BRIGADE/Plus, it is important to have knowledge about how certain choices impact the response and to verify the model. This is done both globally and locally in Section 3.9.

8.1.1 Global verification of deflection

The global deflection verified in Section 3.9 results in a good correlation between hand calculations and FE-results with 1% difference. In the verification, the welds are modelled as tied to simplify the calculations of the stiffness of the plate. As the result becomes similar, it is concluded that the bridge deck behaves as intended globally.

8.1.2 Local verification using load plates

The design program uses load plates as a solution to model the tandem loads. As presented in Section 3.9, the solution correlates well with a solution using partitions but with a small difference of approximately 2% that is non conservative. This is important to have in mind when using the design program. The reason that the load plates result in non conservative results is most likely due to the ties at the boundaries between the load plate and the top plate. Each node in the load plate ties to the closest node in the top plate. Sometimes the tie is created with a node that is not located directly under the load plate. This results in a larger area for the load to distribute on and hence a non conservative result. However, the solution using load plates enables a simple way of moving the tandems which motivates the usage of load plates.

8.2 Impact of assumptions and simplifications

When creating the design program, some choices and simplifications are made which affects the results from the design program. Both the RSM and the FLS evaluation methods are conservative ways of verifying their respective capacities. As a result, a CCSSP bridge deck designed using this design program is overdimensioned in terms of the risk of buckling due to biaxial compression and in the fatigue damage of the welds. As the fatigue damage is critical in all cases tested in this thesis, it is especially relevant to keep in mind that this evaluation is conservative. It is not possible to say that it is equally critical for other cross sections as this thesis only covers some configurations. However, based on the results from this thesis it is relevant to investigate if there is a less conservative way to perform the FLS evaluation of the CCSSP bridge deck. The reason why such an investigation is not performed in this thesis is mainly because the presented evaluation method enables a relatively short analysis time which means that it is possible to use the design program to perform an optimization of the CCSSP bridge deck.

8.3 FFD results

Resolution IV in the FFD is used in this thesis as a way of performing the parametric study. With resolution IV, all main effects can be investigated, as described in Section 2.15.1. However, some two-factor interaction is confounded by other two-factor interaction. This means that in order to get a full understanding of the impact of

the two- or three-factor interaction effects from the cross section parameters on the investigated dependent parameters, it is necessary to perform higher resolution- or full factorial design. This, however, does not mean that the results in this thesis are not useful. Figures 7.1, 7.2 7.3 describe the main effects of the independent cross section parameters on the dependent parameters. These effects are not confounded by any other effects when using resolution IV.

The cross section configuration which is chosen as starting values only generates results within a domain close to the chosen geometry. The conclusions drawn based on the FFD does therefore only apply to the studied cases. In reality, however, the impact of the cross section parameters on the behaviour of the CCSSP may look different with geometries that are more unlike the ones studied in this thesis. This is illustrated in Figure 8.1 which shows the entire domain of all theoretical cross sections of a CCSSP bridge and illustrates the theoretically small subdomain of cross sections studied in this thesis.

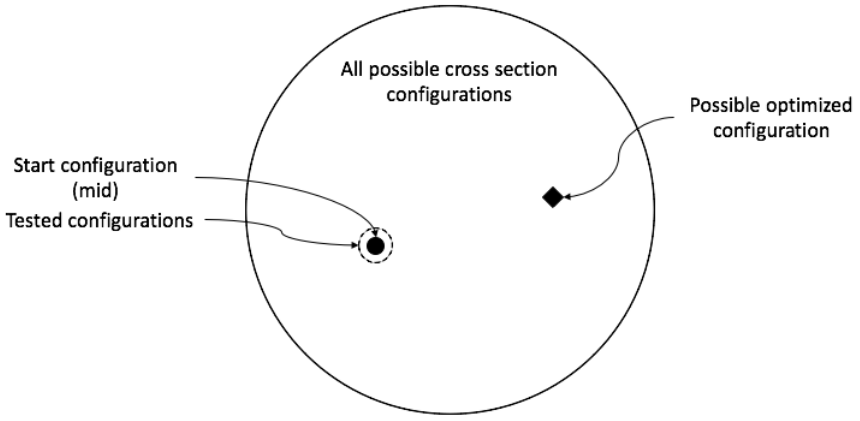

Figure 8.1: *Illustration of the tested subdomain vs. the full domain*

This thesis was not able to present a geometry which fulfils all the demands. In particular the fatigue damage has remained high through all tests. Considering the aspect that there might be other CCSSP bridge deck cross sections which are impacted differently than those studied in this case, this may also mean that with other geometries in another area of the entire domain the fatigue damage might not be critical. The same applies when using the design program to perform an optimization of the CCSSP bridge deck. In this case, the optimal solution may be far away from the studied subdomain. This is also illustrated in Figure 8.1.

8.4 Future optimization using the design program

The design program created in the thesis, enables an optimization of a CCSSP in future studies. It would be of interest to find an optimized cross section configuration of a simply supported CCSSP in order to compare it to a concrete or timber deck with the same dimensions. Especially concrete as it is the most common material on the market today and it is known for its large CO_2-emissions and relatively low

price. The interesting aspects to investigate could be the total weight of the bridge deck, total cost and total CO_2 emissions for example.

The investigations in Chapter 7 show that a narrow cell width is positive with respect to both the UR in SLS and the UR of the welds in ULS for the testes cases. However, a narrow cell width results in a higher mass of the CCSSP bridge deck which is negative when making a comparison between a CCSSP and other alternatives.

9
Conclusion

The design program using Python scripting and BRIGADE/Plus created in the thesis (described in Chapter 6) performs a full capacity check for a CCSSP. The design program calculates the UR in SLS, ULS and the fatigue damage in FLS. From the work in this thesis, which is based on the developed design program, the following can be concluded:

- Local load effects from the patch loads are the most critical loads for a simply supported short span CCSSP.
- The RSM is conservative for a CCSSP bridge deck and can be used in the design program according to Chapter 4.
- The FLS evaluation method presented in Chapter 5 is verified and can be used in the design program.

The parametric study, presented in Chapter 7, shows that for the studied cases, the UR in SLS is decreased when increasing the height, h, and by parameters which reduce the cell width, $2p$. The UR of the Von Mises stress in the welds in ULS is decreased by parameters which reduce the cell width, $2p$, and by increasing the plate thicknesses. The fatigue damage in the welds, D, is decreased by increasing the weld width, a. The required reduction of fatigue relevant stresses can be fulfilled by considering contact in the weld region.

As a final conclusion, this thesis indicates that a CCSSP can be used as a simply supported bridge deck. Performing an optimization or considering contact in the weld region could confirm this. However, it should be compared to other alternatives on the market, such as concrete or timber bridge decks, in order to determine of it is a competitive solution. Possible areas of investigation are cost and CO_2 impact.

9.1 Future studies

With the aim and limitations stated in the thesis, some areas are not covered and could be of interest to study in the future. These are to:

- Investigate if there is a less conservative method than the RSM to evaluate biaxial compression of the CCSSP bridge deck.
- Investigate if there is a way of verifying the FLS of the CCSSP in a less conservative manner than the method used in this thesis.
- Use the design program produced in this thesis to find an optimal design of the CCSSP for a chosen situation
- Investigate and make a thorough comparison between a concrete-, timber- and CCSSP bridge deck. This is of high interest to draw a conclusion regarding if the CCSSP solution is useful for short span bridges. The comparison could for instance involve emissions of CO_2 and total cost to produce.
- Investigate how to consider contact between the core and face plates in the weld region in the design program of the CCSSP bridge deck.

References

Alwan, U. L. a., & Järve, D. (2005). *New Concept for Industrial Bridge Construction*. Chalmers University of Technology. doi:10.1016/S1097-8690(05)71972-7

Araghi, S. N., & Shanmugam, N. E. (2012). Strength of biaxially loaded orthotropic plates. *Thin-Walled Structures*, *53*, 40–47. doi:10.1016/j.tws.2011.12.016

Beneus, E., & Koc, I. (2014). *Innovative road bridges with steel sandwich decks*. Chalmers university of Technology.

Bickel, P., Diggle, P., Fienberg, S., Gather, U., Olkin, I., & Zeger, S. (2006). *A Modern Theory of Factorial Designs*. doi:10.1007/0-387-37344-6

Blaauwendraad, J. (2010). *Plates and FEM*.

Bright, S., & Smith, J. (2007). A new design for steel bridge decks using laser fabrication. *85*, 49–57.

Caccese, V., & Yorulmaz, S. (2009). Laser Welded Steel Sandwich Panel Bridge Deck Development: Finite Element Analysis and Stake Weld Strength Tests.

Chen, W.-F., & Duan, L. (2014). *Bridge Engineering Handbook: Construction and Maintenance* (Second Edi).

Davies, J. M. (1993). Sandwich panels. *Thin-Walled Structures*, *16*(1-4), 179–198. doi:10.1016/0263-8231(93)90044-B

Det Norske Veritas. (2002). *Buckling strength of plated structures, Recommended practice DNV-RPC201* (technical report Number OCTOBER). Høvik, Norway. Retrieved from http://davidmuir.com/offshore/ODB/Norwegian_Codes/RP-C201.pdf

Difs, J. O. N., & Ro, A. (2017). Multi-scale modelling of corrugated core steel sandwich panels subjected to out- of-plane loads.

Al-Emrani, M., & Åkesson, B. (2013). *Steel Structures*. Gothenburg.

Eurocode 1990. (2002). 1990: Basis of structural design.

Eurocode 1991-1-1. (2011). 1991-1-1: Actions on structures - Part 1-1: General actions - Densities, self-weight, imposed loads for buildings.

Eurocode 1991-2. (2003). 1991-2: Actions on structures - Part 2: Traffic loads on bridges.

Eurocode 1993-1-1. (2005). Eurocode 1991-1-1: General rules and rules for buildings.

Eurocode 1993-1-5. (2006). 1993-1-5: Design of steel structures - General rules - Plated structural elements.

Eurocode 1993-1-8. (2005). EN 1993-1-8: Design of steel structures - Design of joints.

Eurocode 1993-1-9. (2005). Eurocode 1993-1-9: Design of steel structures - Fatigue.

Eurocode 1993-2. (2006). 1993-2: Design of steel structures - Part 2: Steel bridges.

Frank, D. (2014). *Fatigue strength assessment of laser stake welds in web-core steel sandwich panels* (Doctoral dissertation, Aalto University).

Fricke, W., Robert, C., Peters, R., & Sumpf, A. (2016). Fatigue strength of laser-stake welded T-joints subjected to combined axial and shear loads. *Weld World*, *60*(March 2016), 593–604. doi:https://doi-org.proxy.lib.chalmers.se/10.1007/s40194-016-0322-z

Giroux, L., & Easterling, W. S. (1993). Shear Lag Effect in Steel Tension Members. *Engineering Journal / American Institute of Steel Construction*, *30*.

Libove, C., & Hubka, R. E. (1951). *Elastic constants for corrugated-core sandwich plates*. NACA TV 2289.

Liu, G., & Quek, S. (2014). FEM for 3D Solid Elements. In *The finite element method* (Pages 249–287). doi:10.1016/b978-0-08-098356-1.00009-6

Mensinger, M., Feldmann, M., Sedlacek, G., Naumes, J., Ndogmo, J., Kuhlmann, U., & Braun, B. (2009). Buckling verification according to Eurocode 3 - Part 1.5: Amelioration of the stress limit approach.

Ndogmo, J., Mensinger, M., & Both, I. (2016). Buckling Behaviour of Stiffened Plate Under Biaxial Compression and Shear. *Procedia Engineering*, *156*(12), 272–279. doi:10.1016/j.proeng.2016.08.297

Nilsson, P. (2015). *Steel-sandwich elements in bridge applications*. Chalmers University of Technology. Gothenburg.

Nilsson, P. (2017). *Laser-welded corrugated core steel sandwich panels for bridge application*. Chalmers University of Technology. Gothenburg.

Nilsson, P. (2020). *Laser-welded corrugated core steel sandwich panels for bridge application*.

Nilsson, P., Atashipour, S. R., & Al-Emrani, M. (2019). *Corrugated core sandwich panels: numerical modelling strategy for structural analysis*. Chalmers University of Technology. Gothenburg.

Nilsson, P., Al-Emrani, M., & Atashipour, S. R. (2017a). *A numerical approach to the rotational stiffness of stake welds* (technical report Number 13-15). Chalmers University of Technology, Department of Civil and Environmental Engineering, Division of Structural Engineering. Copenhagen.

Nilsson, P., Al-Emrani, M., & Atashipour, S. R. (2017b). Transverse shear stiffness of corrugated core steel sandwich panels with dual weld lines. *Thin-Walled Structures*, *117*(December 2016), 98–112. doi:10.1016/j.tws.2017.04.008

Nilsson, P., Al-Emrani, M., & Atashipour, S. R. (2020). Fatigue-strength assessment of laser welds in corrugated core steel sandwich panels. *Journal of Constructional Steel Research*, *164*, 105797. doi:10.1016/j.jcsr.2019.105797

Nilsson, P., Hedegård, J., Al-Emrani, M., & Atashipour, S. R. (2019). The impact of production-dependent geometric properties on fatigue-relevant stresses in laser-welded corrugated core steel sandwich panels. *Welding in the World, Le Soudage Dans Le Monde, 63(6): 1801-1818*, *63*(6), 1801–1818. doi:10.1007/s40194-019-00769-2

NIST/SEMATECH. (2003). e-Handbook of Statistical Methods. doi:https://doi.org/10.18434/M32189A

Peck, M. ((2006). *Concrete : Design, construction, examples.* (M. Peck, Editor). Walter de Gruyter GmbH.

Persson, L. (2016). *A parametric study of shear-induced fatigue in corrugated steel sandwich elements*. Chalmers university of Technology.

Pousette, A., Thelandersson, S., Salokangas, L., Malo, K. A., Fortino, S., & Wacker, J. (2017). Durable Timber Bridges Final Report and Guidelines. *SP Rapport*, (25).

Roland, F., & Metschkow, B. (1997). Laser welded sandwich panels for shipbuilding and structural steel engineering. *Proceedings of the International Conference on Marine Technology, ODRA*, *24*, 183–194.

Romanoff, J., & Varsta, P. (2006). Bending response of web-core sandwich beams. *Composite Structures*, *73*(4), 478–487. Retrieved from https://www.sciencedirect.com/science/article/pii/S0263822305000668

Samvin, D., & Skoglund, O. (2016). *Design of slender steel members A comparison between the reduced stress*.

Swedish Wood. (2016). *Design of Timber Structures Structural aspects of timber construction*. Retrieved from www.swedishwood.com

Trafikverket. (2016). *Krav Brobyggande v3.0*.

Trafikverket. (2019). Klimatkrav - Trafikverket. Retrieved from https://www.trafikverket.se/for-dig-i-branschen/miljo---for-dig-i-branschen/energi-och-klimat/klimatkrav/

Transportstyrelsen. (2018). *Transportstyrelsens föreskrifter och allmänna råd om tillämpning av Eurokoder - TSFS 2018:57.*

Wolchuck, R. (1963). Design Manual for Orthotropic Steel Plate Deck Bridges. New York City: American Institute of Steel Construction, AISC.

Wouters, M. (2005). *Hybrid Laser-MIG welding - An investigation of geometrical consideration* (Doctoral dissertation, Luleå University of Technology).

Zizza, A. (2016). Buckling Behaviour of Unstiffened and Stiffened Steel Plates Under Multiaxial Stress States.

A

Global verification of model

This Appendix contains simplified hand calculations used to verify the global behaviour of the FE-model described in Chapter 3.

Global verification of the model

Calculate the deflection by hand and compare it to the FE-results for a model with tied welds

By: Hanna Lassing & Anna Libell
2020-02-01

Dimensions and material properties

$f_1 := 60mm$ Length of the top part of the corrugation

$f_2 := 60mm$ Length of the top part of the corrugation

$L_{span} := 10m$ Bridge deck span

$B := 7.593m$ Bridge deck width

$t_2 := 8mm$ Thickness top plate

$t_1 := 5mm$ Thickness bottom plate

$t_c := 8mm$ Thickness core

$h := 0.2m$ Height CCSSP

$h_{core} := h - \frac{t_2}{2} - \frac{t_1}{2} = 0.194\,m$ Heigth of the core (simplified)

$E := 210GPa$ Youngs modulus

$A_{deck} := B \cdot L_{span} = 75.93\,m^2$ Area bridge deck

$m_{deck} := 15978.64kg$ Mass bridge deck (from Brigade)

$y_{tp} := \frac{B \cdot t_2 \cdot h + B \cdot t_1 \cdot 0}{B \cdot t_2 + B \cdot t_1} = 0.123\,m$ Center of gravity (only the top and bottom plates contributes)

$$I_{yplate} := \frac{B \cdot {t_2}^3}{12} + B \cdot t_2 \cdot \left(h - y_{tp}\right)^2 + \left[\frac{B \cdot {t_1}^3}{12} + B \cdot t_1 \cdot \left(y_{tp}\right)^2\right] = 9.349 \times 10^{-4}\,m^4$$

$$I_{ycore} := \left[\frac{f_2 \cdot {t_c}^3}{12} + f_2 \cdot t_c \cdot \left(h - y_{tp} - \frac{t_2}{2} - \frac{t_c}{2}\right)^2\right] \cdot 24 \ldots = 4.925 \times 10^{-4}\,m^4$$
$$+ \left[\frac{t_c \cdot {h_{core}}^3}{12} + t_c \cdot h \cdot \left(\frac{h_{core}}{2} - y_{tp}\right)^2\right] \cdot 48 \ldots$$
$$+ \left[\frac{f_1 \cdot {t_c}^3}{12} + f_1 \cdot t_c \cdot \left(y_{tp} - \frac{t_2}{2} - \frac{t_c}{2}\right)^2\right] \cdot 24$$

$I_y := I_{yplate} + I_{ycore} = 1.427 \times 10^{-3} \cdot m^4$ Moment of intertia

Loading situation

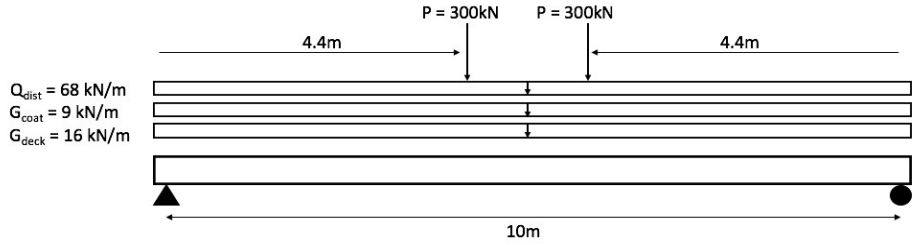

$P_1 := 300kN$ Point load (from tandem)

$P_2 := 300kN$ Point load (from tandem)

$a := 4.4m$ Distance to first point load (from the right)

$b := 4.4m$ Distance to first point load (from the left

$G_{deck} := \frac{m_{deck} \cdot g}{L_{span}} = 15.67 \cdot \frac{kN}{m}$ Self-weight of the bridge deck

$\gamma_{coating} := 1250 \frac{N}{m^2}$ Coating weight

$G_{coat} := \frac{\gamma_{coating} \cdot A_{deck}}{L_{span}} = 9.491 \cdot \frac{kN}{m}$ Self-weight of the coating

$q_{dist} := 9 \frac{kN}{m^2}$

$Q_{dist} := q_{dist} \cdot B = 68.337 \cdot \frac{kN}{m}$ Distributed load

$Q_{tot} := Q_{dist} + G_{deck} + G_{coat} = 93.498 \cdot \frac{kN}{m}$ Total uniform load on the bridge deck

Deflection

$$p_1 := \frac{P_1 \cdot a \cdot L_{span}^{\ 2}}{48 \cdot E \cdot I_y} \cdot \left(3 - \frac{4 \cdot a^2}{L_{span}^{\ 2}} \right) + \frac{P_2 \cdot b \cdot L_{span}^{\ 2}}{48 \cdot E \cdot I_y} \cdot \left(3 - \frac{4 \cdot b^2}{L_{span}^{\ 2}} \right) = 40.836 \cdot mm$$

$$p_2 := \frac{Q_{tot} \cdot 5 \cdot L_{span}^{\ 4}}{384 \cdot E \cdot I_y} = 40.614 \cdot mm$$

$p_{tot} := p_1 + p_2 = 81.45 \cdot mm$ Total displacement from hand calculations

$p_{abaqus} := 82.31mm$ Total displacement from Bridgade

$p_{diff} := p_{tot} - p_{abaqus} = -0.86 \cdot mm$

Comparing reaction force with applied load

$Load := P_1 + P_2 + Q_{tot} \cdot L_{span} = 1.535 \times 10^6 \cdot N$

$Load = 1.535 \times 10^6 N$ Total applied force

$R_{tot} := 1.535 \cdot 10^6 N$ Reaction force from Bridgade

Conclusion: The deflection are similar in hand calculations and in FE-results.
The reaction force are equal to the applied load

B

Determining minimum thickness of the core to resist buckling

This Appendix contains calculations of how to check for the smallest possible thickness of the core in order to avoid column buckling. It is applied to the case described in Chapter 4.

Column buckling of the core

Determine the minimum thickness of the core to resist buckling

By: Hanna Lassing & Anna Libell
2020-03-23

Assumption: A pinned-pinned connection between the face plates, this is conservative.

Steel properties

$f_y := 355MPa$ Yeild stress in plate

$E := 210GPa$ Youngs modulus

$\gamma_{M1} := 1.1$ Safety factor from Eurocode 1993-2

Dimensions

$h := 0.21m$ Length of core acting as a column

$A(t) := 0.5m \cdot t$ Cross-section area of the core (dependant on the thickness that is searched for)

$I(t) := \frac{h \cdot t^3}{12}$ Moment of inertia for the core (dependant on the thickness that is searched for)

Load

$Q := \frac{600kN}{4}$ Maximum load from one tandem load on each loading plate

$N_{b.Ed} := \frac{Q}{2} = 75 \cdot kN$ Maximum load on one weld

Calculations to solve the minimum thickness

$\alpha := 0.34$ Buckling curve b) is assumed

$N_{cr}(t) := \frac{E \cdot I(t) \cdot \pi^2}{h^2}$ Critical normal stress (dependant on the thickness that is searched for)

$\lambda(t) := \sqrt{\frac{A(t) \cdot f_y}{N_{cr}(t)}}$ Slenderness (dependant on the thickness that is searched for)

$$\phi(t) := 0.5 \cdot \left[1 + \alpha \cdot (\lambda(t) - 0.2) + \lambda(t)^2\right]$$

$$\chi(t) := \min\left(\frac{1}{\phi(t) + \sqrt{\phi(t)^2 - \lambda(t)^2}}, 1\right)$$

$$N_{b.Rd}(t) := \frac{\chi(t) \cdot A(t) \cdot f_y}{\gamma_{M1}}$$

$t := 4mm, 5mm .. 6mm$

$N_{b.Rd}(t) =$

43.745	·kN
83.427	
140.538	

Solve minimum thickness to avoid buckling in the core

Conclusion: To avoid buckling problems in the core, the minimum thickness requred is 5mm

C

Determining the interaction of column- and plate-like buckling for a CCSSP

This Appendix contains calculations of the reduction factor for buckling of the top plate field of the CCSSP. It uses the interaction formula between plate- and column-like buckling and determines the interaction between the two phenomena in the two directions of the plane.

Column-like or plate-like buckling

Determine how the plate buckles

By: Hanna Lassing & Anna Libell
2020-02-27

Steel properties

$f_y := 355MPa$	Yeild stress in plate
$E := 210GPa$	Youngs modulus
$\upsilon := 0.3$	Poissons ratio
$\gamma_{M1} := 1.1$	Safety factor from Eurocode

Dimensions

$t := 8mm$	Thickness top plate
$a := 10m$	Length of the plate
$b := 286mm$	Width between the welds

Coordinate system used in calculations

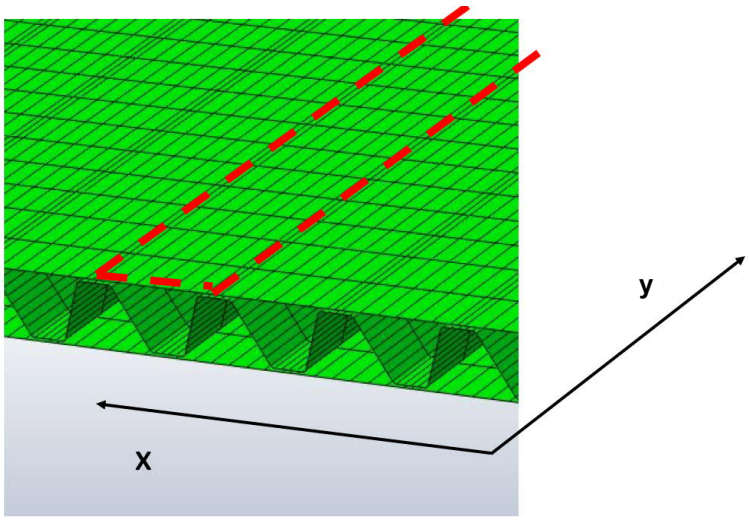

Calculate the critical stresses in x-direction

$$\sigma_{cr.c.x} := \frac{\pi^2 \cdot E \cdot t^2}{12 \cdot \left(1 - \upsilon^2\right) \cdot a^2} = 121.472 \cdot kPa$$

Critical stresses

$$\sigma_{E.x} := \frac{\pi^2 \cdot E \cdot t^2}{12 \cdot \left(1 - \upsilon^2\right) \cdot b^2} = 148.506 \cdot MPa$$

No stiffeners on between the welds

$$k_{\sigma.p} := 1$$

$$\sigma_{cr.p.x} := k_{\sigma.p} \cdot \sigma_{E.x} = 148.506 \cdot MPa$$

$$\xi_x := \frac{\sigma_{cr.p.x}}{\sigma_{cr.c.x}} - 1 = 1.222 \times 10^3$$

Conclusion: Plate-like buckling dominates

Calculate the critical stresses in z-direction

$$\sigma_{cr.c.z} := \frac{\pi^2 \cdot E \cdot t^2}{12 \cdot \left(1 - \upsilon^2\right) \cdot b^2} = 148.506 \cdot MPa$$

$$\sigma_{E.z} := \frac{\pi^2 \cdot E \cdot t^2}{12 \cdot \left(1 - \upsilon^2\right) \cdot a^2} = 121.472 \cdot kPa$$

$$\sigma_{cr.p.z} := k_{\sigma.p} \cdot \sigma_{E.z} = 1.215 \times 10^{-4} \cdot GPa$$

$$\xi_z := \frac{\sigma_{cr.p.z}}{\sigma_{cr.c.z}} - 1 = -0.999$$

Conclusion: Column-like buckling dominates

D

Design Program - file overview

This Appendix describes the contents of the design program written for this thesis. The design program is run in BRIGADE/Plus or Abaqus. It has two main stages:

1. Stage 1 is used to create FE-models and input files for the FE-analyses
2. Stage 2 is used to read the odb-files from the FE-analyses and make controls according to Eurocode

To run the input files in BRIGADE/Plus or Abaqus, the code `RunningJobs.py` can be used.

D.1 Stage 1: Creating input files

The main file for stage 1 of the design program is `INPUTFILE.py`. In this file, the following codes are used:

- `Input.py`
  Contains the input data for the CCSSP, such as geometry, material data, etc. (Created by Peter Nilsson, 2017 modified by authors, 2020)
- `PostInput.py`
  Makes post input calculations related to geometry, etc (Created by Peter Nilsson, 2017 modified by authors, 2020)
- `LoadPositions.py`
  Specifies the positions of the tandem loads
- `LoadCombinations.py`
  Calculates the partial factors for the loads in ULS
- `MakeModel.py`
  Creates the model except loads, steps and job (Created by Peter Nilsson, 2017 modified by authors, 2020)
- `MODEL_Buckle.py`
  Creates the model used in the linear buckling analysis
- `MODEL_LM1.py`
  Creates the model used in the linear static analysis with LM1 for ULS and SLS controls
- `MODEL_FLM_A.py`
  Creates the model used in the linear static analysis with FLM4 and axel type A for fatigue assessment
- `MODEL_FLM_B.py`

Creates the model used in the linear static analysis with FLM4 and axel type B for fatigue assessment

- `ADDINGWELDS.py`
  Adds spring and connector elements to the positions of the welds in the linear static models (Created by Peter Nilsson, 2017 modified by authors, 2020)
- `pnPyFuncs.py`
  Calculate the spring stiffness, function created by (Created by Peter Nilsson, 2017)
- `FunctionModule.py`
  A number of functions collected in one file. See section D.3 for more information

D.2 Stage 2: Performing Eurocode controls

The main file for stage 2 of the design program is `CONTROLS.py` which uses BRIGADE/-plus odb-files and performs controls of the models according to Eurocode. In this file, the following codes are used:

- `Input.py`
  Contains the input data for the CCSSP, such as geometry, material data, etc. (Created by Peter Nilsson, 2017 modified by authors, 2020)
- `PostInput.py`
  Makes post input calculations related to geometry, etc. (Created by Peter Nilsson, 2017 modified by authors, 2020)
- `LoadPositions.py`
  Specifies the positions of the tandem loads
- `SPRINGOUTPUT.py`
  Writes output files for forces and mending moment in the springs which represents welds, after the linear static analyses have been run (Created by Peter Nilsson, 2017 modified by authors, 2020)
- `WeldsULS.py`
  Retrieves results and makes Eurocode controls for the weld stresses in ULS
- `SLS.py`
  Retrieves results and makes Eurocode controls for the deflection in SLS
- `ULS.py`
  Retrieves results and makes Eurocode controls for plate stresses in ULS
- `FLS.py`
  Retrieves results and makes Eurocode controls for fatigue damage in FLS
- `FunctionModule.py`
  A number of functions collected in one file. See section D.3 for more information

D.3 Functions

A number of functions have been created by the authors used in the Design program. These can be found in the module `FunctionModule.py` and are:

- `PathList`
  This function makes a list of all nodes on the chosen path. The input is a choice of axis for the path, the set on which the path shall be made and a coordinate which all nodes on the path shares
- `PathFromNodeList`
  This function makes a path in the chosen model, based on a node list of the nodes chosen for the path
- `ResultFromPath`
  This function retrieves results of a chosen variable from a chosen path
- `RetrieveEigenvalue`
  This function retrieves the eigenvalue of a linear buckling analysis
- `TextFileToWeldForces`
  This function reads and processes the spring forces from a text-file written by `SPRINGOUTPUT.py`
- `SpringForceToStress`
  This function calculates weld stresses using spring forces
- `ULS`
  This function calculates the utilization ratio, η, for normal stresses in ULS
- `ULSshear`
  This function calculates the utilization ratio, η, for shear stresses in ULS
- `SLS`
  This function calculates the utilization ratio, η, for deflection in SLS
- `RSM`
  This function calculates the utilization ratio, η, for the RSM in ULS
- `ULSwelds`
  This function calculates the utilization ratio, η, for stresses in the welds in ULS
- `DamageAccumulationMethod`
  This is a function which, given the weld stress $\Delta\sigma_i$ in each cycle of the bridge's total life calculates the total damage done to the weld with respect to fatigue

E

Design Program - Eurocode controls

In this Appendix all the Eurocode controls performed in the Design Program are summarized.

E.1 SLS

E.1.1 Deflection

$$\delta = \frac{L}{400} \tag{E.1}$$

$$\eta = \frac{u}{\delta} \cdot 100 \leq 100\% \tag{E.2}$$

E.2 ULS

E.2.1 Stresses in x-direction

$$\eta = \frac{\sigma_{x,Ed}}{f_y/\gamma_{M0}} \cdot 100 \leq 100\% \tag{E.3}$$

Where $\gamma_{M0} = 1.0$.

E.2.2 Stresses in y-direction

$$\eta = \frac{\sigma_{y,Ed}}{f_y/\gamma_{M0}} \cdot 100 \leq 100\% \tag{E.4}$$

Where $\gamma_{M0} = 1.0$.

E.2.3 Shear stresses

$$\eta = \frac{\tau_{Ed}}{\sqrt{3} f_y/\gamma_{M1}} \cdot 100 \leq 100\% \tag{E.5}$$

Where $\gamma_{M1} = 1.0$.

E.2.4 Von Mises stress

$$\eta = \frac{\sigma_{VM}}{f_y \cdot \gamma_{M0}} \cdot 100 \leq 100\% \tag{E.6}$$

Where $\gamma_{M0} = 1.0$.

E.2.5 RSM

$$\eta = \left(\frac{\sigma_{x,Ed}}{\rho_x f_y/\gamma_{M1}}\right)^2 + \left(\frac{\sigma_{z,Ed}}{\rho_z f_y/\gamma_{M1}}\right)^2 - \left(\frac{\sigma_{x,Ed}}{\rho_x f_y/\gamma_{M1}}\right)\left(\frac{\sigma_{z,Ed}}{\rho_z f_y/\gamma_{M1}}\right) + 3\left(\frac{\tau_{Ed}}{\chi_w f_y/\gamma_{M1}}\right)^2 \cdot 100 \leq 100\% \tag{E.7}$$

Where $\gamma_{M1} = 1.1$.

E.2.6 Weld stresses

Equation E.8 is used to transform the force in each spring ([N]) to the force per element ([N/m]) along each weld. This is done with the forces from all three nodes of each element. These are seen in figure E.1. The same procedure is used to transform the bending moment, M_x ([Nm]), in the springs to moment in each element ([Nm/m]) as seen in Equation E.9.

$$P_{norm,k} = \frac{\frac{P_{j-1}}{2} + P_j + \frac{P_{j+1}}{2}}{elSize_k} \quad [N/m] \tag{E.8}$$

$$M_{norm,k} = \frac{\frac{M_{j-1}}{2} + M_j + \frac{M_{j+1}}{2}}{elSize_k} \quad [Nm/m] \tag{E.9}$$

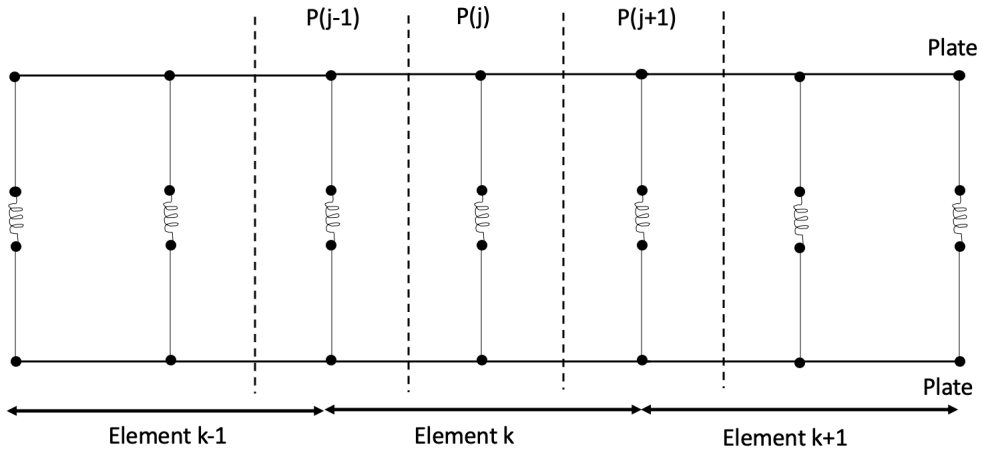

Figure E.1: *Normalization of weld stresses*

$$A = a[m] \tag{E.10}$$

$$W = \frac{a^2}{6}[m^2] \tag{E.11}$$

$$\sigma_{90} = \frac{P_z}{A} + \frac{M_x}{W} \tag{E.12}$$

$$\tau_0 = \frac{P_x}{A} \tag{E.13}$$

$$\tau_{90} = \frac{P_y}{A} \tag{E.14}$$

$$\sigma_{VM} = \sqrt{\sigma_{90}^2 + 3 \cdot (\tau_0^2 + \tau_{90}^2)} \tag{E.15}$$

$$\frac{\sigma_{VM}}{f_u/(\beta_w \cdot \gamma_{M2})} \cdot 100 \leq 100\% \tag{E.16}$$

$$\frac{\sigma_{90}}{0.9 \cdot f_u/(\gamma_{M2})} \tag{E.17}$$

Where $\beta_w = 0.9$ & $\gamma_{M2} = 1.25$.

E.3 FLS

$$n_i = \%_{lorry} \cdot \%_{position} \cdot Lifetime \cdot N_{OBS} \tag{E.18}$$

$$N_i = 2 \cdot 10^6 \left(\frac{\Delta\sigma_C/\gamma_{Mf}}{\gamma_{Ff}\Delta\sigma_i} \right)^m \tag{E.19}$$

$$D = \sum D_i = \sum \frac{n_i}{N_i} \tag{E.20}$$

DEPARTMENT OF ARCHITECTURE AND CIVIL ENGINEERING
CHALMERS UNIVERSITY OF TECHNOLOGY
Gothenburg, Sweden
www.chalmers.se

CHALMERS
UNIVERSITY OF TECHNOLOGY